FERMILAB-PUB-79-108-E

INCLUSIVE PRODUCTION OF LARGE TRANSVERSE MOMENTUM HADRONS AND HADRON PAIRS

H. Jöstlein, R. J. Engelmann, R. J. Fisk,* M. L. Good,
A. S. Ito, D. M. Kaplan, R. D. Kephart,
R. L. McCarthy, and H. Wahl†
State University of New York at Stony Brook
Stony Brook, New York 11794

and

S. W. Herb, D. C. Hom,‡ L. M. Lederman,
J. C. Sens,# H. D. Snyder,§ and J. K. Yoh
Columbia University, New York, New York 10027

and

J. A. Appel, B. C. Brown, C. N. Brown, W. R. Innes,
and K. Ueno
Fermi National Accelerator Laboratory, Batavia, Illinois 60510

*Present address: Fermi National Accelerator Laboratory, Batavia, Illinois 60510

†Present address: CERN, Geneva, Switzerland.

‡Present address: Riverside Research, 80 West End Ave., New York, New York 10023

§Present address: Gallaudet College, Washington, D.C.

#Present address: Foundation for Fundamental Research on Matter, The Netherlands

ABSTRACT

We have studied interactions of 200, 300 and 400 GeV protons with beryllium and tungsten targets, in which two large p_t hadrons were produced roughly back-to-back in the proton-nucleon center of momentum system. Both hadrons could be identified. Some results from this work have been published earlier.[1,2,3,4] This paper describes properties of the apparatus, data on the two-particle correlation as a function of the kinematic variables and quantum numbers of the produced hadrons, invariant two-particle cross sections and scaling properties of symmetric hadron pair production.

I. INTRODUCTION

In recent years the study of hadronic interactions leading to one or more large transverse momentum (p_t) particles has received much attention, both experimentally and theoretically. Such interactions are believed to be sensitive to the small scale structure of hadronic matter. Current ideas about the constituent nature of hadrons are able to explain most large p_t observations qualitatively in a consistent way. However, many detailed questions cannot yet be answered satisfactorily. Of particular interest are the nature of the constituents dominating a given process (quarks, gluons, di-quarks, mesons, . . .), the origin, magnitude and role of the transverse momentum of constituents within the hadron and the nature of the interaction between constituents. Previous publications from this experiment[1,2,3,4] have shed light on some of these questions; additional results are presented in this article, together with a discussion of experimental details.

II. EXPERIMENTAL DETAILS

These studies were made with a two-arm magnetic spectrometer (Fig. 1) with Cerenkov particle identification in each arm. Use of high luminosity permitted observation of the rare processes which produce two large p_t hadrons (pair mass from 4 to 10 GeV).

A) Running Conditions

Data were taken with three beam energies (200, 300 and 400 GeV protons), two target materials (beryllium and tungsten) and various intensities and magnet currents. Table I lists the major running conditions and integrated luminosities.

B) Beam and Monitors

The beam was obtained by slow extraction from the Fermilab proton synchrotron. Beam intensities between $2 \cdot 10^9$ and $3 \cdot 10^{10}$ protons per accelerator cycle (typically 1 second spill every 10 seconds) were used. The beam intensity was monitored using a secondary emission monitor (SEM) which was calibrated several times during the course of the experiment by comparing the SEM rate to the rate of production of ^{24}Na and ^{52}Mn in copper foils. The resulting calibration constants varied by less than 5% during the approximately one year of operation. Integrated proton fluxes were derived from these foil calibrations using cross sections[5] per Cu nucleus of 3.5 mb for the production of ^{24}Na and 4.0 mb for ^{52}Mn.

In addition to the SEM intensity monitor a pair of fast monitors consisting of small scintillation counter telescopes viewed the target through the magnet apertures in each arm. Almost all charged particles were swept away from these counter telescopes (called N_1 and N_2) so that the sensitivity of the N counting rate to the magnetic field was less than 5%. About 98% of the N counts came from the target. The beam intensities as measured by the SEM and by the N counters increased in proportion from small intensities up to

twice the highest intensities used in data taking. A logic level, generated whenever the experiment was ready to accept triggers, was used to gate these fast monitors. Thus the total number of counts (N) measured the integrated luminosity without the need for dead-time corrections.

Three different targets were used. Each was a rectangle of thin sheet metal, standing on its long edge with the beam impinging on the short edge. Their properties are listed in Table II. The wide "Be3" target was used to measure the full targeting ratio N/SEM for beryllium. It intercepted all of the beam, which was focused to a spot 0.08 cm high by 0.03 cm wide (FWHM). The ratio N/SEM varied by about 5% during the course of the experiment. The monitor constant may be expressed as an effective cross section σ_N for a proton striking a target nucleus to produce a monitor count. The integrated luminosity is then expressed as $L = N/\sigma_N$. The monitor cross section σ_N is determined from the full-targeting ratio N/SEM. The narrow "Be7" target used in data taking typically intercepted 70% of the beam. This geometric efficiency is taken into account by the N monitor. In the case of tungsten, it was not possible to calibrate the monitor using a thick target, because secondaries would have been noticeably attenuated. Instead, several careful target scans were made (see Fig. 2). The normalized monitor rates N/SEM at the points where the target was displaced by integral multiples of its own width were added to measure the amount of beam not hitting the target in its usual position. This procedure yielded the monitor ratio and cross section for the W

target. The method was verified by applying it to the Be7 target where an independent determination of the monitor constant had been made using the thick Be3 target. Monitor cross sections are listed in Table III.

The attenuation of the primary beam in the targets was taken into account assuming protons were removed from the beam after they had interacted. Another small correction was made for interactions of the high p_t hadrons on the way out of the target.

C) Accidental Coincidences

Accidental coincidences between the two spectrometer arms must be considered carefully when performing a pair production experiment. The time structure of the proton beam is relevant here. In the present mode of operation of the Fermilab synchrotron, the rf accelerating voltage is left on during the slow extraction of the beam. This results in a spill delivered in "rf bunches" of about 1 nsec duration each, separated by 18.9 nsec. The timing of the fast logic circuits used in triggering the apparatus was set up such that sets of particles from different rf bunches could not combine to satisfy the trigger requirements when neither set would do so alone. Under these conditions we can write the rate in each spectrometer arm (per rf bunch) as $B_i = B_{int}\ \epsilon_i$, where B_{int} is the average number of inelastically interacting protons per rf bunch, and ϵ_i is the average number of particles per inelastic interaction detected in arm i.

The probability of observing an accidental pair event (two tracks from the same rf bunch but from separate nuclear collisions)

per rf bunch is then

$$B_{1,2}^{acc} = B_{int}^{2}\,\varepsilon_1\varepsilon_2.$$

This is an exact result if the number of interactions per rf bunch follows a Poisson distribution with average value B_{int}. For a data set including N_{in} inelastic interactons in the target, the physically interesting correlation function R is defined as

$$R \equiv \frac{N_{1,2}^{real}/N_{in}}{(N_1/N_{in})\ (N_2/N_{in})} \qquad (1)$$

where $N_{1,2}^{real}$ is the number of real (i.e. originating from a single interaction) pair events, while N_1 and N_2 are the number of single hadrons in each arm. R can be evaluated for any kinematic region, e.g. the region of acceptance of our pair spectrometer. The average number of real pairs per rf bunch can then be written as $B_{1,2}^{real} = B_{int}\,\varepsilon_1\varepsilon_2 R$. The ratio (accidental pairs/real pairs) simplifies to $B_{1,2}^{acc.}/B_{1,2}^{real} = B_{int}/R$, independent of acceptance and efficiencies. In planning a pair measurement one therefore chooses a beam intensity matched to the R value expected in the region of interest. Since R increases rapidly with increasing mass of the pair (see Sect. III and Fig. 23), the fraction of accidental events drops rapidly with increasing mass, permitting the use of large beam intensities for the study of the high mass region.

The above formulae apply not only to the two spectrometer arms, but to any pair of monitor counters. If the monitor counters

accept pairs of low effective mass, where the R-function is small, then the pair rate of these monitors will be dominated by accidentals, provided B_{int} is larger than R. (If B_{int} is not large compared to R, a correction for real pairs is made.) Such a pair of counters can then be used to determine the expected level of accidental coincidences, characterized by the effective number of rf bunches in an accelerator cycle or a whole run (presuming B_{int} stays constant):

$$K_{eff} = \frac{N_1 N_2}{N_{1,2}^{acc}}.$$

K_{eff} contains all the information about the spill duty factor needed to calculate the number of accidental coincidences due to single particles in each arm from different proton interactions in the target. This is true even if the mean intensity varies during data taking, because at the intensities used both the N monitor pair and the pair of spectrometer arms require coincidences between two detector signals, causing the accidental rates to vary as the square of the intensity.

In addition to problems with uneven slow spill structure, a particular difficulty was the presence of rf bunches with much larger than average intensity, called "superbuckets". These superbuckets caused a large increase in trigger rate and some rise in the fraction of accidentals. In order to monitor their occurrence, a short gas filled Cerenkov counter was installed in the proton beam line. The output signal of this fast counter was proportional to

the number of protons in each rf bunch. By discriminating against large pulse heights, triggers coming from superbuckets were vetoed. This veto was also imposed on the monitors to ensure correct proton flux integration.

D) The Magnetic Spectrometers

Downstream of the target the secondaries in each arm passed through a 5 m collimator, made from steel and tungsten, with its opening centered about a ray emerging from the target center in the horizontal plane at $\tan\theta = 0.0725$ (θ is the production angle in the lab). The opening of the collimator was larger than the final fiducial solid angle. A 5 cm long tungsten collimator, installed to define the vertical acceptance for the concurrent electron pair experiment, was carefully surveyed and defined the hadron aperture via software cuts. The fiducial volume used in the final analysis is listed in Table IV and shown in Figs. 3 and 4. A cartesian coordinate system was defined for each spectrometer arm, with the z coordinate pointing along the center of the arm in the direction of flight of the secondaries, the x-axis pointing horizontally away from the beam line and the y-axis oriented such as to form a right-handed system.

The collimators were followed by a pair of magnets, one in each arm, which deflected charged particles vertically. The magnets were 3.05 m long with an aperture 25 cm high, tapering from 46 cm to 60 cm width. The apertures contained vacuum chambers to reduce scattering. (For the same purpose, the target area and

collimators up to the magnet entrances were filled with He gas). Looking downstream, the left spectrometer arm accepted only particles bent upward out of the neutral beam (the region within line of sight of the target), while the right arm accepted only particles bent downward. The arms were therefore called the "up arm" and the "down arm". This arrangement decouples the momentum measurement from the production angle measurement, sweeps low p_t particles out of the aperture (rather than across it) and maximizes the acceptance for pairs with small net transverse momentum.

The magnets were connected in series so that their currents were equal. The two polarities could, however, be varied independently. Most data were taken at magnet currents of 1288 and 961 A. The corresponding field integrals were 3.48 and 2.58 Tesla -m, imparting transverse momentum kicks of 1.043 and 0.774 GeV respectively. The magnet current and the field at one point in each magnet were monitored continuously and found stable within 10^{-3}. The field integrated over z was uniform to ±1%. The x and y dependence of the integral was expressed as a second order polynomial fitted to field measurements made with a very long flip coil.

E) Acceptances

The requirement that charged particles be bent out of the neutral beam into the detectors, but not too far out, results in the momentum acceptance shown in Fig. 5. At low momentum (p), tracks are bent out of the fiducial volume and miss the rear detector planes. At intermediate momenta we accepted tracks within the full aperture of the 5 cm W collimator. At high momentum the acceptance

falls due to failure of high momentum tracks to be swept out of the neutral beam into the detectors.

Plotted against p_t rather than p, the resulting acceptance is a superposition of many such curves. Since $p_t = p \sin\theta$, a range of momenta contribute at each p_t value. To calculate single arm acceptances as a function of p_t we must know how the events are distributed in the production angle θ, or, equivalently the rapidity y. In a given system, the rapidity y is defined as a function of the energy (E) and momentum of a particle parallel to the incident beam ($p_{\parallel}$) as $y \equiv \frac{1}{2} \ln \frac{E + p_{\parallel}}{E - p_{\parallel}}$. In calculating the p_t acceptance we assume that the invariant cross section is independent of y within the small range of y accepted. The single particle acceptance A at each p_t value is then defined by the equation

$$\frac{dN}{dp_t} = L\, p_t \left(E \frac{d^3\sigma}{dp^3}\right) A,$$

where N is the number of observed events, L is the integrated luminosity and $E \frac{d^3\sigma}{dp^3}$ is the invariant single particle cross section. The acceptance A is computed by integrating over the fiducial volume of our spectrometer by the Monte Carlo method: $A = \int \frac{p}{E} \frac{d\Omega}{\sin^2\theta}$. This integral is Lorentz invariant and can be evaluated in the c.m. or lab system. Its value is approximately equal to our c.m. solid angle at 400 GeV, since the $\sin^2\theta$ factor in the denominator is close to 1.0 in the c.m. system for our experiment at this beam energy. The resulting single arm acceptance is plotted versus p_t in Fig. 6. The same figure also shows the acceptance requiring Cerenkov identification of the hadron (to be discussed later). Unlike the c.m. solid angle, the invariant single arm acceptance is independent of the inci-

beam energy. The mean c.m. rapidity depends, however, on the beam energy and moves from an average of about 0.0 at 400 GeV to 0.2 at 300 GeV and 0.4 at 200 GeV. The rapidity for accepted pairs is close to the average rapidity of the two secondaries. The fraction of pairs accepted as a function of y is shown in Fig. 7 for all three beam energies. It does not depend strongly on mass.

The small vertical aperture of our apparatus requires observed events to be nearly coplanar. The horizontal (x) projections of the transverse momenta are therefore equal to p_t within 0.4% for accepted events ($p_{t,x} = 0.999\ p_t$ on average), so we neglect the distinction between p_t and $p_{t,x}$. Only pairs with a small vertical (y) component of the pair transverse momentum (called p_y) are accepted, as seen in Fig. 8. The width of our p_y acceptance increases with mass, but reaches a value of only about 0.4 GeV/c at the largest observed masses of 10 GeV. The width of the p_{out} event distribution is reported to be much larger than our acceptance, as is apparent from the data sample from Ref. 6, also shown in Fig. 8 (small differences in the definitions of p_{out} and p_y are negligible here).

It is useful to define the pseudo-mass $m' \equiv p_{t,1} + p_{t,2}$, where $p_{t,1}$ and $p_{t,2}$ denote the magnitudes of the transverse momentum of the particle in each of the arms. The mass of a hadron pair is calculated from $m^2 = m_1^2 + m_2^2 + 2\ (E_1E_2 - p_1p_2 \cos\alpha)$, where α is the opening angle of the pair. If $m_1 << p_1$ and $m_2 << p_2$ this simplifies to $m^2 \simeq 4\ p_1p_2 \sin^2(\frac{\alpha}{2})$, which can be approximated (to better than 2% accuracy for our events) by $m^2 \simeq (m')^2 - (p_t')^2$,

where $p_t' \equiv p_{t,2} - p_{t,1}$ is almost exactly the x-component of the pair transverse momentum for those pairs accepted by our apparatus. Because of the relationship $m' \equiv p_{t,1} + p_{t,2}$, the pair acceptance at a given m' is roughly a convolution of the p_t acceptances in the two arms. Two kinds of pair cross sections were considered. One assumed that an intermediate dihadron state was formed and decayed isotropically in its rest system. The corresponding fraction of all pairs accepted at a given mass will be called "pair acceptance". To calculate the pair acceptance one needs to know the dihadron production dynamics. The second kind of cross section we considered was the invariant two particle cross section near $p_y = 0$ and $y_{pair} = 0$. We measure this type of cross section directly without any model assumptions.

The pair acceptance was used in our search[1] for dihadron resonances. Invariant two particle cross sections will be shown in Section IV. Figures 9 and 10 show the "pair acceptance" for charged hadron pairs as a function of pair mass and pair transverse momentum (p_t'). The steep increase as p_t' approaches zero is due to the fact that transverse momentum vectors pointing in any azimuthal direction are accepted when p_t' is small. Note also that the acceptances requiring Cerenkov particle identification are considerably smaller than the geometric acceptance of the spectrometer alone, and do not extend to very high masses or pair transverse momenta.

F) Counters, Chambers and the Hadron Calorimeter

The instrumentation of the spectrometer arms downstream of the analyzing magnets is shown in Fig. 11. Three coarse scintillation

counter nodoscopes (T_o, T_1 and S_2) were the primary trigger elements. Two additional fine-grained hodoscopes, V_1 (38 elements) and V_2 (55 elements), measured horizontal (x) track positions.

Nine proportional wire chambers recorded track impact positions in each arm. Two threshold gas Cerenkov counters allowed identification of a fraction of the hadrons in each arm. A total absorption hadron calorimeter measured the hadron energy and was used both in triggering and rejecting background during the off-line analysis. The hadron calorimeter consisted of a lead glass array, 61 cm deep, followed by a "swimming pool calorimeter".[7] The water calorimeter, shown in Fig. 12, consisted of a large volume of purified water, 5.5 m long in the up-arm, 3.2 m long in the down-arm. Cerenkov light produced by a hadron and by its shower was collected by a plane of wavelength-shifter-doped acrylic panels covering the downstream end and connected to a set of photomultiplier tubes. Since both the lead glass and the water calorimeter responded to Cerenkov light only, large fluctuations in the output signal were observed. The calorimeter pulse height F was the sum of the responses from the lead glass and the water calorimeter, balanced such as to minimize the pulse height spread for hadronic showers. Figure 13 shows a typical spectrum of calorimeter pulse height (F), normalized to the particle momentum (p) measured by the magnetic spectrometer. The F response has been normalized to yield $F \tilde{=} p$ for hadrons. The F/p distributions show full width/mean ratios of approximately 0.8, which was adequate for the two tasks of the calorimeters: (1) to generate signals proportional to p_t and m' for triggering (see below), and (2) to reject

background off-line. We observed a significant dependence of the calorimeter response on the hadron species (Fig. 14), which was taken into account in the analysis.

Since no detectors were placed upstream of the analyzing magnets, the momentum of a hadron was inferred from its trajectory downstream of the magnet, presuming it originated in the target. It was possible for a low p_t hadron to scatter off the magnet coils or other material in such a way as to simulate a (rare) large p_t particle. These background tracks usually failed to produce a large calorimeter pulse height F, which allowed us to reject them with a cut on the ratio F/p. The extrapolated target distribution in the non-bending (x) plane allows an independent determination of the level of this type of background. Figure 15 shows a scatter plot of the apparent target x position versus the ratio F/p. For F/p below our cut value of 0.35, there is a large number of events not originating in the target. After cutting on F/p and x_{target}, the remaining background is negligible, except at the highest p_t (above 5 GeV), where it may approach 10%. In view of the poor statistical accuracy of the background determination for high p_t data no correction has been made. The error due to this background is negligible compared to the statistical error for all data shown.

G) The Trigger

The trigger employed a two-level system developed at Nevis Laboratories. The primary triggers consisted of two single arm triggers and a pair trigger. The single arm triggers required a

coincidence of T_o, T_1 and S_2. The pair trigger required a coincidence of the two single arm triggers. The primary triggers caused hodoscope and calorimeter information to be strobed into registers. The second stage trigger consisted of a number of units capable of sensing the status of the bits set in some of these registers, providing an output if certain conditions were met. With these logic units it was easy to implement complicated trigger requirements such as hodoscope "roads". Using signals from the V_1 and V_2 hodoscopes, a "matrix unit" rejected tracks not pointing back to the target in the (non-bending) horizontal plane. This unit divided V_1 into 10 bins, V_2 into 14 bins. The active V_1V_2 combination also provided an estimate of the polar production angle θ, assigning one of four possible angular regions to the track in each arm. The hadron calorimeter measured the total energy deposited within its volume. By using the angular information from the V_1V_2 hodoscopes it was possible to construct an analog signal crudely proportional to the transverse momentum p_t of a particle. This was done by weighting the calorimeter pulse height by a factor proportional to the average value of $\sin\theta$ appropriate for the angular region in which the track registered. The requirement that this "p_t signal" exceed a given threshold eliminated the numerous low-p_t secondaries from the trigger. In addition we used the relation $m' \equiv p_{t,1} + p_{t,2} \simeq m$ to construct a sum signal which was roughly proportional to the mass of the hadron pair. A sum signal exceeding a set threshold indicated a high-mass pair, allowing suppression of triggers from the abundant low-mass pairs. Triggers were normally

vetoed if more than one angular region registered a track. Losses due to this requirement (M1) and other inefficiencies are listed in Table V. Figure 16 displays the trigger efficiency for single arm (p_t) and mass triggers. The trigger efficiencies were measured (data points) and also calculated by a Monte Carlo method starting with the observed species dependent F/p distributions.

The secondary trigger level allowed concurrent use of several triggers, each prescaled if required. Prescaled single arm triggers were taken along with the pair triggers during all of the data runs to monitor the performance of the apparatus, to calculate the number of accidental pairs and to determine two particle correlation functions (see Sect. III).

H) Performance of the Apparatus

The nine proportional wire chambers in each spectrometer arm had wire spacings of 2 and 3 mm. The resulting resolution in momentum, transverse momentum and mass is shown in Fig. 17. The contribution of multiple scattering due to a total of 0.13 radiation lengths of material in each arm, plus 0.05 r.l. in the Be target (or 1 r.l. in the W target) was small compared to the track measurement errors. The e^+e^- mass spectra taken simultaneously with the dihadron data afforded a direct check of the mass resolution at the J/ψ peak. Figure 18 shows the e^+e^- mass spectrum, measured with the magnetic spectrometer (the lead glass was used only as an electron identifier). The observed resolution of 13 MeV r.m.s. agrees closely with the calculated one.

contribution was minimized by focusing the mirrors on a spot halfway between the target and the magnet centers. The measured light yield for this mirror/phototube combination was N_o = 180 photoelectrons/cm, as defined by $N = N_o L \sin^2\psi$, where N = observed number of photoelectrons, L = length of radiator and ψ = Cerenkov cone opening angle ($\cos\psi = 1/\beta n$). These measurements were made in a test beam, using 6 GeV pions and also electrons, with a test counter of variable radiator length.

The second counter, $\check{C}_2$, contained no helium gas. It was therefore possible to avoid windows and to place the phototubes inside the gas volume, where very short wavelength UV light can reach them. The glass envelopes of the phototubes used (Amperex 58 DVP) are not transparent to UV light. In order to make use of that light normally absorbed in the glass, the faces of the tubes were coated by vacuum evaporation with 200 $\mu g/cm^2$ of p-terphenyl, a fluorescent material. This treatment improved the light yield from an original N_o = 60 to a value of 150 photoelectrons/cm. Conservative light yields of 150 ($\check{C}_1$) and 100 ($\check{C}_2$) were used in establishing the momentum ranges over which particles could be identified, and in the entries of Table VII, which lists properties of the Cerenkov counters.

The threshold momenta observed for each gas agreed with expectations based on its index of refraction. Threshold curves are shown in Fig. 20. The momentum band in which only pions registered in $\check{C}_1$, and kaons (but not protons) registered in $\check{C}_2$, is called the triple identification band. Pions could be distinguished from protons and kaons over a much wider momentum range, as listed in Table

VII. An example of the response of the two Cerenkov counters to negative hadrons is shown in Fig. 21.

The success of a Cerenkov identification system is characterized by its efficiency and by the absence of contamination. Due to the large number of photoelectrons available, the efficiency for $\beta = 1$ particles was always greater than 0.998, and consistent with 1.0, as measured with electrons. The large light output allowed operation close to the thresholds, thereby maintaining a large usable momentum range. We defined identification ranges such that the Cerenkov counters responded with at least 95% efficiency near the thresholds. This can lead to a 5% misidentification of kaons as protons.

In addition, extra tracks could pass through the Cerenkov counters. These tracks were usually of low momentum, emerging from the magnets at large vertical angles and missing some of the detectors, thus escaping reconstruction. They were most copious during "high mass" data runs because of the associated high beam intensity. Each Cerenkov counter was divided into three cells. Accidental hits were studied by observing how often a cell not associated with a reconstructed track responded. The level of accidentals did not exceed 10 % (except for $\bar{p}$). Accidental contamination and inefficiencies for all hadron species are listed in Table VIII.

Our results for species ratios in inclusive single hadron production as a function of p_t are shown in Fig. 22, together with results from the CP group.[8] The two experiments are in good agreement with regard to the K/π ratios. However, the p/π^+ and $\bar{p}/\pi^-$ ratios show a small discrepancy (about 1.5 times our systematic error) in the $p_t > 3$ GeV region.

III. THE HIGH-MASS PAIR CORRELATION

A) Introduction

If the probability of producing two hadrons in an inelastic proton-nucleon collision is the product of the probabilities of producing each hadron inclusively, then such pair production is said to be uncorrelated.

Correlations might be introduced by several effects: when producing large p_t hadrons, it might be that a collision "hard enough" to make one large p_t particle would be more likely to yield another one than would an average collision; also, transverse momentum balance might enhance the production of hadron pairs with large p_t on each side. (In general, however, the balancing occurs through the emission of many low p_t hadrons.[12]).

Indeed it is found[13] that there is a significant enhancement of the emission of a second large p_t π^o even on the same side as a first one (approximately a factor of 40 at 3 GeV/c), consistent with the idea that hard collisions which produce single large p_t hadrons are also effective in producing pairs of large p_t hadrons. On the opposite side where one expects help from transverse momentum balance, the enhancement exceeds 200 at 3 GeV/c and rises rapidly with increasing p_t.

Data from the present experiment (CFS) are in agreement with the CCRS data at the common c.m. energy. We have extended the study to large x_t values and to the very important question of quantum number correlations at large mass.

The enhancement is quantitatively expressed as the correlation function R, defined in Eq. 1. R can also be written in terms of cross sections for single hadron and pair production

$$R = \frac{E_1 E_2 \frac{d^6\sigma_{1,2}}{dp_1^3\, dp_2^3} \Big/ \sigma_{in}}{E_1 \frac{d^3\sigma_1}{dp_1^3} \Big/ \sigma_{in} \; E_2 \frac{d^3\sigma_2}{dp_2^3} \Big/ \sigma_{in}} \qquad (2)$$

because all acceptances and efficiencies cancel (σ_{in} is the inelastic cross section).

B) Data from the Be Target

The mass and energy dependences of the correlation function R for p-Be collisions are shown for symmetric pairs ($|p_t'| < 1.1$ GeV) in Fig. 23. Measurements at the ISR[14] and bubble chamber data[15] indicate R values of around 1.6 for h^+h^- and 1.3 for doubly charged hadron pairs at low p_t. Above a pseudomass ($m' \equiv p_{t,1} + p_{t,2}$) of 5 GeV we find that the correlation increases roughly as exp (1.4 m'). This is the line in Fig. 23.

The correlation function is nearly independent of the beam energy, in contrast to single- and two-particle production cross sections, which depend more strongly on the beam energy. This can be seen in another way by inserting fit functions e, f and h from Table X into the definition of R (Eq. 2), resulting in $R \sim (1-x_t)^{-4.3} \left(\frac{m'}{2}\right)^{+8.7}$. The $(1-x_t)$ factor raises the 200 GeV data above the 400 GeV data by about a factor of 2 over the range of the data, consistent with Fig. 23.

At fixed pseudomass m' we see in Fig. 24 that R varies only slowly with the net transverse momentum $p_t' \equiv p_{t,1} - p_{t,2}$. There is no gross dependence of these features of R on species or charge combination.

The abundance of π, K and p in inclusive single hadron production (e.g. relative to all charged hadrons) can be used to define a "natural" abundance of pairs composed of these species as the product of the single inclusive abundances. If we divide the observed pair abundances by these "natural" abundances (evaluated at the appropriate p_t), we can obtain a measure of the strength of quantum number correlations. The correlation function R has exactly this property and is therefore well suited to this study.

Figure 25a shows R functions (in 2 mass ranges) for all species combinations for which we have sufficient statistical accuracy. The R functions have been divided by the correlation R for h^+h^- pairs (all hadrons regardless of identification) in order to facilitate comparison between the two mass regions shown. The full circle data points are as measured on Be. Only data in the "triple identification" momentum band have been included. The pair trigger for the data set of Fig. 25 was the coincidence of two single arm triggers (each with a p_t threshold), making the determination of R insensitive to trigger efficiencies. Systematic errors are estimated to be negligible and hence only statistical errors are shown.

Combinations involving only three "favored species", π^+, π^- and K^+, show a stronger correlation than the others. In addition we see some evidence that correlations between a favored species and an unfavored species are stronger than correlations between two unfavored species, as suggested by the (hand-drawn) broken lines representing the normalized correlation function in each of the three groups. We label this species dependence of R hence the "factorizing enhancement" because it appears to depend on the species observed in each arm separately. In addition we observe an enhancement in the number of K^+K^- and $\bar{p}p$ pairs, above other combinations containing K^- or $\bar{p}$, at least in the low mass (4-6 GeV) region.

C) Extrapolation to Nucleon Target

Nuclear size effects have been ignored so far. The CP group has shown[8] that the cross section per nucleon for inclusive hadron production at large p_t is enhanced in nuclear targets. We have published data[2] on the nuclear enhancement of hadron pair production. Figure 26 summarizes these findings. The nuclear enhancement of pair production depends very little on the pseudo-mass m' and becomes significant only for very asymmetric pairs, when e.g. $p_{t,1} >> p_{t,2}$. Extrapolation of the data on R to a "nucleus" of nucleon number 1 (not the same as a proton) is accomplished by multiplying the R values by

$$F = A_{Be}^{-\alpha_p + \alpha_{s1} + \alpha_{s2}}$$

where A_{Be} is the nucleon number of Be (9.012), α_p is the exponent for pairs, assuming their production cross section depends on the nucleon number as $A^{\alpha p}$ (see Ref. 2) and α_{s1}, α_{s2} are the same exponents for single inclusive hadron production, evaluated at $p_{t,1}$ and $p_{t,2}$. Table IX shows our data published earlier[2] on nuclear enhancement as a function of species. Although these data are of limited statistical accuracy, we apply corrections wherever available (W target data were taken only for opposite charge pairs). The corrected correlation ratios are shown as open circles in Fig. 25a. The error flags are increased to allow for the uncertainty in the determination of the nuclear enhancement. Pairs containing π^+, π^- and K^+ continue to show stronger correlation than others. The R-ratios for K^+K^- and $\bar{p}p$ pairs, however, return to the level of the other combinations.

D) The Effect of Constituent k_t

The R function as defined in Eq. 2 compares the species composition of single hadrons and pairs at the same p_t ($\equiv m'/2$ for pairs). However, it has been suggested[16,17] that the transverse momentum generated in constituent scattering leading to large p_t inclusive single hadron production is augmented by about 1 GeV of additional transverse momentum Δp_t from the initial transverse momentum k_t of the quarks within the hadrons (see Fig. 27). Symmetric pair production is not biased by k_t because of symmetry. Therefore it might be more appropriate to define a modified correlation function

$$R' \equiv \frac{\sigma_{12}(p_{t,1}, p_{t,2})/\sigma_{in}}{\frac{\sigma_1(p_{t,1} + \Delta p_t)}{\sigma_{in}} \quad \frac{\sigma_2(p_{t,2} + \Delta p_t)}{\sigma_{in}}}$$

which compares pair production and single inclusive production at the same transverse momentum transfer of the constituent scattering process, rather than at the same transverse momentum of the observed hadrons. Since the species composition of large p_t hadrons depends on p_t, this function R' will differ from R, even after being normalized to $R'(h^+,h^-)$.

The species for which we find factorizing enhancement, i.e. π^+, π^- and K^+, are the mesons containing a valence quark from beam or target. Their inclusive single production cross sections are found to fall less steeply with increasing p_t than cross sections of K^-, p and $\bar{p}$. This can be seen from Fig. 28, which replots data from the CP group[8] as the species composition of positive and

negative hadrons. The boost due to constituent k_t causes single hadrons to reflect the species composition at a lower p_t than that of members of the corresponding pairs. Assuming an average Δp_t of 1 GeV, we calculate R' from R for the two mass bins shown, and plot the result in Fig. 25b (without increasing the relative error bars and without any corrections for nuclear effects). The corrections follow directly from the change in species/hadron composition with p_t (Fig. 28), and are, of course, model dependent in the choice of Δp_t. In the light of the uncertainties associated with these corrections we do not consider the remaining species dependence of the normalized R' values to be significant.

E) Discussion of Correlations

The meaning of R, the correlation function, may be clarified by considering a very crude picture in which large p_t single hadrons are always made in pairs of equal and opposite p_t. The observed pair cross section into a sufficiently large acceptance would then equal the single hadron cross section. As a consequence, R would behave like the inverse of the single hadron production cross section at $p_t = m'/2$. The single hadron cross

section falls roughly like $e^{-3.5\ p_t}$ in the range of our data. This would lead to an R function proportional to $e^{+3.5\ p_t}$ or $e^{+(3.5/2)m'}$ for symmetric pairs. In Fig. 23, R rises exponentially with a slope of 1.4, which is only slightly flatter than the "maximum correlation" limit in this crude picture. The absolute value of this maximum R depends on the size of the acceptance needed to detect the second hadron, and is therefore model dependent.

The same comparison can be made in a more precise way by relating our R function to dn/dx_e, the differential conditional probability to find an "away" hadron with a transverse momentum $p_{t,2} \equiv x_e \cdot p_{t,1}$ opposite a trigger hadron with transverse momentum $p_{t,1}$ in a given solid angle $\Delta\Omega$. Simple quark scattering models predict that the away side multiplicity dn/dx_e will scale, i.e. be independent of the trigger transverse momentum in the p_t region where hard scattering dominates. In a previous paper[3] we have shown that for $(p_{t,1} + p_{t,2}) > 5.6$ GeV, dn/dx_e approximately scales. If σ_{12} denotes the partial pair cross section accepted by our apparatus, then

$$\frac{dn}{dx_e} = \frac{\dfrac{d^2\sigma_{12}}{dp_{t,1}dx_e}}{\dfrac{d\sigma_1}{dp_{t,1}}} = p_{t,1}\,\frac{\dfrac{d^2\sigma_{12}}{dp_{t,1}dp_{t,2}}}{\dfrac{d\sigma_1}{dp_{t,1}}}$$

and

$$R = \frac{\sigma_{in}\,\dfrac{d^2\sigma_{12}}{dp_{t,1}dp_{t,2}}}{\dfrac{d\sigma_1}{dp_{t,1}}\;\dfrac{d\sigma_2}{dp_{t,2}}}$$

so that

$$\frac{dn}{dx_e} = p_{t,1}\,\frac{R}{\sigma_{in}}\,\frac{d\sigma_2}{dp_{t,2}}$$

where

$$d\sigma_2/dp_{t,2} = p_{t,2}\;(E_2\; d^3\sigma/dp_2{}^3)\;A_{max}$$

is the relevant production cross section into the acceptance A_{max}, arbitrarily defined as the maximum value of the acceptance $A(p_t)$ as used in Section II E, independent of $p_{t,2}$. We see from this relation that x_e scaling implies (up to the factor $p_{t,1}$) the cancellation of the drop in single inclusive production cross sections with p_t by

the simultaneous rise in R. Qualitatively, the resulting similarity of the p_t dependence of single hadron- and pair production cross sections is an indication that "all singles are made as part of a pair" (maximum correlation), or, at least, by the same mechanism. In Fig. 29 we plot $E\,d^3\sigma/dp^3$, R and dn/dx_e vs. p_t,1 for symmetric pairs ($p_{t,1} \simeq p_{t,2} \simeq m'/2$). x_e-scaling is evident, giving support to the constituent scattering picture.

Constituent scattering models can be classified into two groups according to whether or not flavor is exchanged in the dominant interaction. Since gluons do not carry flavor, models based on elastic quark and gluon scattering[16,17] imply that there should be essentially no quantum number correlations between two hadrons produced at high p_t on opposite sides of an interaction (R should be independent of species). Other models, such as the constituent interchange model[18] (CIM), which invoke flavor exchange, allow such correlations to exist. Consider as an example the CIM in its naive form. This model, devised to explain the p_t^{-8} behavior seen in single pion production, takes as the basic process the interaction of a single quark with a "diquark", which may or may not be a meson, but pre-exists in one of the colliding hadrons. In the final state there is a quark (jet) on one side, a large p_t meson on the other, both having about the same magnitude of p_t. Several hadrons share the p_t of the jet, so usually none of them has large p_t by itself. The meson appears with large p_t. If this process occurs, it can make a strong contribution to single large p_t hadron production without becoming important for pair production (note that

the large ratio of jet/single production cross sections measured by other experiments[16] already argues against such a model). The R function is essentially the ratio of pair production over the product of the singles production cross sections. For those species pre-existing as diquarks in the hadron, i.e. for the "favored species" containing valence quarks of the nucleon (π^+, π^-, K^+) one would expect an increase in single hadron production, resulting in lower R functions. Although we do observe quantum number correlations in our uncorrected Be data, we find that, contrary to the above expectations of the CIM model, the R functions are higher for the favored species than for the others. Furthermore the observed species dependence of the R functions is at least qualitatively explained by other effects (nuclear enhancement and constituent k_t). Hence our results favor models which do not invoke flavor exchange.

F) Discussion of the Correlation Data in the Constituent Scattering Model (CSM)

1. The Model

Constituent scattering (see e.g. Ref. 16, 17 and 18) is believed to be a relevant description of the processes leading to large p_t single hadrons and pairs. In such models, constituents from each hadron (quarks, gluons, ...) collide and, upon leaving the interaction region, each gives rise to a jet of particles which "transports" the net color carried in each quark or other constituent back to the interaction volume where it can be neutralized.

Whatever may be the underlying dynamics of the production of high mass hadron pairs, the process can be divided into two parts. In the first of these, the primary interaction, there is a possibility that whatever happens to produce one of the hadrons may influence the production of the other. In the second part, the hadronic matter on one side is sufficiently removed from the hadrons on the other side that they should have no effect on each other. This second part is referred to as the "dressing" part of the process.

2) Primary Enhancement

An important question is whether the primary interaction is equally strong between quarks of all flavors, or indeed between all constituents important for hadronic interactions. Evidence for a quantum number dependence of the primary interactions could best be found in enhancements which depend on the species of both hadrons making up a pair. As an example, processes proceeding through $q\bar{q}$ annihilation, or gluon fusion to $q\bar{q}$, would always produce pairs of quarks with zero net flavor. Consequently, although all types of hadrons may be produced as the quarks emerge, one would expect to see enhanced K^- production opposite a K^+, and enhanced $\bar{p}$ production opposite a detected proton, especially if each of these has large p_t. After the data have been corrected for nuclear enhancement, no such effect is seen (Fig. 25a). The primary interaction shows no quantum number dependence.

3) Factorizing Enhancement

We have applied the term "Factorizing Enhancement" to the observed quantum number dependent correlation described in Section III B. At first sight one might think that species dependence of the jet development might lead to an enhancement of this type. However, in any model such as the CSM, in which single high p_t hadrons and pairs have the same origin, this species dependence of the decay function affects numerator and denominator of R in the same way and cancels out. It is therefore difficult to accommodate factorizing enhancement of the R function in the constituent scattering model, because single hadron- and pair-production have a common origin. Any such enhancement seen (after corrections) would point to a different origin of single hadrons and hadron pairs.

As can be seen from Fig. 25b, there appear to be no enhancements of any species over others after correction for nuclear target effects other than the consequences of the different trigger biases in single and pair measurements.

4) Nuclear Enhancements

Finally, we turn to the nuclear enhancements seen in the correlation function. The most striking effect is the enhancement of K^+K^- and $\bar{p}p$ pairs in nuclei. This effect is not understood at present, but may shed light on the process of hadron formation in nuclear matter. Since the effect depends

on both hadrons, its explanation is unlikely to be found in the nuclear development of the decay functions.

This effect aside, the correlation function R can be affected by nuclear enhancement in two ways, through the single inclusive hadron production cross sections in the denominator and through the two particle inclusive cross section in the numerator.

Extensive measurements of nuclear enhancement in single particle production have been made by the CP group,[8] yet a compelling explanation is still lacking. The CFS group has studied[2] nuclear enhancement in two particle production. Assuming nuclear enhancement depends on the nucleon number A as A^{α} (just as in the single production case) the values for α as a function of m' and p_t' are shown in Fig. 26 for zero charge hadron pairs (h^+h^-). These results can be summarized by stating that the exponent α does not depend on the pseudomass m' of the pair, but rises sharply when the momentum imbalance $|p_t'|$ gets very large.

We shall discuss these findings in the framework of the constituent scattering model, described above. Again we assume the primary interaction to be hard elastic quark-quark scattering (in the following discussion we consider quarks, but it should apply equally well to other kinds of constituents, if they exist). The primary interaction is assumed to be unaffected by the presence of nuclear matter, but the dressing function, describing the transition from a large p_t quark to a hadron jet, is assumed to be modified if the transition takes place in nuclear matter.

If we ignore its quark- or hadron- species dependence, the dressing function depends in general on only two variables, p_{quark} and $z \equiv \frac{p_{hadron}}{p_{quark}}$. Explicit calculations[16,17,19] show that the z values of single large p_t hadron (and, presumably, high mass symmetric pair) production are rather high and cluster around 0.8, independent of p_{quark}. The quark transverse momentum p_{quark} is therefore roughly proportional to m' in symmetric hadron pair production. Since the nuclear enhancement does not depend on m' we conclude that it does not depend on p_{quark}.

On the other hand, the nuclear enhancement effect rises with p_t' and is therefore consistent with being caused by the presence of low z (below 0.25) hadrons. In the constituent scattering model very asymmetric pairs originate from large p_t primary interactions where one of the observed hadrons emerged with a small momentum fraction z_{low} (z_{low} is less than the ratio of the hadron momenta of the pair), while the other hadron had a momentum close to that of the quark ($z_{high} \approx 1$). The strong nuclear enhancement seen in very asymmetric pair production hence may be traced to the z dependence of the dressing function.

Let us go one step beyond these rather direct consequences of experimental data and the constituent scattering model and try to understand why the dressing function might be enhanced by surrounding nuclear matter at low z-values, but not at high ones. To this end we need a more detailed understanding of the process which turns a pair of high p_t quarks

into two hadron jets. As the two quarks separate after their violent elastic collision, an energetic field is set up by the color charges of the quarks. The field energy rises (linearly?) with separation, until enough is available to create another quark-antiquark pair. This pair will be made with a (vector) momentum distribution centered about zero in the c.m. system of the original quarks. The original quarks continue to speed away from the new pair, until sufficient field energy has built up on each side to make another pair. Each of these pairs will have its momentum distribution centered about zero in a different system, i.e. the c.m. system of one of the original quarks and one of the newly made ones, and will therefore tend to be of higher p_t in the laboratory frame. The process continues, with the pairs created later in the chain having higher and higher p_t. This is shown schematically in Fig. 30, which is based on material by D. Duke and H. Miettinen.[20]

In this description, the slow hadrons, i.e., those at low z, are made early in the process, while the fast ones are made later, when the original quarks have already separated substantially. It is even possible to estimate the final separation of the original quarks at the time when the process stops. This separation is the product of the number of $\bar{q}q$ pairs made ($\simeq$ the number of hadrons made) and the average separation between those pairs. We can estimate the number of $\bar{q}q$ pairs made from the observation that the number of additional particles opposite a large p_t pion increases roughly

linearly with p_t at the rate of one extra particle for each GeV of transverse momentum[12] such that e.g. a p_t = 4 GeV hadron will have on average four additional ("jet") particles on the opposite side (which has a typical, unbiased jet). The separation between quarks at the time when a new pair is created must be somewhat larger than the diameter of a hadron, since the quarks within hadrons can separate easily to such distances without pair creation. We find then that the p_t = 4 GeV hadron in our example is made a distance of 4 to 8 fm from the point where the primary constituent scattering took place, a distance comparable to the diameter of a large nucleus.

Hence this leading p_t = 4 GeV hadron may be made after the original quark has left the region of nuclear matter; hadrons made early in the jet development, on the contrary, which have a small momentum fraction z, will be made inside the nucleus.

This may explain why low z hadrons suffer nuclear effects, while high z hadrons are not affected. However, the details of hadron formation in nuclear matter are unknown and the enhancement cannot be predicted in detail. The nuclear enhancement observed in single large p_t hadron production does not follow naturally from the ideas exposed above, while the absence of nuclear enhancement in dimuon production[21] at large mass is understood since no jet formation is involved.

G) Summary

The correlation function R is found to depend weakly on the pair transverse momentum p_t', and to rise sharply (like an

exponential or a power law) with increasing pseudomass m'. The s-dependence of the correlation function is weak over the 4-8 GeV m'-range common to the 200, 300 and 400 GeV data. The value of R rises only slightly more slowly than the "maximum correlation" limit, a conclusion also reached from the observed x_e-scaling behavior.

Normalized to the R-function for all hadron pairs (regardless of identification) the correlation function shows two types of quantum number dependence. Firstly, there is an increase in the number of K^+K^- and $\bar{p}p$ pairs, at least in the lower (4-6 GeV) m' region. This is a consequence of anomalous nuclear enhancement in the Be target. The origin of this enhancement remains largely unexplained, although a possible explanation of the p_t' dependence of nuclear enhancement is proposed. Secondly, the normalized correlation function is larger for pairs containing π^+, π^-, or K^+ (the mesons containing valence quarks of the colliding nucleons). It is shown that this "factorizing enhancement" may be explained by the p_t dependence of the species ratios and the trigger bias in single inclusive hadron production resulting from the motion of the constituents inside the colliding nucleons.

IV. INVARIANT TWO PARTICLE CROSS SECTIONS

A) Definitions

In discussing our resonance search[1] we have presented cross sections for the production of hadron pairs of mass m, calculating the acceptance under the assumption that an intermediate state of

mass m was formed which subsequently decayed isotropically in its rest frame. This artificial assumption implies the equality of the transverse momentum distributions in the scattering plane (component p_t') and normal to the scattering plane (component p_{out}), in contradiction to large p_t dihadron production data (compare the wide p_t' distributions in Fig. 31 with e.g. the p_{out} sample shown in Fig. 8).

As an alternate, and model independent, way of presenting our pair production data we compute the cross section density in momentum space near $y_1 \simeq y_2 \simeq 0$ and $p_{out} \equiv p_{y1} + p_{y2} \simeq 0$. We form the following invariant two particle cross section:

$$S \equiv E_1 E_2 \frac{d^6\sigma}{dp_1^3 \, dp_2^3} \Bigg|_{\substack{y_1 \simeq y_2 \simeq 0 \\ p_{out} \simeq 0}}$$

Using the single particle invariant acceptances A_1, A_2 as defined earlier, we can express S in terms of the number of observed pair events N_{12} with $p_{t,1}$ and $p_{t,2}$ as

$$S = \frac{d^2N_{12}/dp_{t,1}\, dp_{t,2}}{L \cdot A_1 \cdot p_{t,1} \cdot A_2 \cdot p_{t,2}} \quad .$$

where L is the integrated luminosity. We assume that the p_{out} distributions and the rapidity distributions are flat and uncorrelated within our acceptance.

Note that the correlation function R and the invariant two particle cross section S have nearly the same p_t' dependence, because the product of single hadron cross sections in the denominator of R is approximately constant at fixed m' due to their nearly exponential shape.

B) p_t' Dependence of the Two Particle Cross Section

Data for h^+h^-, $\pi^+\pi^-$, π^+K^-, $K^+\pi^-$ and $p\pi^-$ pairs are shown in Figs. 31 and 32. We see that, in general, the dependence of S on the transverse momentum p_t' of the hadron pair is weak. The data in these figures are quoted per Be nucleus. If we assume a nuclear enhancement of the form A^α, we may parameterize our result[2] for h^+h^- pairs as $\alpha = 0.98 + (p_t')^2/40\ GeV^2$. Since there is no significant dependence on the pseudomass $m' \equiv p_{t,1} + p_{t,2}$, all data points, if expressed per nucleon, would be multiplied by the same function $A^{-\alpha(p_t')}$, which drops as p_t' increases. This function is shown as a dashed line in Fig. 31.

The solid lines in Fig. 32 resulted from calculations by the Bielefeld [19] group. The predictions, normalized to inclusive single pion production data, have been divided by a common factor of 3 to match our high mass pion pair data and are then in rough agreement with all data points. The low rate of hadron pair production seen in our experiment was an important factor in a recent

theoretical re-evaluation [17,22] of the constituent scattering model.

It is natural to compare the p_t' spectra at fixed pseudomass m' to the p_t' spectra at fixed mass, shown in Ref. 1 and Fig. 33. The average value of $|p_t'|$ had been found in that reference to be proportional to the mass. This proportionality is equally well described by a flat p_t' distribution at constant pseudomass $m' \equiv p_{t,1} + p_{t,2} \simeq \sqrt{m^2 + p_t'^2}$, as seen by the lines in Fig. 33. In the constituent scattering model the mass of the hadron pair, of course, has no physical importance.

C) Scaling Properties of Symmetric Hadron Pair Production

Inclusive single pion production in the p_t range from about 2 to 6 GeV/c at 90^o in the c.m. system can be parameterized (see Fig. 19 and Table X) as

$$E \frac{d^3\sigma}{dp^3} = p_t^k \, f(x_t), \text{ where } x_t \equiv \frac{2\,p_t}{\sqrt{s}} \text{ and } k \simeq -8.5$$

Field theories based on single gluon exchange between the interacting quarks, or simply dimensional analysis, predict k to be 4 (a value approached by experimental data[23] at much higher p_t). R. D. Field has argued[17,22] that the observed power k = -8 may be due to a combination of effects and that the fundamental k = -4 behavior may become evident at larger values of p_t than currently accessible to experiment. He suggested that roughly two powers of p_t are due to the internal motion of the constituents inside the colliding hadrons while two more powers of p_t are a consequence of various

scale breaking effects expected in QCD. The transverse momentum of the internal motion (k_t) adds vectorially to the transverse momentum exchanged between the colliding constitutents, increasing the observed p_t for some events, decreasing it for others. The net effect of this k_t "smearing" is a rise in cross section proportional to the second derivative of the cross section versus p_t. This increase is strongest at low p_t, thus steepening the cross section as a function of p_t. If not taken fully into account, it will lead to an overestimation of the basic scattering cross section as extracted from single hadron production, which in turn leads to an overestimation of pair production where this enhancement is smaller or absent.

In the QCD-parton model[17,22] (QPM) pair production back-to-back at 90^o in the c.m. system proceeds in a way similar to inclusive single hadron production. However, for symmetric pairs smearing should have a negligible effect. (Whenever p_t on one side is increased, it decreases on the other, keeping m' and hence the cross section S unchanged as seen, e.g., in Fig. 31). Field therefore suggested studying symmetric pairs, produced with beams of different energy. Dimensional analysis suggests a dependence p_t^{-6} for our form of the two particle invariant cross section (for symmetric pair production we define $p_t \equiv m'/2$). Various QCD effects, just as in the case of single inclusive production, should steepen this dependence to p_t^{-8}. Smearing corrections should be negligible, and therefore roughly the same p_t power law is expected[22] for single and two

particle inclusive production. The quantity $\Delta k \equiv k_{\pi^+\pi^-} - 1/2\ (k_{\pi^+} + k_{\pi^-})$ is expected to be approximatley zero in the QPM model; note that Δk is insensitive to overall normalization errors.

The dimensionless variable x_t is generalized for pairs to be defined as $x_t \equiv \frac{p_{t,1} + p_{t,2}}{\sqrt{s}} = \frac{m'}{\sqrt{s}}$. Figures 34 and 35 show our 200, 300 and 400 GeV data for the production of symmetric h^+h^- and $\pi^+\pi^-$ pairs as a graph of S versus x_t for $|p_t'| \leq 1.1$ GeV. The data at all three energies are well described by scaling fits. Table X lists the parameters of the best fits in two x_t ranges.

Fits g and h are shown as lines in Figs. 34 and 35.
They describe the data well at all three energies. The power k of p_t is roughly the same for fits to all data points and for fits restricted to $x_t > 0.24$, where data exist at all three energies. Systematic errors, except for the normalization errors, have been added to the statistical errors of the data points in quadrature. The effect of these systematic errors is, however, not fully reflected in the quoted fit errors since they are correlated for neighboring data points. We estimate the effect of the imperfect knowledge of relative efficiencies and normalizations to be 0.14,0.18 and 0.12 of the cross sections for single hadrons, pairs and their ratio, in that order, corresponding to an error in k of 0.4, 0.5 and 0.4 units respectively. Together with the fit errors, we estimate the total error on k as ±0.5 units for single hadrons, ±0.6 units for pairs and ±0.5 units for the error of Δk.

The fit parameters listed in Table X show that the power k of p_t for pairs agrees with the average of the powers for single inclusive production. Above $x_t = 0.24$ we find for $\pi^+\pi^-$ that
$\Delta k = +0.2 \pm 0.5$ for the B_e data

and $\Delta k = +0.5 \pm 0.5$ for the nucleon analysis. At these x_t values where we have data at all three energies, it is possible to read off the k parameter from the cross section ratios at common x_t, but different beam energies. The b parameter describes the shape of the x_t distributions. Correspondingly there is little correlation between the fit values for b and k. Below $x_t = 0.24$ we have only 400 GeV data (p_t is too low for scaling fits at the other two energies) and therefore b and k become strongly correlated. It is known[8] that scaling fits to single inclusive hadron production begin to work in fact only above $p_t = 3$ GeV. The fits beginning at $x_t = 0.17$ ($p_t = 2.3$ GeV at 400 GeV beam) take advantage of the correlation between the b and k parameters to follow the data into the non-scaling region. Only the fits above $x_t = .24$ should therefore be considered for this investigation of scaling in symmetric pair production. In this x_t range the data are in agreement with $\Delta k = 0$ and with the expectations of the modified hard scattering model with internal parton k_t smearing.

The QPM model[17,22] describes the p_t dependence of both our single pion and our pion pair data if the quark motion is taken to be of the magnitude deduced from the transverse momentum distribution of hadronically produced muon pairs.[21] In both this and the μ pair experiment the large value for $k_t \approx 1$ GeV may be due to either primordial quark motion, or to gluons participating in the scattering process, or both.

Note that the common scaling form is not just a consequence of dimensional arguments. Simple dimensional considerations fail to

predict the right power behavior in our p_t range. The fact that symmetric pair production follows the same scaling form as single inclusive production thus lends significant support to the hypothesis of a common origin of single hadrons and pairs.

The spectrometer polar angle acceptance is fixed in the laboratory and is centered about $\theta = 90^o$ (c.m. system) for 400 GeV beam momentum (see Table IV). At smaller beam momentum the polar angle acceptance moves forward in the c.m. system, and as a result we are comparing two-particle invariant cross sections taken at different rapidity values. Figure 7 shows typical y_{cm} acceptances (they are similar for single particle and pair production) for the three beam momenta. If the cross sections S were to fall rapidly with y_{cm}, then the 200 GeV data would be too low, and the p_t power would need a correction making it steeper. The y-acceptance of this experiment is too narrow to extract the y-dependence of S reliably. A large drop of S with y_{cm} is, however, not expected theoretically[24] and it is unlikely that the power of p_t is much affected. We have also verified, by comparing our angular distributions from Be and W targets, that also within 10% accuracy, no y-dependence of σ_p or σ_s is introduced by the nuclear targets. The determination of Δk is sensitive only to the difference of the y distributions of single and pair cross sections. A 10% difference in cross section at 200 or 400 GeV changes k by only 0.3 units.

Note that nuclear enhancement has been measured[2] to be small for symmetric hadron pairs at 400 GeV, but no measurements exist at 200 and 300 GeV.

In conclusion, it has been shown that symmetric two particle production cross sections can be remarkably well described by a p_t- and x_t- dependent scaling form similar to the one describing single particle inclusive production, lending weight to the idea of a common origin of the two processes. The value of the power k of p_t agrees well for single hadron production and for pair production, a result expected in the QPM model.

V. CONCLUSIONS

1) Two hadron correlations at large transverse momentum are extremely strong, and serve as evidence that high mass hadron pair productions results dominantly from constituent scattering. This evidence takes three related forms:
   - The rise of R with m' is nearly maximal
   - dn/dx_e is nearly independent of m'
   - Scaling laws of the same form fit both symmetric pair production and singles production.
2) In the scaling form mentioned above, symmetric pair production and singles production exhibit approximately the same power of p_t, confirming the role and magnitude of k_t smearing as expressed in the QCD-parton model.
3) Once nuclear effects and constituent k_t are taken into consideration, we see no species dependence of the pair correlation. This observation is in accord with the QCD-parton model and appears damaging to models (such as the CIM) which invoke flavor exchange between constituents.

ACKNOWLEDGEMENTS

We would like to express our thanks and appreciation to the many people from Fermilab and the participating institutions that made this experiment possible. This includes in particular our

expert technicians K. Gray, K. Kephart, L. Lenzi, F. Pearsall, T. Reagan and J. Upton, as well as the dedicated and able crews of the Fermilab Proton Department and the Accelerator Division. We would also like to thank M. Luba for the typing of this manuscript. Much help and expertise was contributed by T. Yamanouchi. Many of us thank the Fermilab for hospitality during the several years of experimentation. Support by the people of the United States of America through the DOE and NSF is gratefully acknowledged.

REFERENCES

[1] R. D. Kephart et al., Phys. Rev. Lett. 39, 1440 (1977).

[2] R. L. McCarthy et al., Phys. Rev. Lett. 40, 213 (1978).

[3] R. J. Fisk et al., Phys. Rev. Lett. 40, 984 (1978).

[4] H. Jöstlein et al., Phys. Rev. Lett. 42, 146 (1979), R. J. Fisk, Thesis, State University of New York at Stony Brook, 1978 (unpublished).

[5] The values used were measured at Brookhaven National Laboratory by J. Hudis et al., Phys. Rev. 129, 434 (1963) and J. B. Cumming et al., Phys. Rev. C 14, 1554 (1976). A recent measurement at Fermilab by S. Baker et al. (unpublished) yielded 3.8 mb for ^{24}Na and 4.6 mb for ^{52}Mn production. If these new members were used, our cross sections would increase by about 10%. In order to maintain continuity with earlier Fermilab experiments we have used the BNL cross sections.

[6] M. Della Negra et al., Nucl. Phys. B 127 (1977) 1.

[7] B. C. Brown et al., Proceedings of the IEEE 1977 Nucl. Sci. Symposium, IEEE Transactions on Nucl. Sci. NS-25, 347 (1978).

[8] L. Kluberg et al., Phys. Rev. Lett. 38, 670 (1977). D. Antreasyan et al., Enrico Fermi Institute preprint EFI 78-29 and M. Shochet, private communication.

[9] Useful reviews are found in M. Della Negra, "Large Transverse Momentum Phenomena", Tutzing Conference (1976). P. Darriullat, "Large Transverse Momentum Hadronic Processes", Tbilisi talk (1976).

[10]Design report, in preparation.

[11]Made by the Eagle Convex Glass Company, P. O. Box 1340, Clarksburg, W. Virginia 26301.

[12]R. Kephart et al., Phys. Rev. D14, 2909 (1976).

[13]F. W. Busser et al., Nucl. Phys. B106, 1-30 (1976).

[14]G. Bellettini, Proc. XVI Int. Conf. on High Energy Collisions, Stony Brook (1973); S. R. Amendolia et al., Phys. Lett. 44B (1973), 313.

[15]R. Singer et al., Phys. Lett. 49B, 481 (1974).

[16]R. D. Field and R. P. Feynman, Phys. Rev. D15, 2590 (1977).
G. C. Fox, "Phenomenology of High p_t Scattering", CALT-68-573.
R. P. Feynman, R. D. Field and G. C. Fox, Nucl. Phys. B128, 1 (1977). Note that Ref. 17 revises some of the assumptions made in Ref. 16.

[17]R. D. Field, Phys. Rev. Lett. 40, 997 (1978).
R. P. Feynman et al., Caltech preprint CALT-68-651 (1978).

[18]R. Blankenbecler, S.J. Brodsky and J.F. Gunion, Phys. Rev. D18, 900 (1978) and referen-es therein.

[19]R. Baier, J. Cleymans, J. Engels and B. Petersson, private communication (see also Ref. 24).

[20]D. Duke and H. Miettinen, Fermilab 1978 "Academic Lecture Series" (unpublished.)

[21]D. C. Hom et al., Phys. Rev. Lett. 37, 1374 (1976).
J. K. Yoh et al., Phys. Rev. Lett. 41, 684 (1978).
D. M. Kaplan, Thesis, State University of New York at Stony Brook, 1978 (unpublished).

K. J. Anderson et al., paper submitted to the XIX Int. Conf. on High Energy Physics, Tokyo, Japan, 1978.

[22] R. D. Field, Caltech preprint CALT-68-688 (1978), and private communication.

Our definition of the two-particle invariant inclusive cross section differs from the one used in this reference by two powers of p_t; it also differs in dimension from our definition of the inclusive single particle cross section. Note that the predictions in this reference have been obtained by integrating over the complete "away side" jet (all azimuth angles ϕ), while our measurements are of the differential cross sections near $\Delta\phi = 180^{\circ}$; also the c.m. rapidity y has been kept zero for the above calculations. Recent calculations by R. D. Field (private communication) arrive, however, at the same conclusions due to a fortuitous cancellation of the effect of the ϕ-integration with the effect of a more careful representation of the p_t range of our data in the theoretical calculations.

[23] A.L. S. Angelis et al., Physics Letters 80B (1979)

[24]R. Baier et al., Nucl. Phys. B118, 139 (1977): rapidity distributions in this reference drop by less than 10% going from $y_{cm} = 0$ to $y_{cm} = 1$. The y distributions in Fig. 21 of the paper by Feynman, Field and Fox (Ref. 16) drop by about 15% going from $y_{cm} = 0$ to $y_{cm} = 0.4$, where the 200 GeV acceptance peaks; this causes a change of less than 0.5 units in the power k of p_t.

TABLE I

Running Conditions

Mass Range (GeV)	Intensity (protons/pulse)	Magnet Current (A)	Trigger* 50% Efficiency Points of PT in p_t (GeV)	MH in m' (GeV)	Full Particle ID Momentum Band (GeV)	Target	Beam Energy (GeV)	Intergrated Luminosity (= protons x Nuclei/cm^2) (10^{34} cm^{-2}) ++ and --	+-
4-5	4×10^9	961	1.8	3.1	22-39	Be	400	229	927
						W	400	-	6
5-6	7×10^9	1288	2.5	4.5	30-50	Be	200	1170	2600
						Be	300	5260	6440
						Be	400	3840	4690
						W	400	11	22
5-6 asymmetric	7×10^9	961	up: 1.8 down: 3.2	4.5	up: 22-39 down: 35-55	Be	300	6100	12800
						Be	400	1740	1790
						W	400	-	1050
6-10	2×10^{10}	961 or 1288	3.2	5.9	35-55	Be	400	16130	92600
						W	400	-	220

*PT designates the "p_t trigger", MH the "mass trigger".

TABLE II

Target Properties

Target Label	Width (cm)	Length (cm)	A	Density (gm/cm^3)	Absorption Length (cm)	Geometric Efficiency (average)	Fraction of beam interacting
Be 3	0.203	10.27	9.012	1.85	37.1	1.00	0.242
Be 7	0.022	10.27	9.012	1.85	37.1	0.7	0.17
W	0.041	1.275	183.85	19.3	9.85	0.95	0.109

TABLE III

N Calibration Constants

	Monitor counts N/ Secondary emission monitor counts$_8$SEM (SEM unit = 10^8 protons)	Effective[a] monitor cross section σ_N (cm^2/nucleus)
Be at 400 GeV	100.5 ± 5.0	(8.98 ± .60) 10^{-31}
Be at 300 GeV	96.0 ± 4.5	(8.58 ± .70) 10^{-31}
Be at 200 GeV	89.7 ± 4.5	(8.02 ± .60) 10^{-31}
W at 400 GeV	77.6 ± 4.0	(1.02 ± .07) 10^{-29}

a) No corrections have been made to σ_N for the absorption of secondaries, hence these cross sections are only valid for the target dimensions used here.

TABLE IV

Fiducial Volume

The two spectrometer arms were nearly identical. Arm averages are listed.

Limits on	Z-position (cm)	Limits from	Limits to
Production angles (lab system)			
$\tan \theta_x$ (horizontal projection)		0.0485	0.0945
$\tan \theta_y$ (vertical projection)		-0.0040	+0.0035
Production angles (c.m. system)			
θ_x for $\beta = 1$ particles at 200 GeV		53.2°	88.5°
300 GeV		63.0°	100.0°
400 GeV		70.6°	108.0°
Azimuth small θ side (rad)		-0.0824	+0.0721
large θ side (rad)		-0.0425	+0.0372
Projected x position at the target (cm)	0	-2.3	2.3
W - collimator y (cm)	676	-3.05	+2.24
Chamber 1 y (cm)	2416	+10.7	+49.8
Calorimeter entrance x (cm)	3655	-81.0	+86.6
y (cm)		+24.0	+91.7

TABLE V

Detector and Cut Efficiencies

	4-5 Gev	5-6 GeV	6-10 GeV
Scintillation counters	0.95	0.94	0.91
Chambers combined	0.997	0.995	0.992
M1 - requirement (only one of 13 angular ranges registered a track)	0.93	0.91	0.89
Single track requirement (off-line, after M1 - req)	0.997	0.993	0.989
Track reconstruction efficiency	0.97	0.96	0.96
Calorimeter F/p cut	(included in the trigger efficiency)		

The efficiencies listed are per spectrometer arm. The arms had nearly equal efficiency. The efficiencies were independent of p_t and mass.

Table VI

Rules Used to Determine the Systematic Errors

Quantity	Rule	Typical Contribution
Mass trigger efficiency	4% error in the threshold	10% or less, different for each point
Single track requirement (M1)	10% of the correction	2% uniformly
Single arm p_t triggers	4% error in the threshold	2% or less, (different for each point) when used for accidentals correction to mass trigger data; 10% or less effect on single particle cross sections
Acceptance calculation	Constant error equal to 5% of the maximum acceptance	5% uniformly
Decay probabilities	Negligible error	Neglected
Overall etticiencies	15% of the correction	3% uniformly
Accidentals correction (Error of B_{int})	+10%/-5% of B_{int}	15% at m' = 4 GeV, falling rapidly with increasing mass
Normalization	±15% constant	±15%, depends on beam energy and running mode
Total:	Add contributions in quadrature	15% uniformly plus 10% point-t point (typically)

Note that some normalized quantities are insensitive to uniform errors.

TABLE VII

Properties of the Cerenkov Counters

	Mass Range (Running Mode)		
	4-5 GeV	5-6 GeV	Above 6 GeV
$\check{C}_1$ gas	He	He	He
(n-1) in $\check{C}_1$	37.2×10^{-6}	37.2×10^{-6}	37.2×10^{-6}
$\check{C}_2$ gas	N_2	42% Ne, 58% N_2	67% Ne, 33% N_2
(n-1) in $\check{C}_2$	286×10^{-6}	193×10^{-6}	140×10^{-6}
# Photoelectrons * (at $\beta = 1$)	$\check{C}_1$ 8.2	8.2	8.2
	$\check{C}_2$ 23	15	11.2
Triple identification band	22-39 GeV	30-50 GeV	34-56 GeV
Pion identification	16-56 GeV	16-56 GeV	16-56 GeV

* These numbers are based on test beam measurements of the phototube system actually used (conservatively derated as explained in the text) and are consistent with the inefficiency of less than 0.2% that was measured with electrons in the spectrometer system during data taking.

TABLE VIII

π, K, p Samples: Losses and Contaminations (%)

				Running Conditions for Mass Range 4-5 GeV	5-6 GeV	6-10 GeV
π:	losses:	$\check{C}1$ or $\check{C}2$ inefficiencies		0.4	0.2	0.2
	contam:	K's with C1	K^+	0.7	1.9	3.4
		accidentals	K^-	0.4	1.1	2.0
K:	losses:	$\check{C}1$ accidentals or $\check{C}2$ inefficiencies		2.2	5.4	9.8
	contam:	π's with $\check{C}1$	π^+	1.0	0.5	0.4
		inefficiencies	π^-	1.8	0.9	0.7
		P's with $\check{C}2$	p^+	3.1	6.9	10.1
		accidentals	$\bar{p}$	2.3	4.9	6.7
P:	losses:	$\check{C}1$ or $\check{C}2$	p^+	3.7	8.2	12.8
		accidentals	$\bar{p}$	5.6	11.9	17.1
	contam:	K's with $\check{C}2$	K^+	0.2	0.1	0.1
		inefficiencies	K^-	0.3	0.1	0.1

TABLE IX

	π^-	K^-	$\bar{P}$	h^-
π^+	0.99 ± 0.03	1.05 ± 0.09	1.29 ± 0.14	1.00 ± 0.03
	1.08 ± 0.11	1.37 ± 0.46	-	1.12 ± 0.08
K^+	0.98 ± 0.09	1.33 ± 0.17	-	1.05 ± 0.05
	-	-	-	1.24 ± 0.22
P	1.11 ± 0.07	1.58 ± 0.21	1.37 ± 0.13	1.16 ± 0.05
	-	-	-	1.14 ± 0.19
h^+	1.00 ± 0.02	1.11 ± 0.06	1.17 ± 0.07	1.01 ± 0.02
	1.15 ± 0.06	1.52 ± 0.20	1.41 ± 0.43	1.18 ± 0.04

The power α of the A dependence of the invariant dihadron production cross section is given as a function of particle species for p_t < 2.1 GeV/c (upper value) and for p_t > 2.1 GeV/c (lower value in each box). h^+ denotes all positive hadrons, h^- all negative hadrons.

TABLE X

Fits to Single Hadron and Symmetric Pair Invariant Cross Sections

$$E\frac{d^3\sigma}{dp^3} \text{ or } E_1E_2\frac{d^6\sigma}{dp_1^3\,dp_2^3} = A(1-x_t)^b\,p_t^k \quad \text{where } x_t = \frac{2p_t}{\sqrt{s}};$$

$$p_t \equiv \frac{m'}{2} \text{ for symmetric pairs}$$

		$x_t > 0.17$				$x_t > 0.24$			
Fit	Cross Section	A ($cm^2/GeV^2, cm^2/GeV^4$)	b	k	χ^2/D.F.	A($cm^2/GeV^2, cm^2/GeV^4$)	b	k	χ^2/D.F.
a.	Single π^+ (Be)	$(3.3\pm0.3)\times10^{-26}$	7.4±0.5	-8.0±0.1	82/40	$(5.5\pm1.5)\times10^{-26}$	6.1±0.8	-8.9±0.2	18/17
b.	(N)	$(4.4\pm0.4)\times10^{-27}$	7.4±0.5	-8.4±0.1	75/40	$(7.2\pm1.9)\times10^{-27}$	6.1±0.8	-9.2±0.2	17/17
c.	π^- (Be)	$(2.9\pm0.2)\times10^{-26}$	9.1±0.1	-7.5±0.1	44/40	$(4.7\pm1.4)\times10^{-26}$	8.1±0.8	-8.2±0.2	14/17
d.	(N)	$(3.9\pm0.3)\times10^{-27}$	9.1±0.1	-7.9±0.1	43/40	$(6.5\pm1.7)\times10^{-27}$	8.1±0.8	-8.6±0.3	14/17
e.	h^+ (Be)	$(13.0\pm0.7)\times10^{-26}$	8.3±0.1	-8.5±0.1	246/56	$(39.\pm5.\ )\times10^{-26}$	7.3±0.2	-9.5±0.1	54/33
f.	h^- (Be)	$(6.9\pm0.4)\times10^{-26}$	11.2±0.1	-7.6±0.1	120/56	$(16.\pm2.\ )\times10^{-26}$	10.7±0.2	-8.4±0.1	38/33
g.	Symmetric $\pi^+\pi^-$	$(1.6\pm0.3)\times10^{-28}$	12.8±0.6	-8.7±0.2	24/47	$(1.7\pm0.7)\times10^{-28}$	14.0±0.8	-8/4±-/2	16/29
h.	h^+h^-	$(6.7\pm0.4)\times10^{-28}$	13.0±0.4	-9.3±0.1	40/60	$(8.4\pm1.9)\times10^{-28}$	13.7±0.6	-9.2±0.2	34/42

Be = beryllium data. N = per nucleon, extrapolated to A=1, using $A^{\alpha(p_t)}$, with $\alpha(p_t)$ from Ref. 8. Systematic errors are listed in Table VI and have been added to the statistical errors of the data points before fitting, except for the normalization errors; these are estimated to contribute an error of ±0.5 units to k. Note that χ^2 values are affected by the non-scaling behavior of the data at low x_t, as well as by the addition of systematic errors.

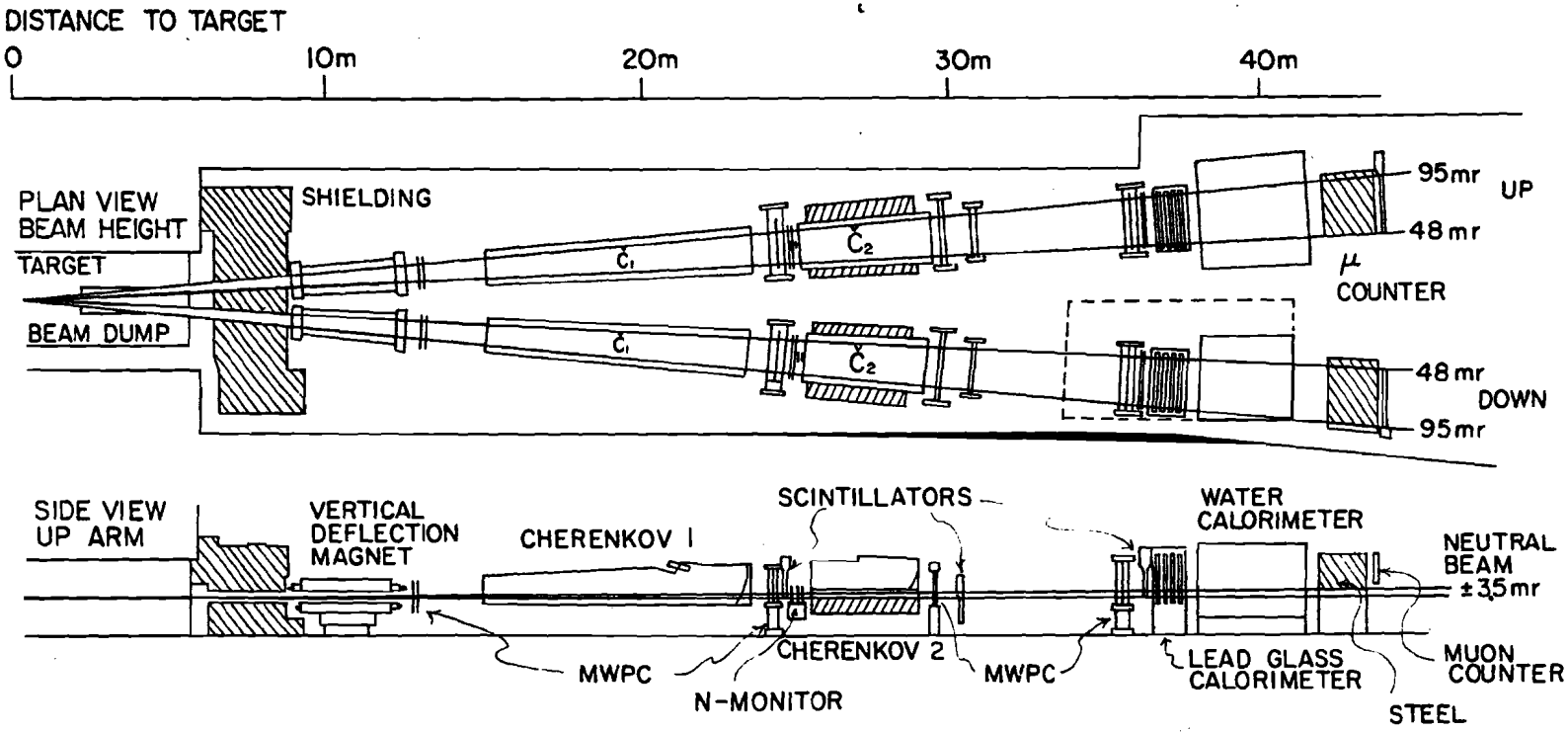

Fig. 1: Plan view of the experimental apparatus and elevation view of the up-arm.

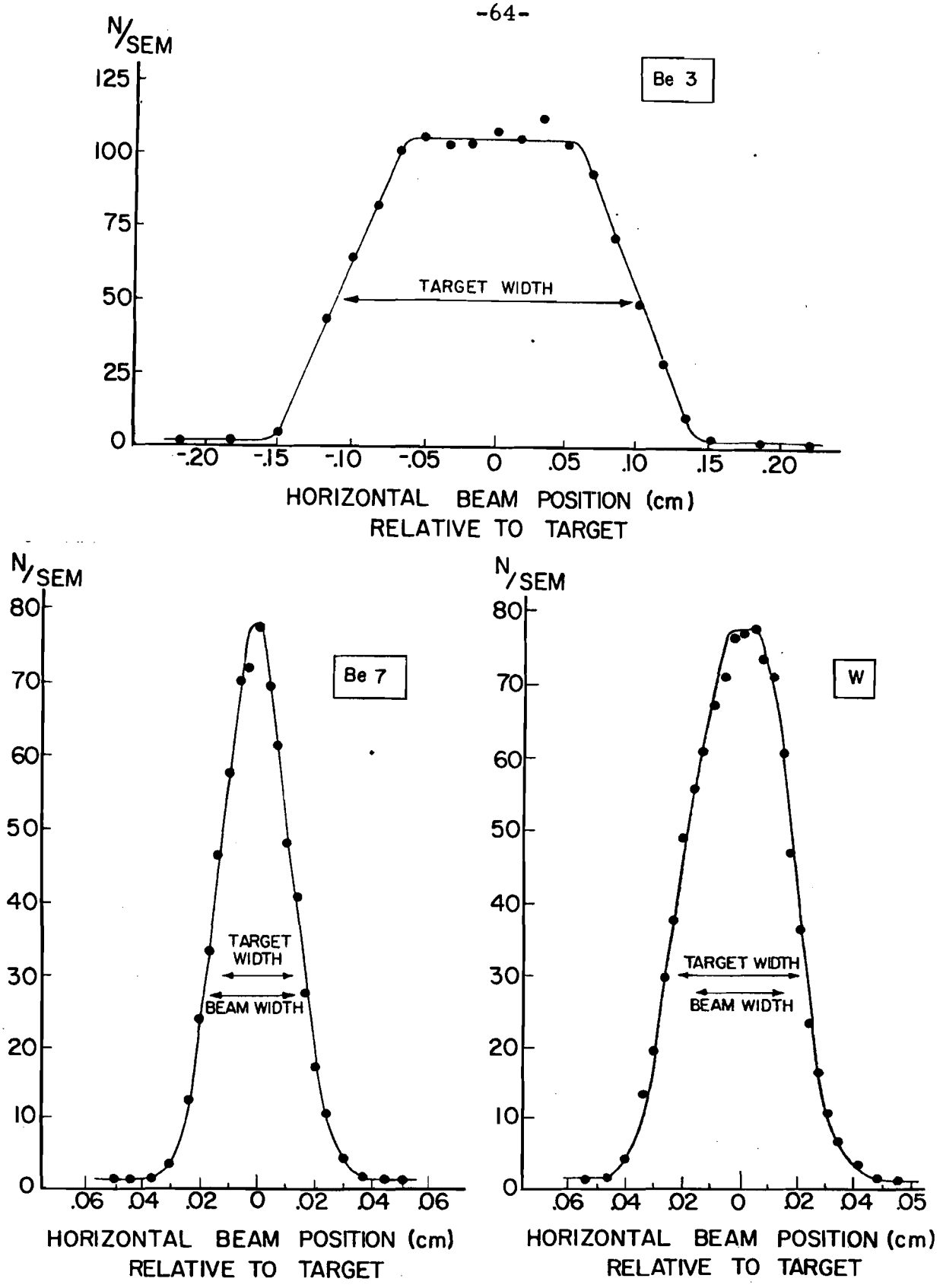

Fig. 2: Target scans used to measure geometric efficiencies and to obtain monitor constants. See Table II for target properties.

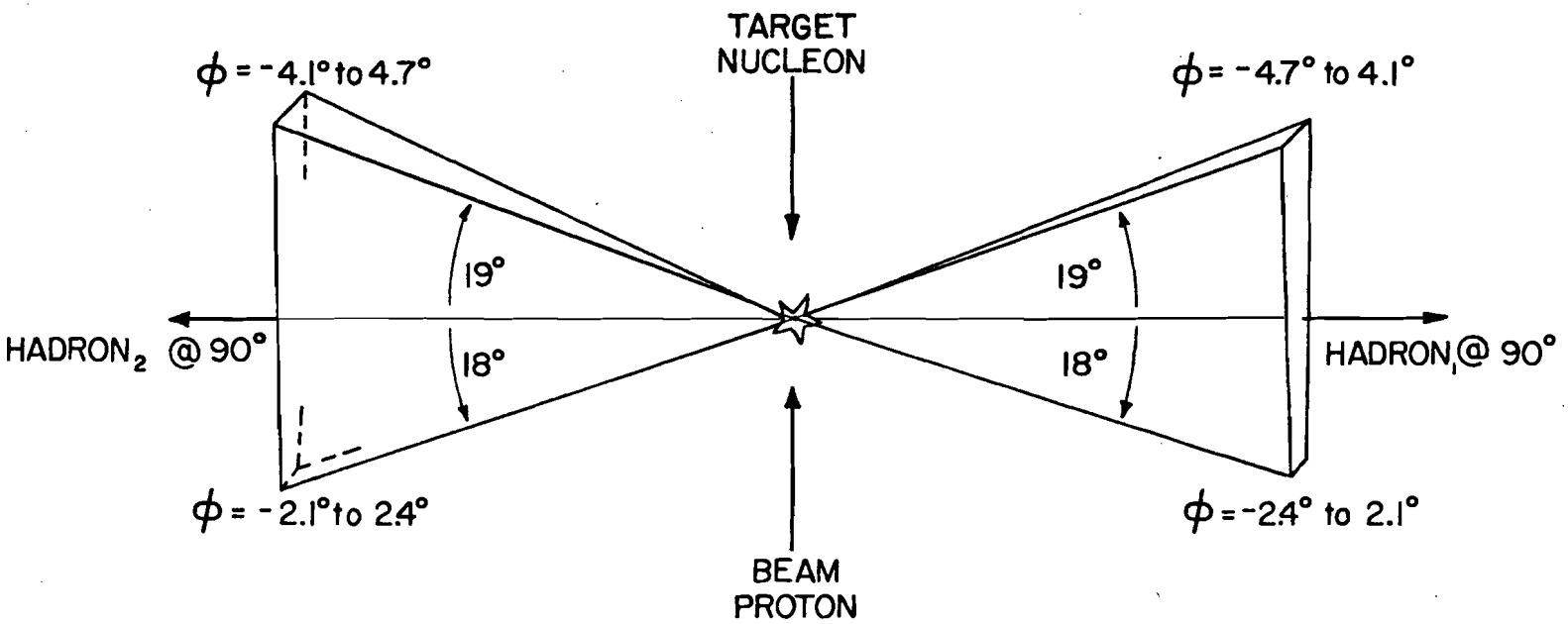

Fig. 3: The acceptance in the c.m. system for 400 GeV beam momentum, as seen from above.

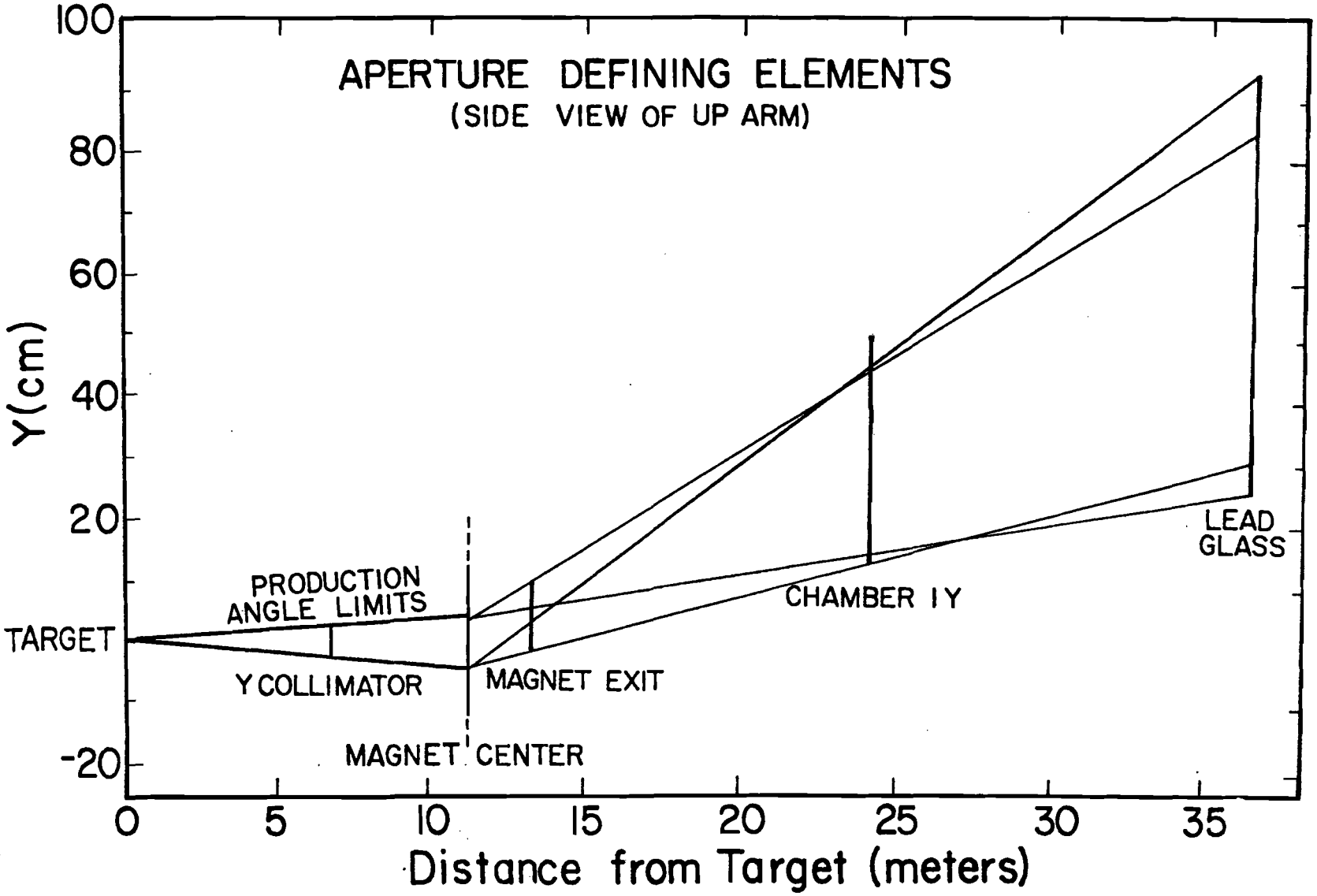

Fig. 4: Aperture defining elements. See Table IV for dimensions.

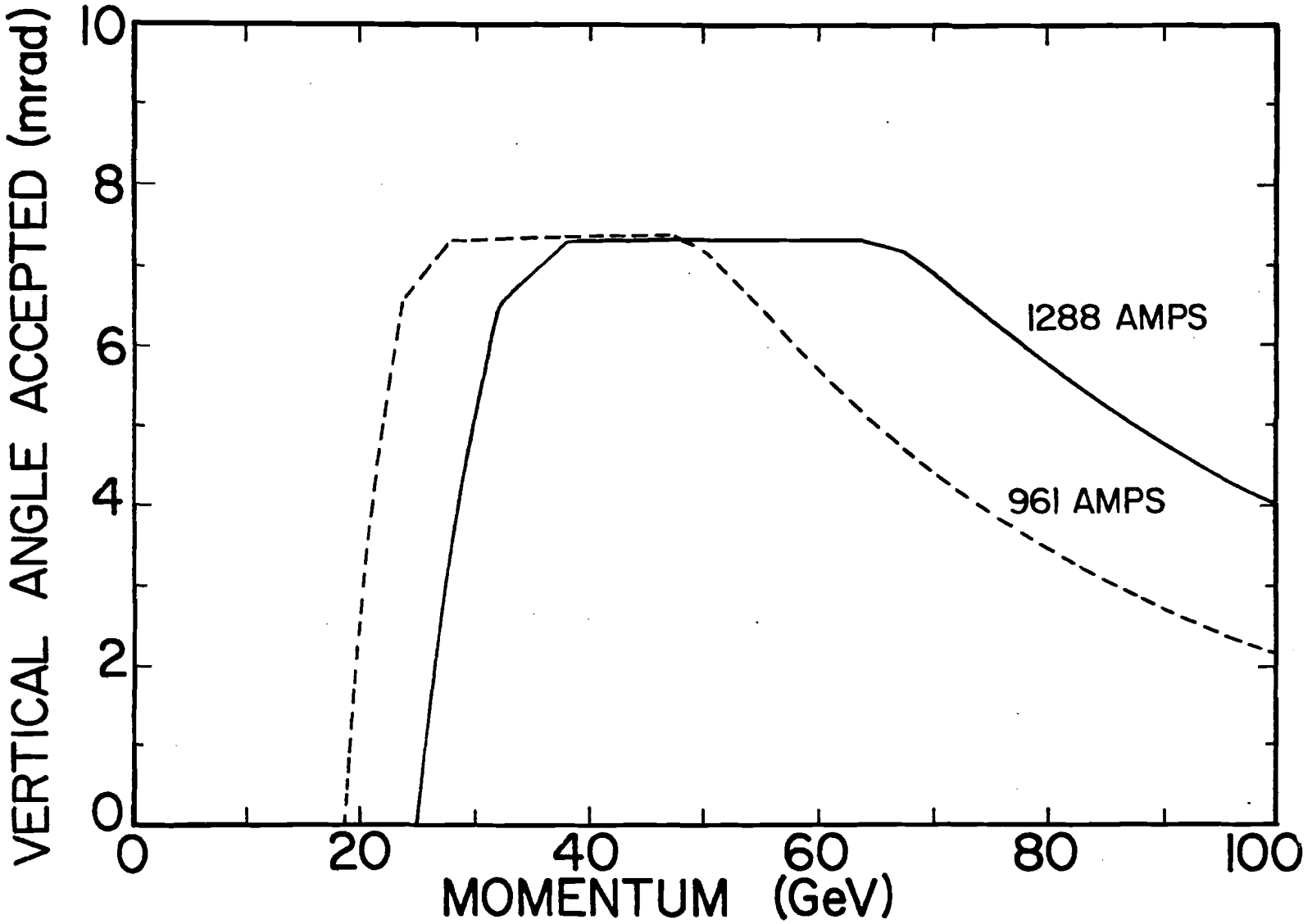

Fig. 5: Vertical angle accepted as a function of momentum. This angular acceptance is independent of the horizontal production angle.

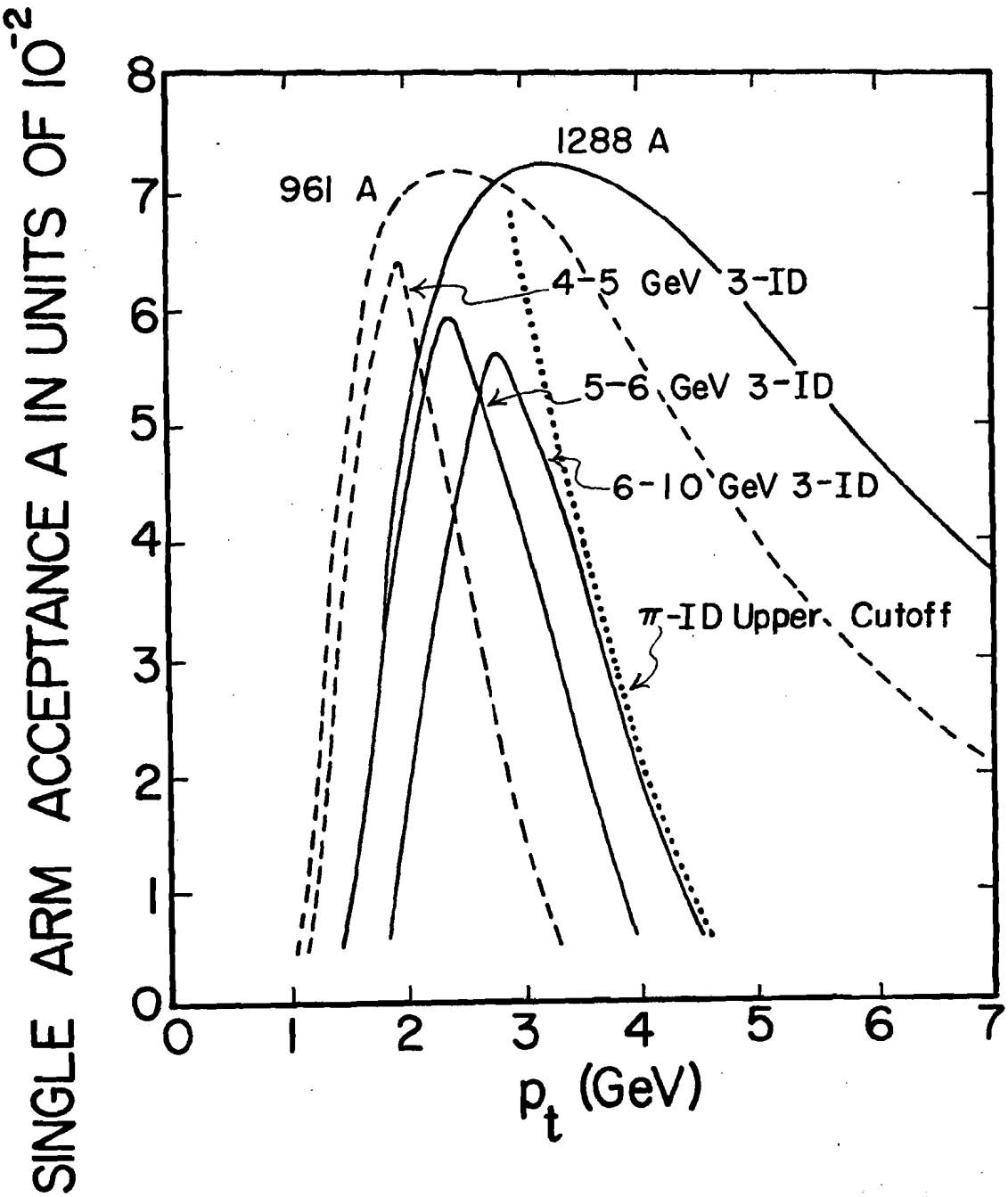

Fig. 6: The invariant single arm acceptance A as a function of p_t. The wide curves are for the spectrometer alone, the narrow ones apply if triple particle identification is required. Pions can be accepted and identified up to the dotted line (1288 A).

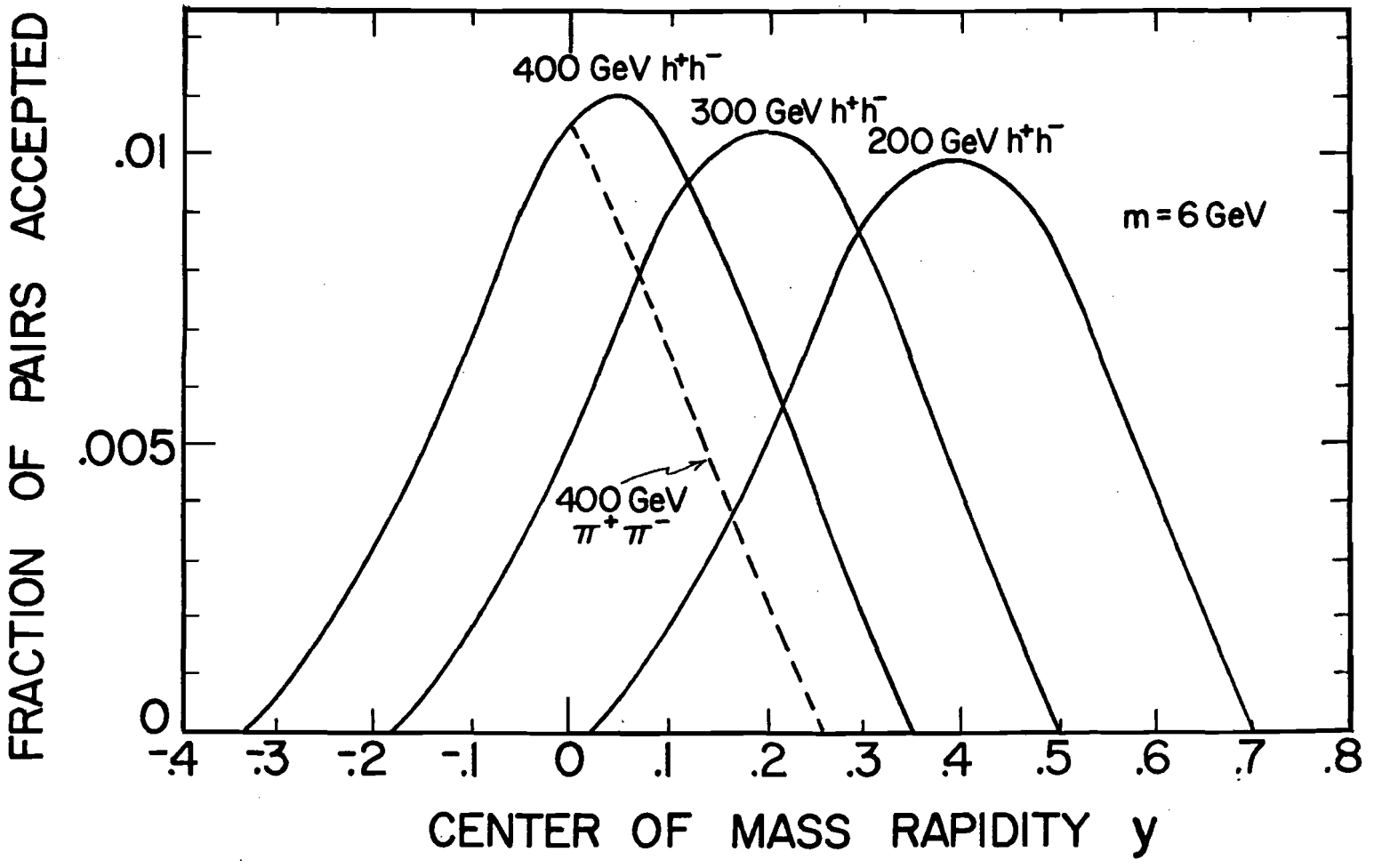

Fig. 7: Fraction of pairs with mass m = 6 GeV accepted, as a function of the c.m. rapidity y. The lines are for h^+h^- pairs. The mass dependence is weak. Single hadron acceptances follow a similar shape. Note the shift to the forward hemisphere as the beam momentum is lowered from 400 GeV. The calculation assumed an isotropic decay model, but the shape is approximately model independent.

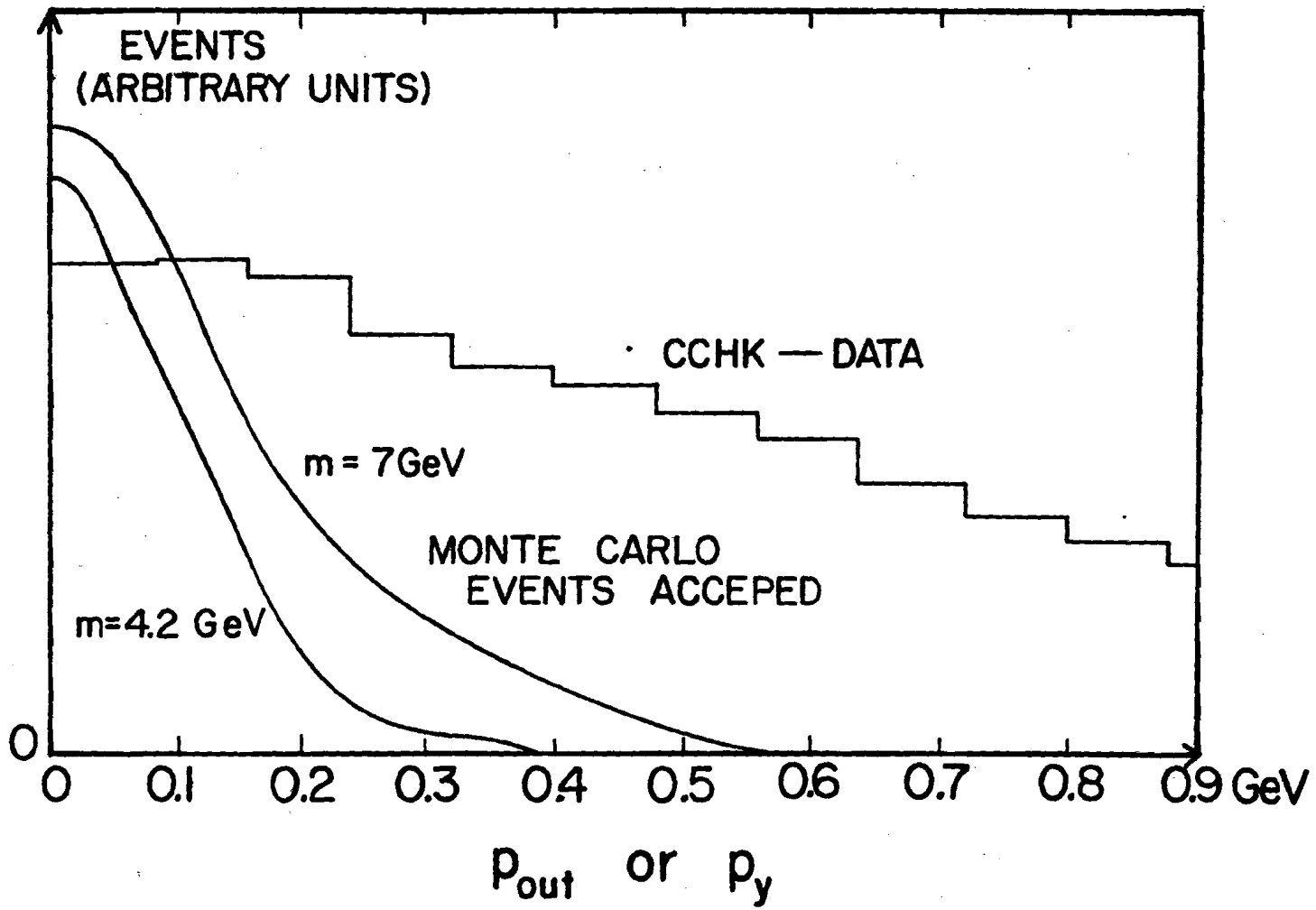

Fig. 8: Distribution of Monte Carlo generated events (isotropic decay model) accepted by our apparatus (smooth lines), together with a data sample from the CCHK collaboration (Ref. 6). The data are reasonably flat within our acceptance. The variable p_y used here differs negligibly from p_{out} used in Ref. 6.

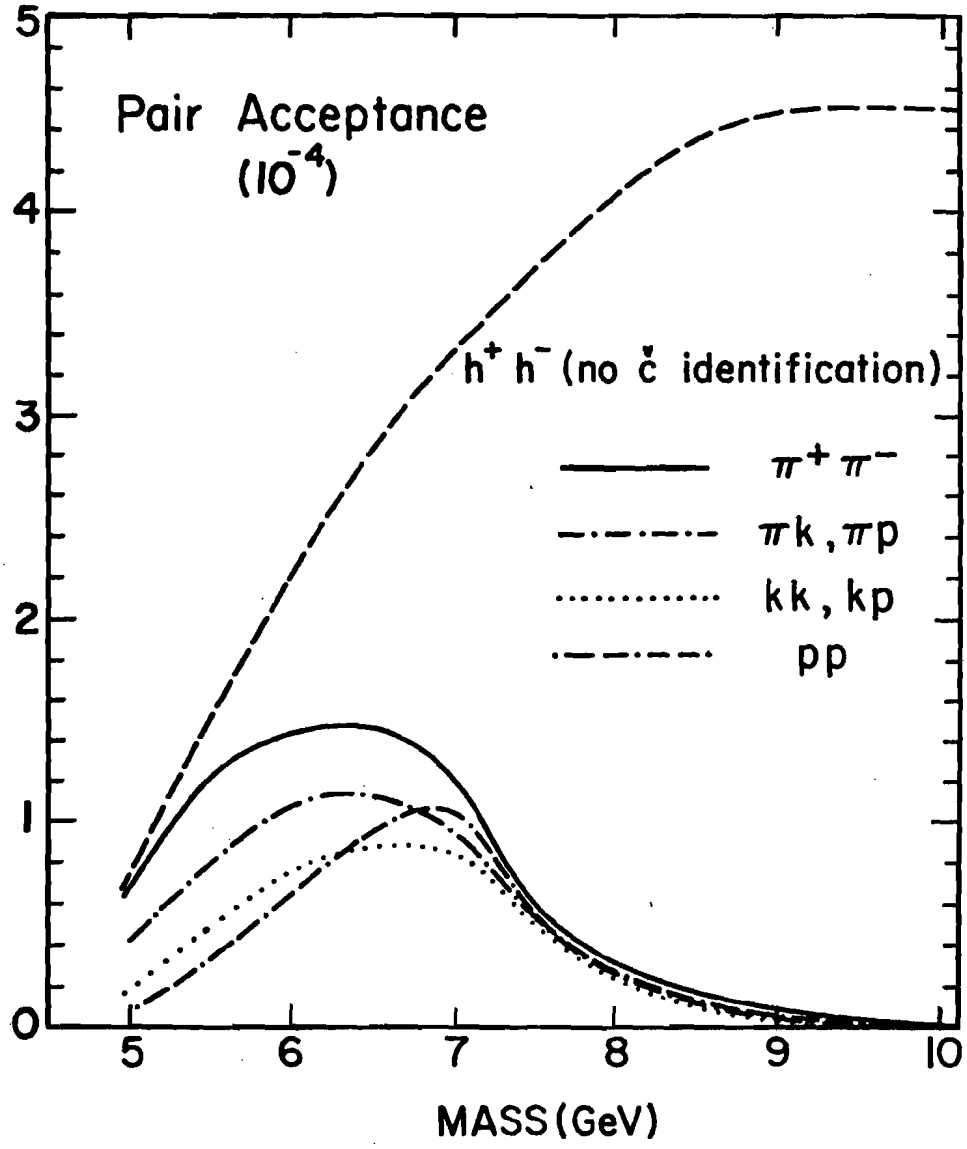

Fig. 9: Fraction of pairs accepted, calculated for the isotropic decay model. The requirement of particle identification cuts off the acceptance at high mass.

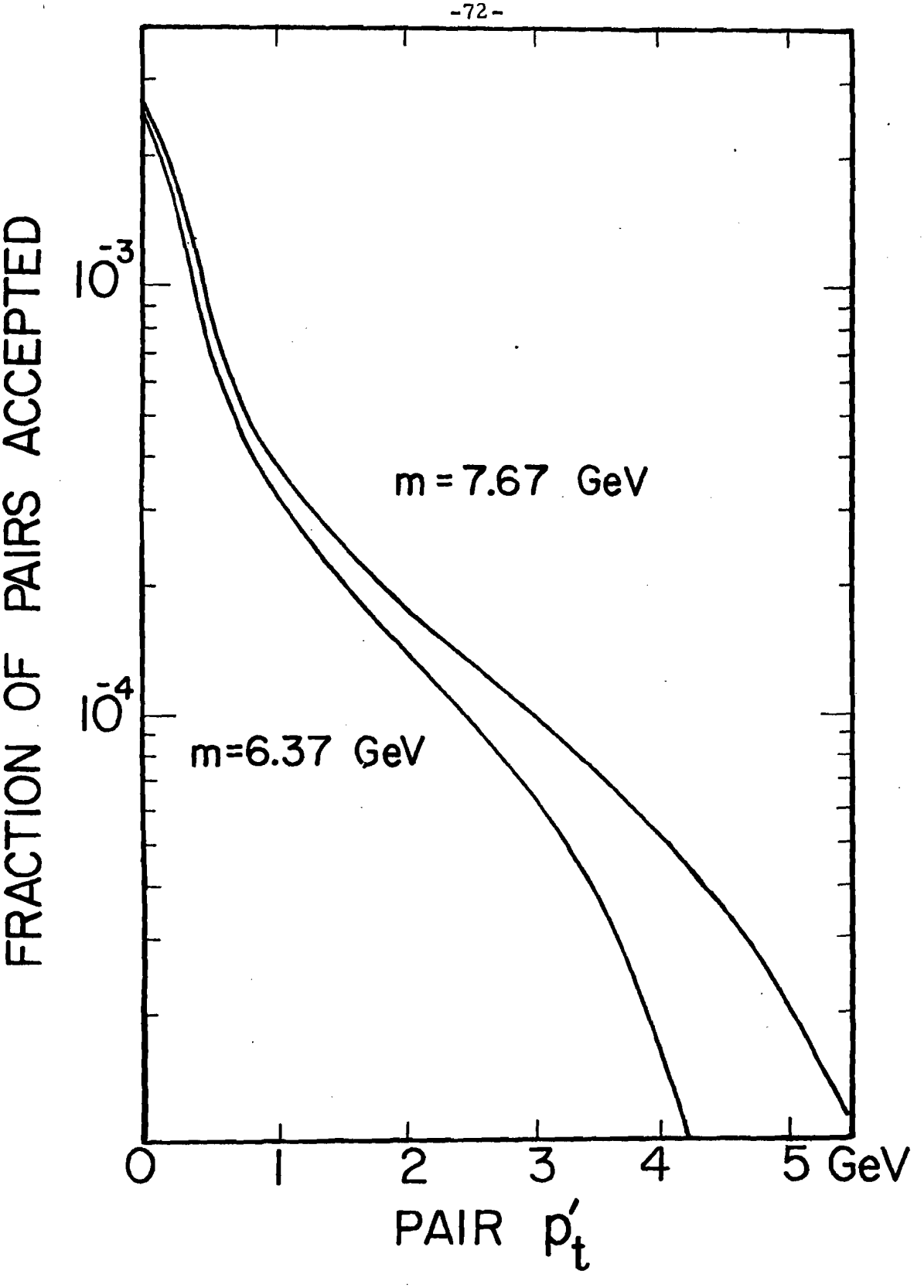

Fig. 10: Fraction of hadron pairs accepted as a function of p_t' in the isotropic decay model. At very low p_t', transverse momenta pointing to any azimuthal direction are accepted. At nigher p_t' the apparatus accepts only p_t' vectors lying in the scattering plane.

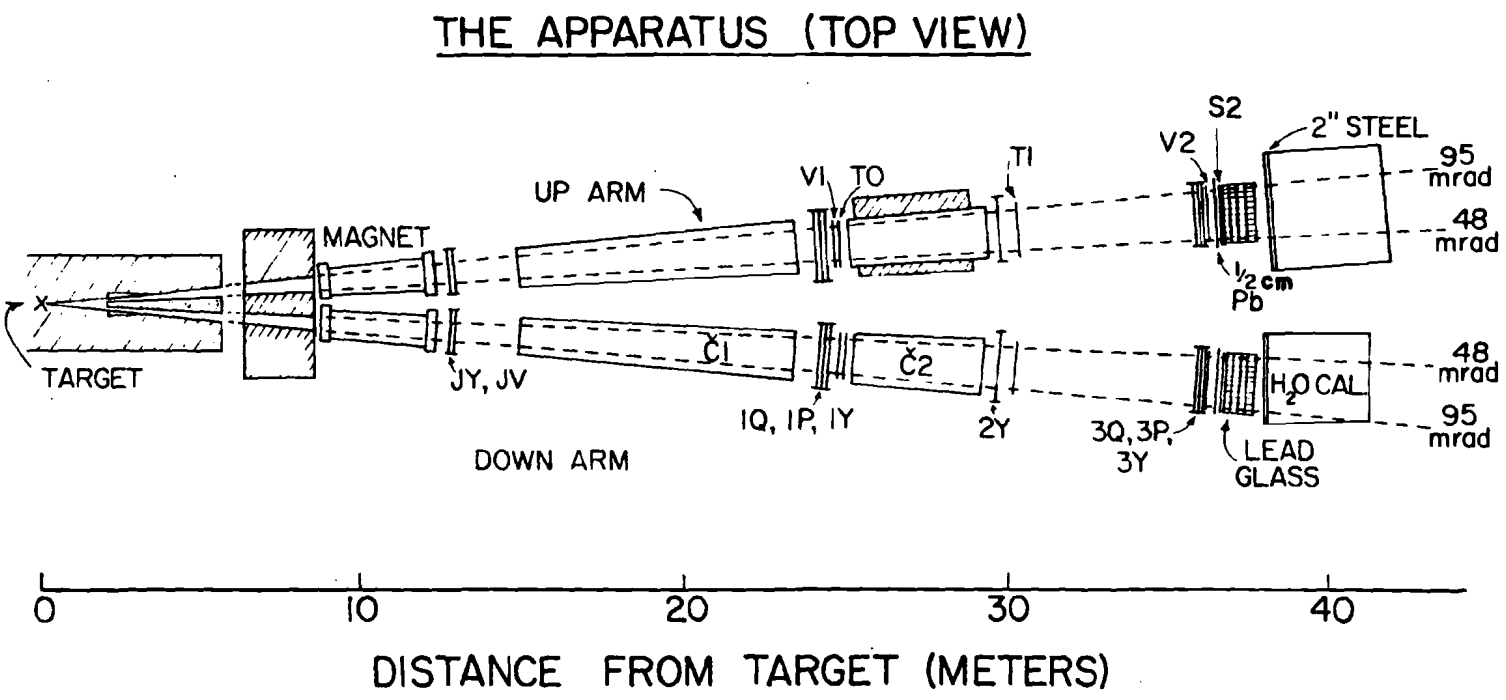

Fig. 11: Plan view of the apparatus, showing the location of the trigger counters (T0, T1, S2), proportional wire chambers (JY,JV,1Q,1P,1Y,2Y,3Q,3P,3Y) and x-measuring hodoscopes (V1 and V2).

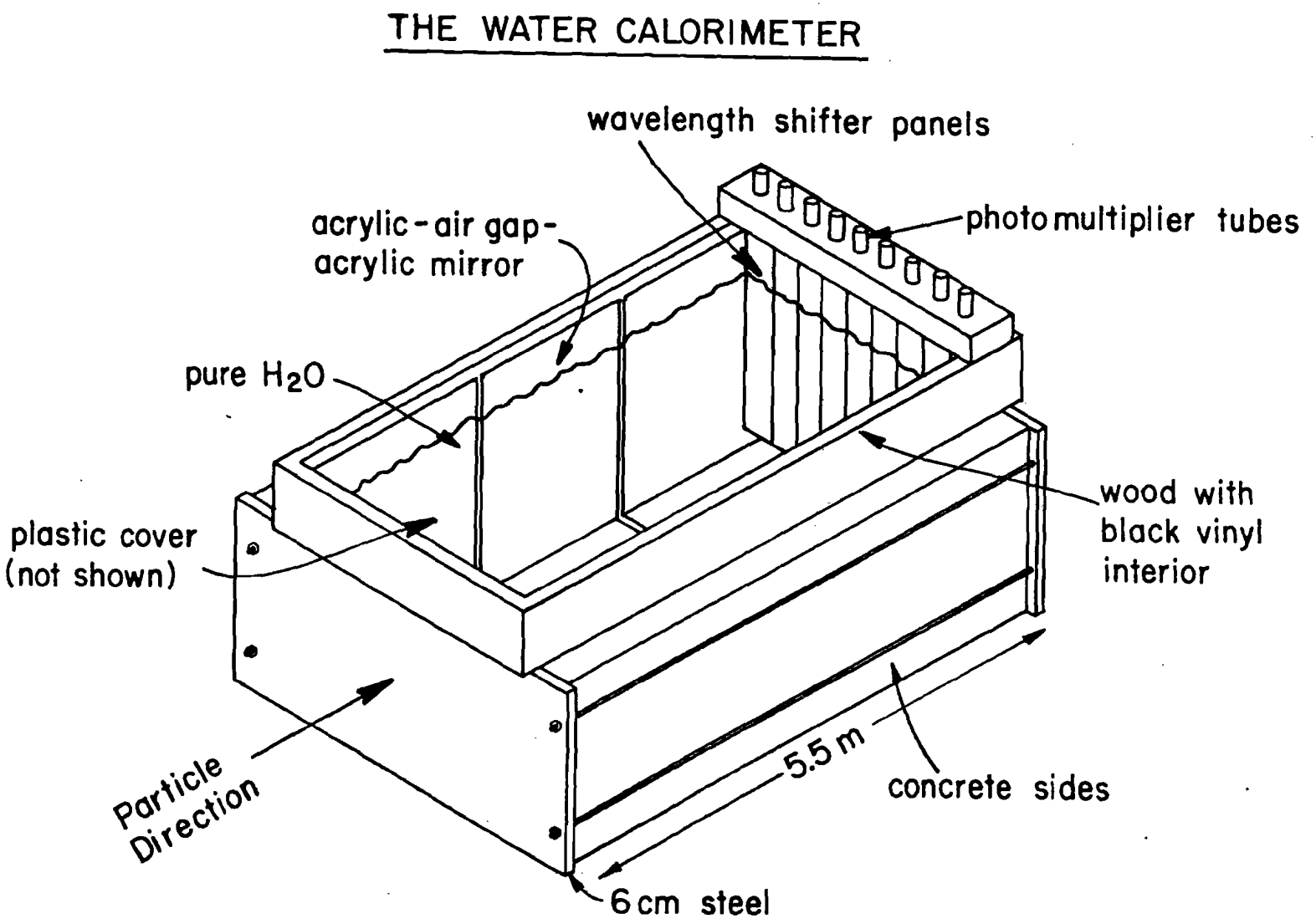

Fig. 12: The up arm water hadron calorimeter.

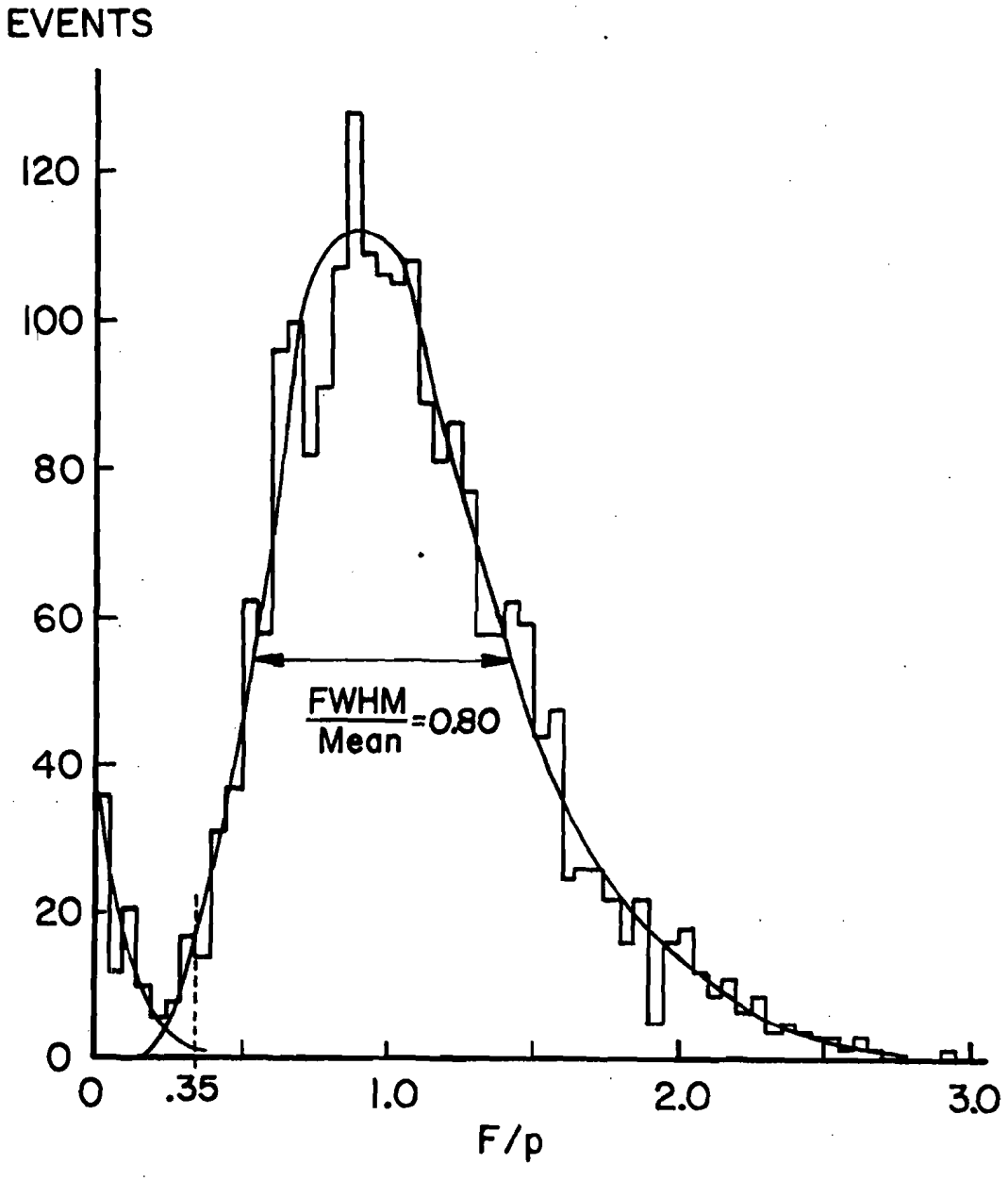

Fig. 13: Distribution of the calorimeter pulse height F/momentum p for hadrons accepted by the magnetic spectrometer. The peak near F = 0 is due to scattered hadrons of small momentum.

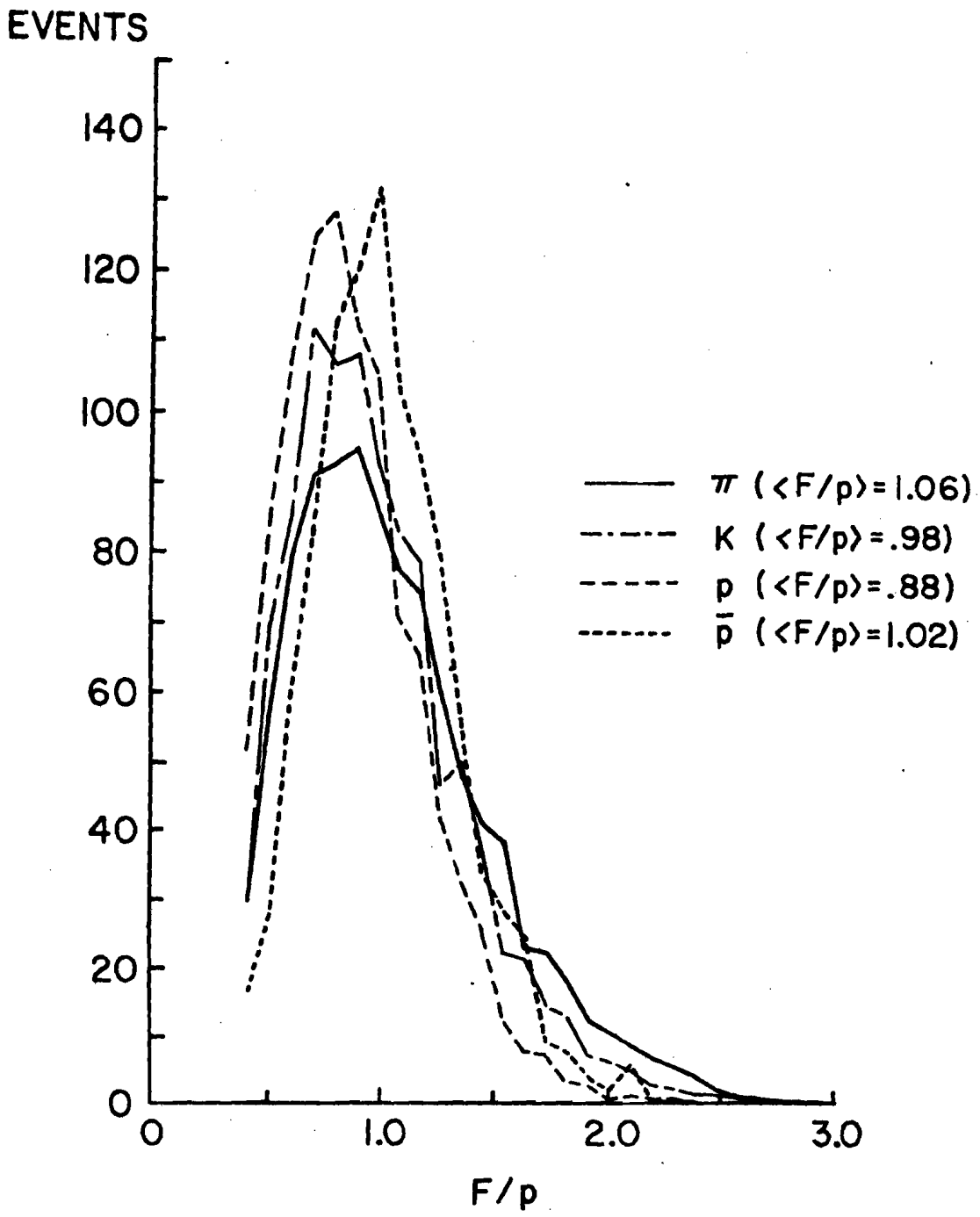

Fig. 14: The normalized response F/p of the hadron calorimeter for π, K and p. The ratio F/p depends significantly on the hadron species.

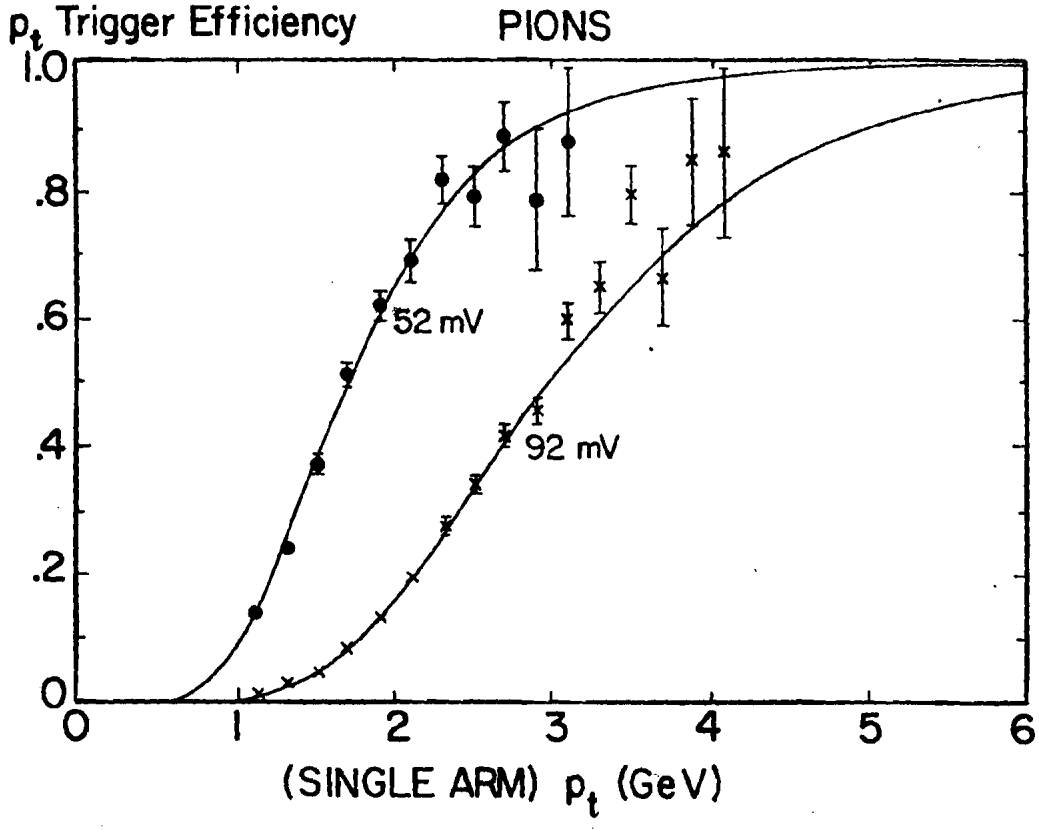

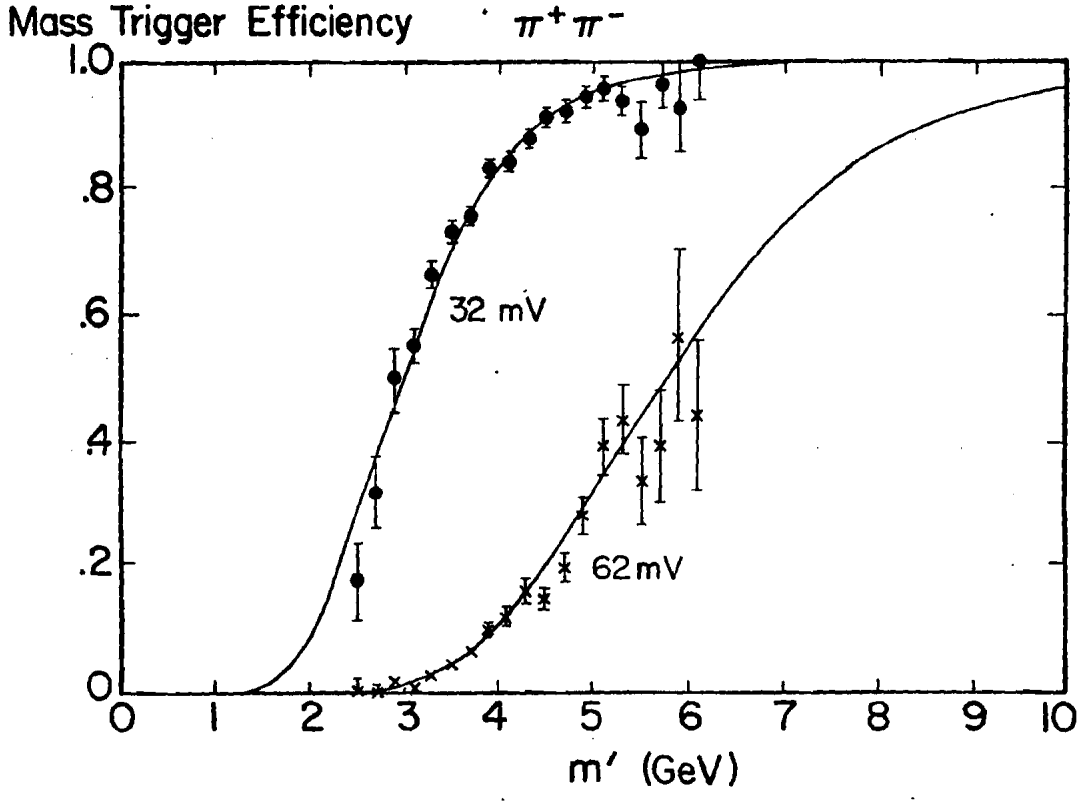

Fig. 16: Trigger efficiency for the p_t and mass-triggers for two threshold settings. The lines are from calculations using measured F/p distributions. The points are from measurements using less restrictive triggers.

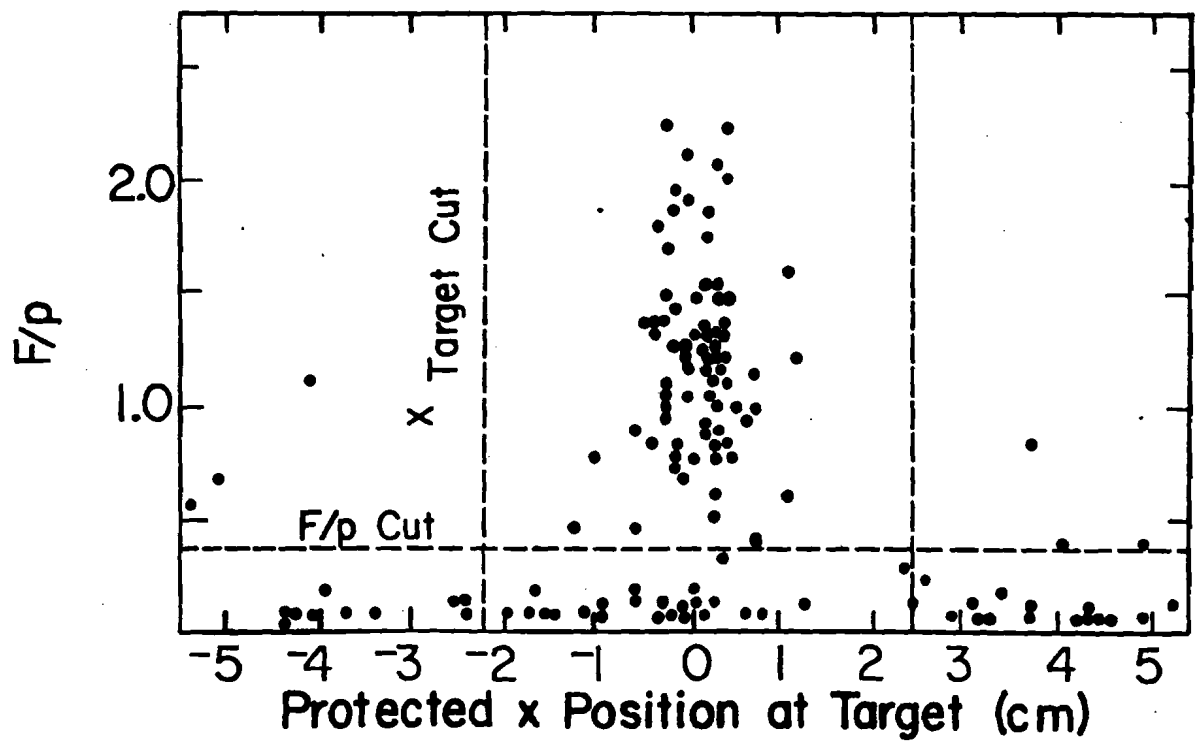

Fig. 15: Scatter plot of the calorimeter signal ratio F/p versus the projected target position x for a typical event sample obtained with a trigger accepting all charged tracks (very high p_t events have relatively more background). A cut on F/p is seen to eliminate much of the background due to events not coming from the target.

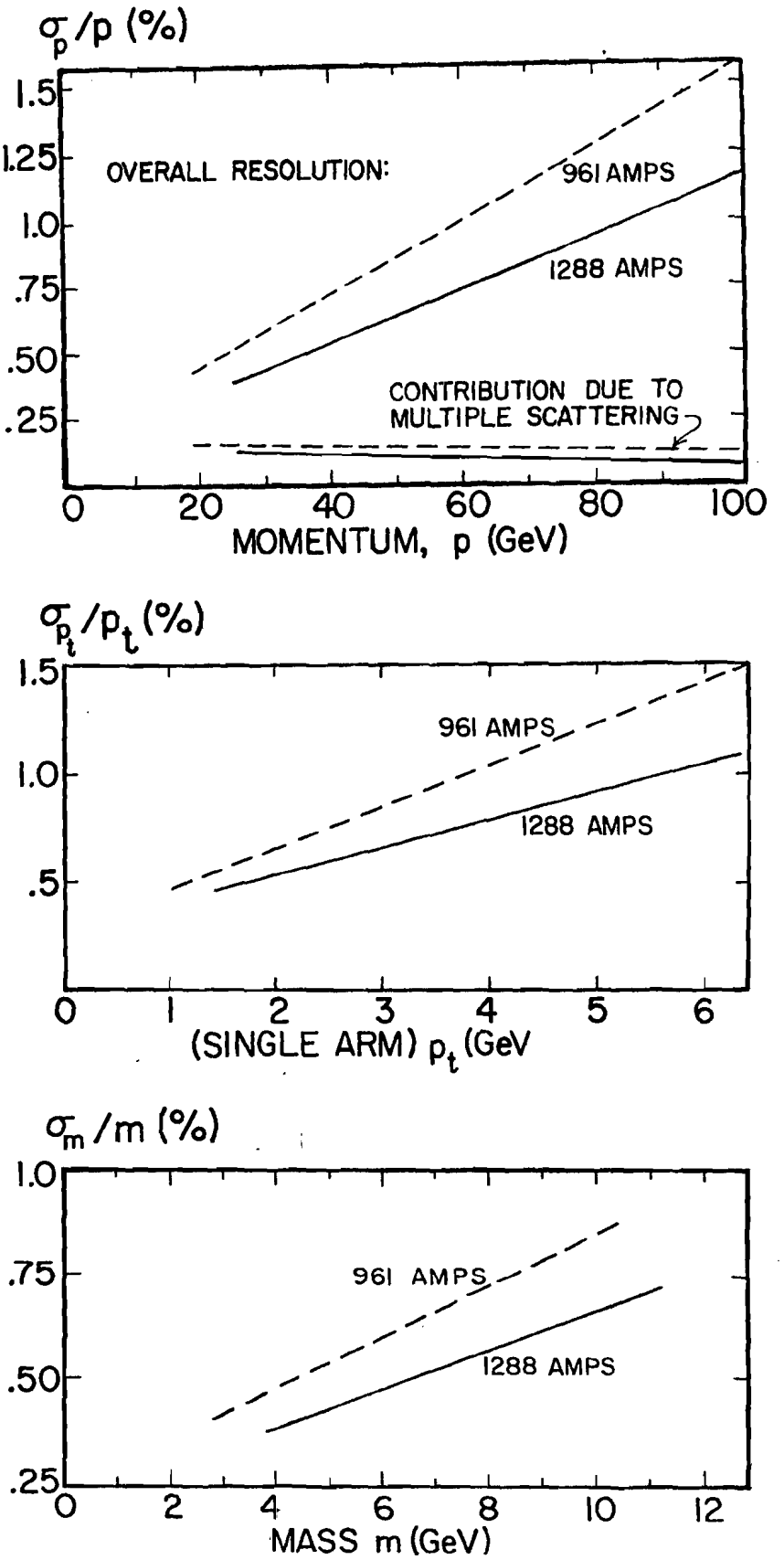

Fig. 17: Calculated resolution, in momentum, p_t and mass as a function of these variables.

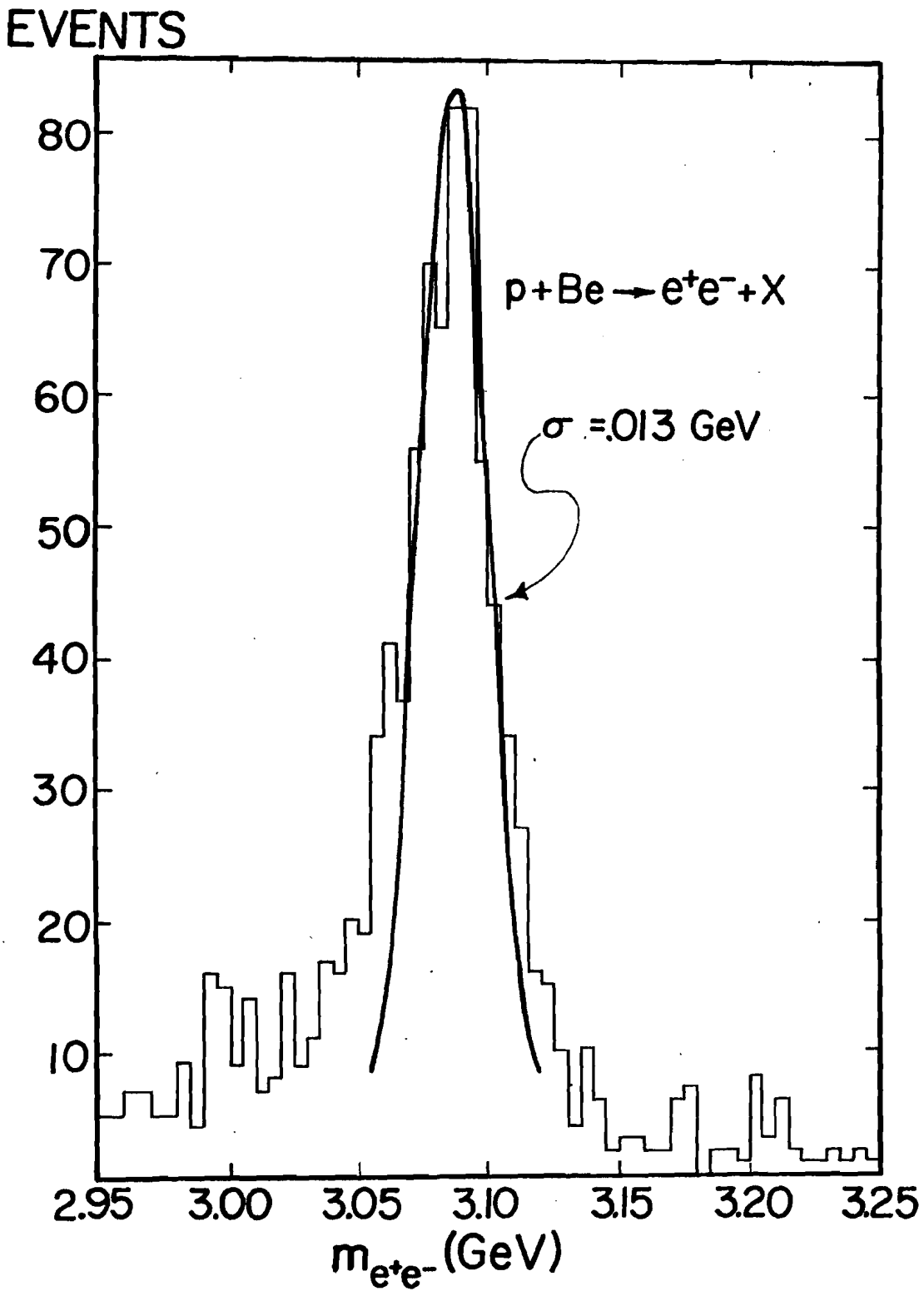

Fig. 18: Observed mass spectrum of the J/ψ and confirmation of the calculated mass resolution.

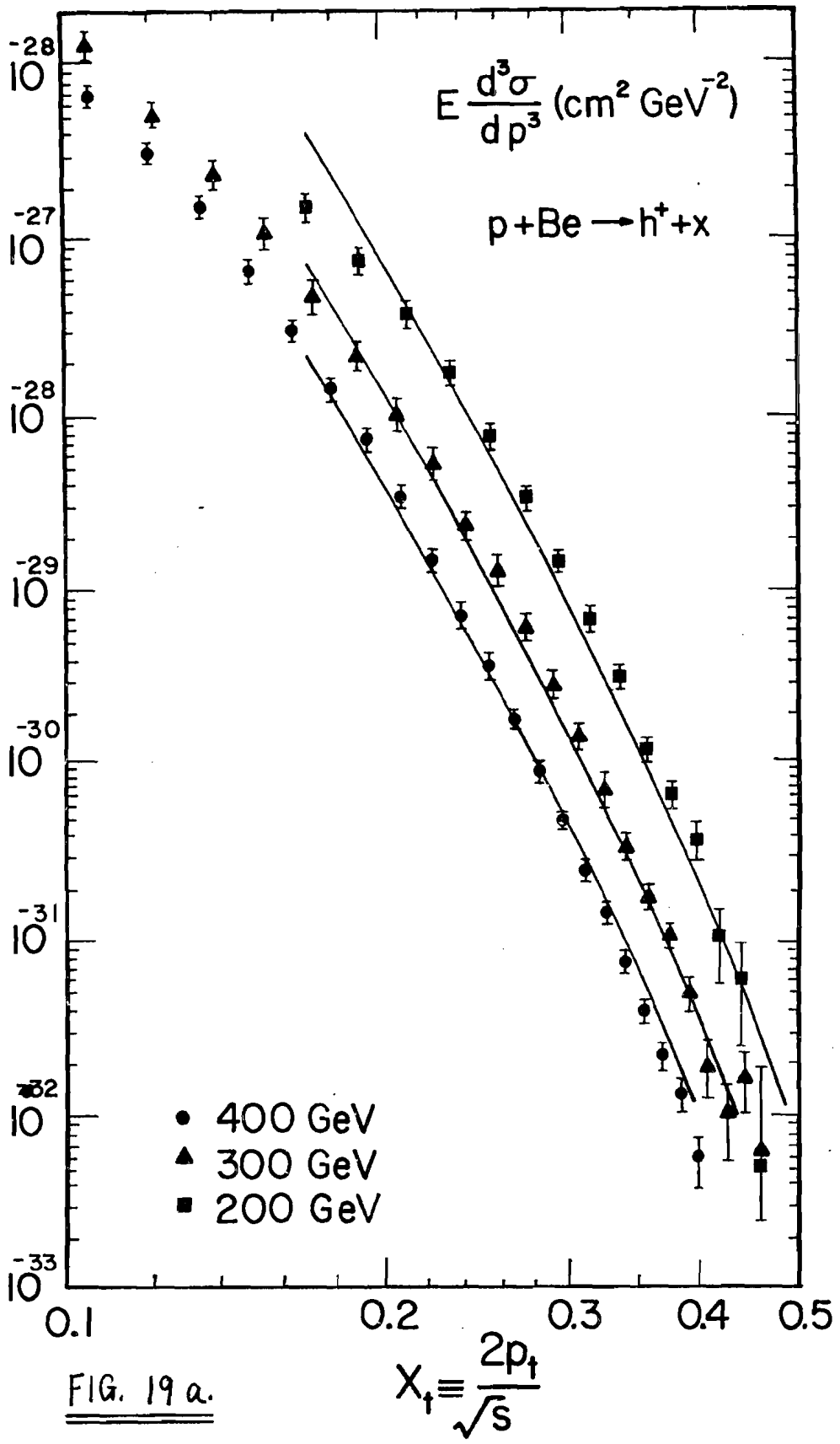

FIG. 19 a.

Fig. 19: Inclusive single hadron production invariant cross sections per Be nucleus, measured with prescaled triggers taken throughout this experiment, for three proton beam energies. The lines are the relevant fits from Table X for the range $x_t \geq +0.24$. Fig. 19 a, b, c, and d shows data for h^+, h^-, π^+ and π^-. Systematic errors (except for the normalization error) have been added in quadrature to the statistical errors. The open symbols in Figs. 19c and 19d are data from the CP group.[8]

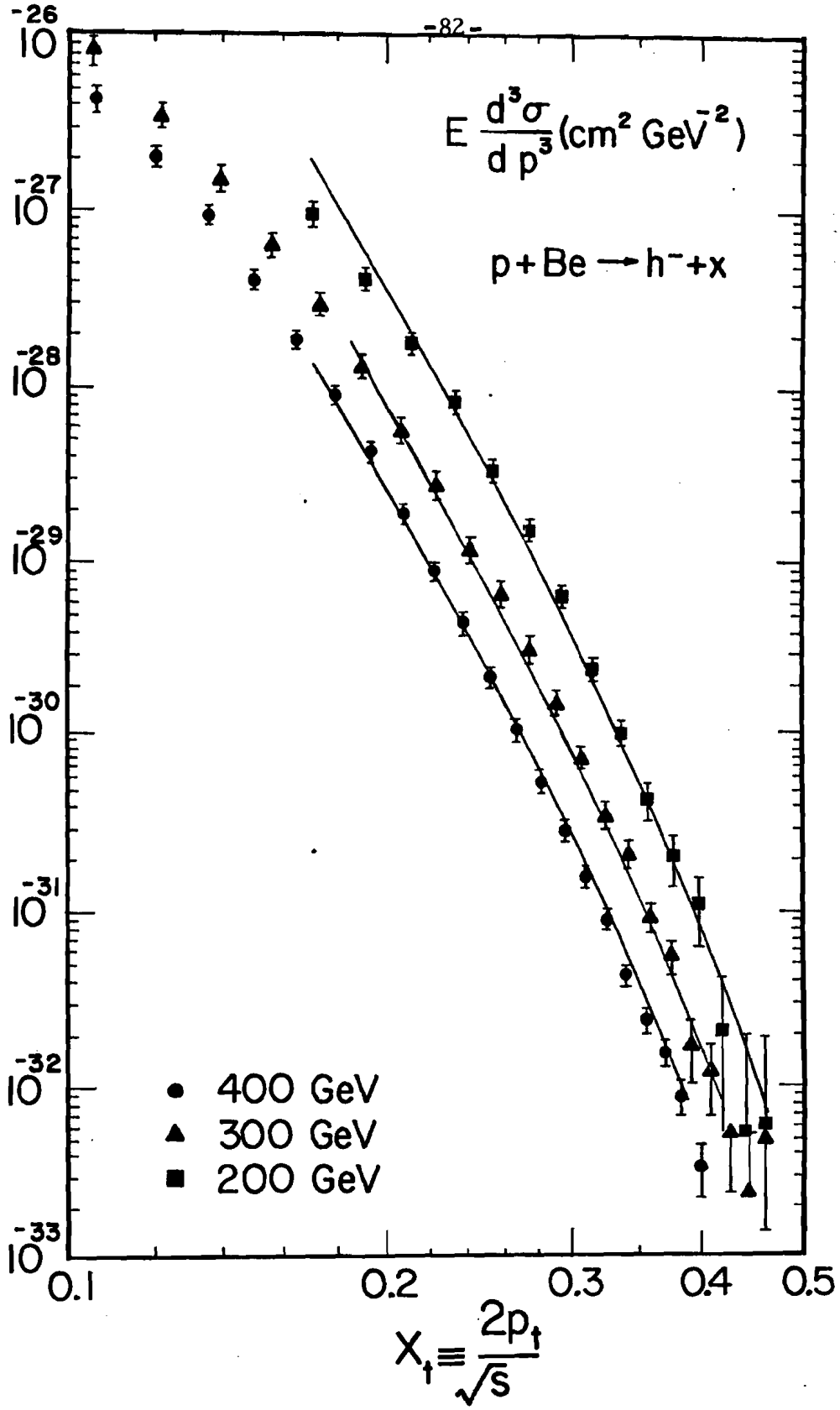
$E\frac{d^3\sigma}{dp^3}(cm^2\,GeV^{-2})$
$p+Be \rightarrow h^- + x$
400 GeV
300 GeV
200 GeV
10^{-26}
10^{-27}
10^{-28}
10^{-29}
10^{-30}
10^{-31}
10^{-32}
10^{-33}
0.1
0.2
0.3
0.4
0.5
$X_t \equiv \frac{2p_t}{\sqrt{s}}$

FIG. 19 b.

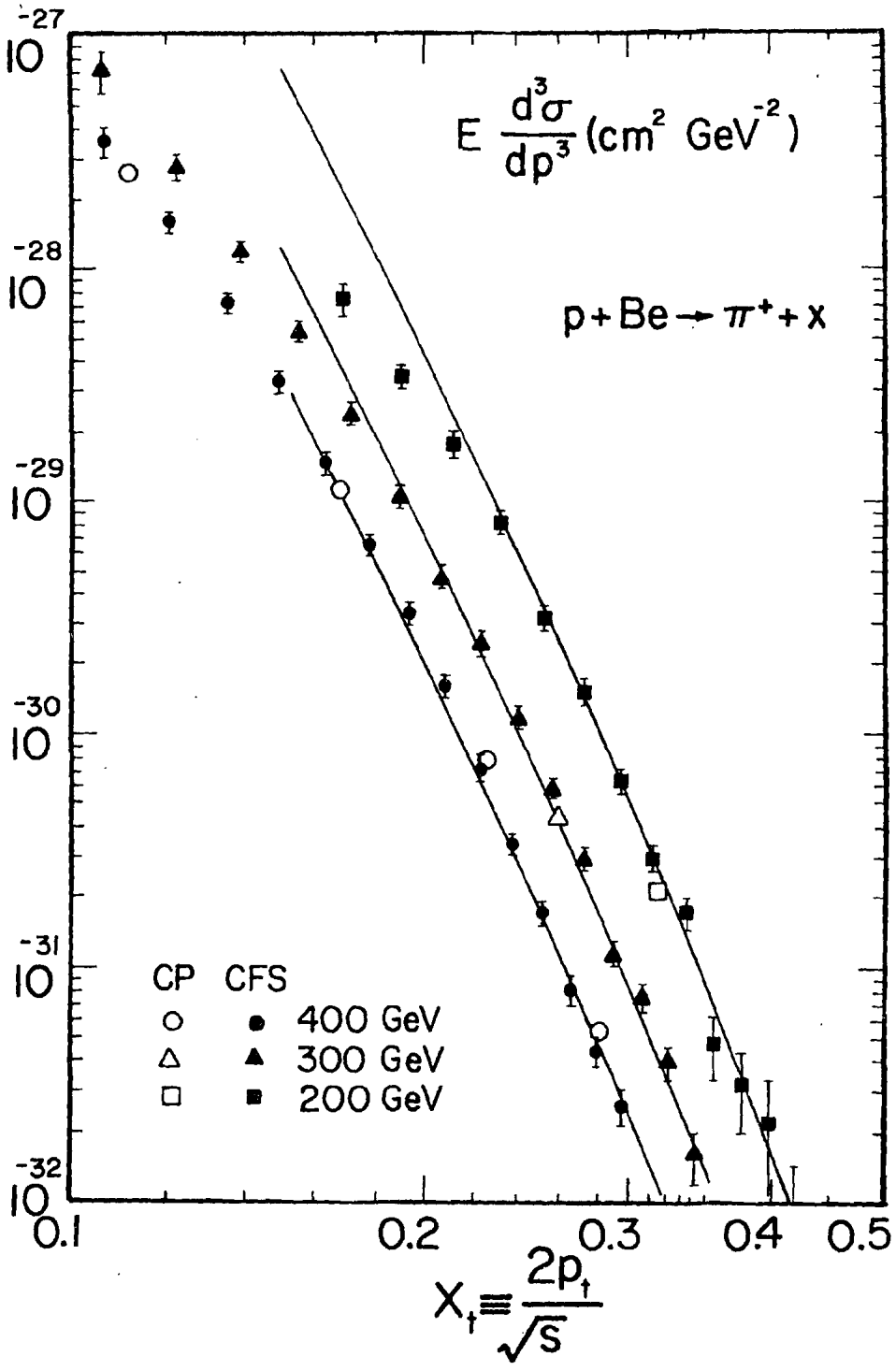
$E\frac{d^3\sigma}{dp^3}(cm^2\ GeV^{-2})$
$p+Be \rightarrow \pi^+ + X$
CP CFS
400 GeV
300 GeV
200 GeV
10^{-27}
10^{-28}
10^{-29}
10^{-30}
10^{-31}
10^{-32}
0.1
0.2
0.3
0.4
0.5
$X_t \equiv \frac{2p_t}{\sqrt{s}}$

FIG. 19 c.

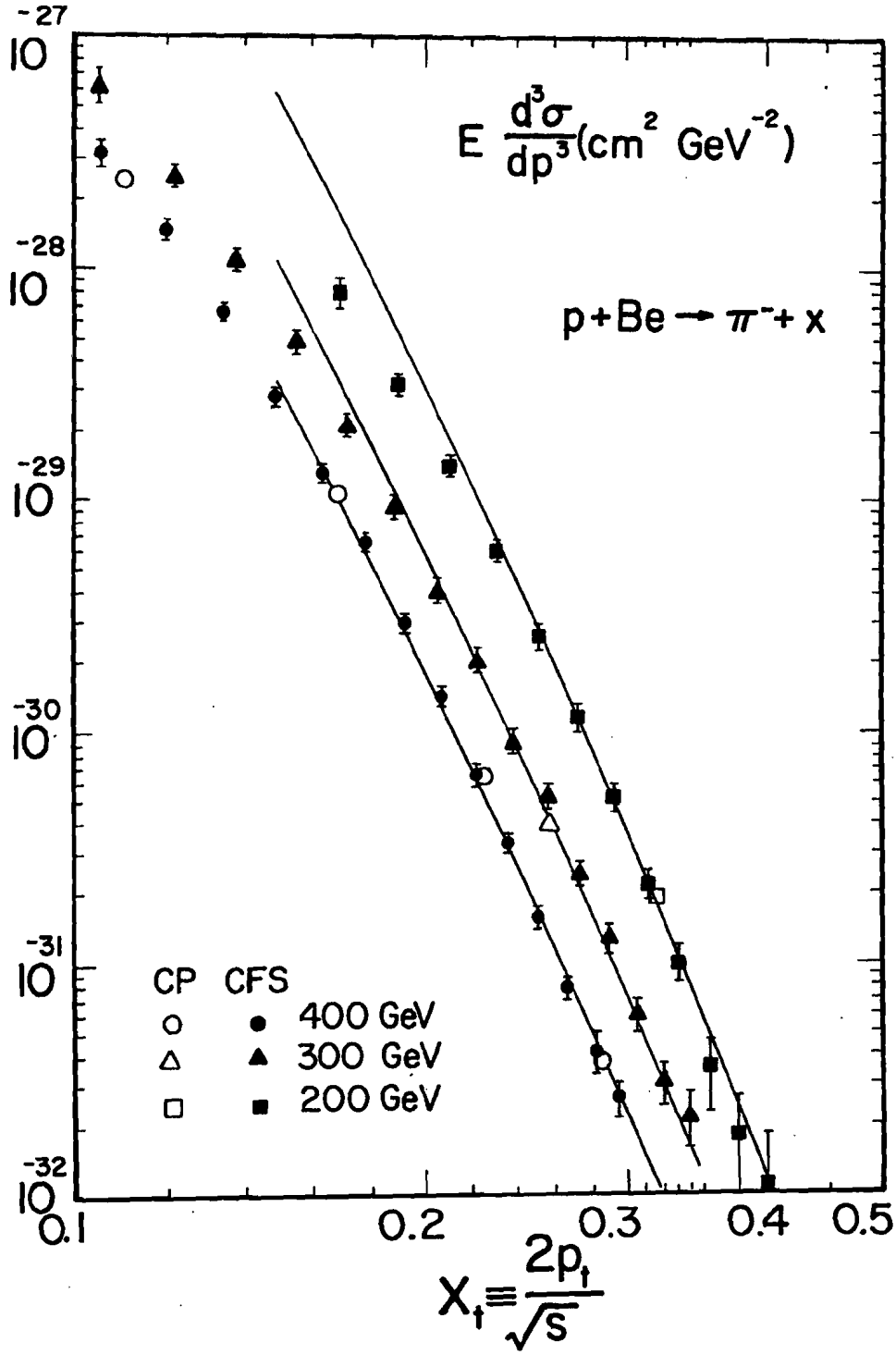
$E\frac{d^3\sigma}{dp^3}(cm^2\ GeV^{-2})$
$p+Be \rightarrow \pi^- + x$
CP CFS
400 GeV
300 GeV
200 GeV
10^{-27}
10^{-28}
10^{-29}
10^{-30}
10^{-31}
10^{-32}
0.1
0.2
0.3
0.4
0.5
$X_1 \equiv \frac{2p_1}{\sqrt{s}}$

FIG. 19 d.

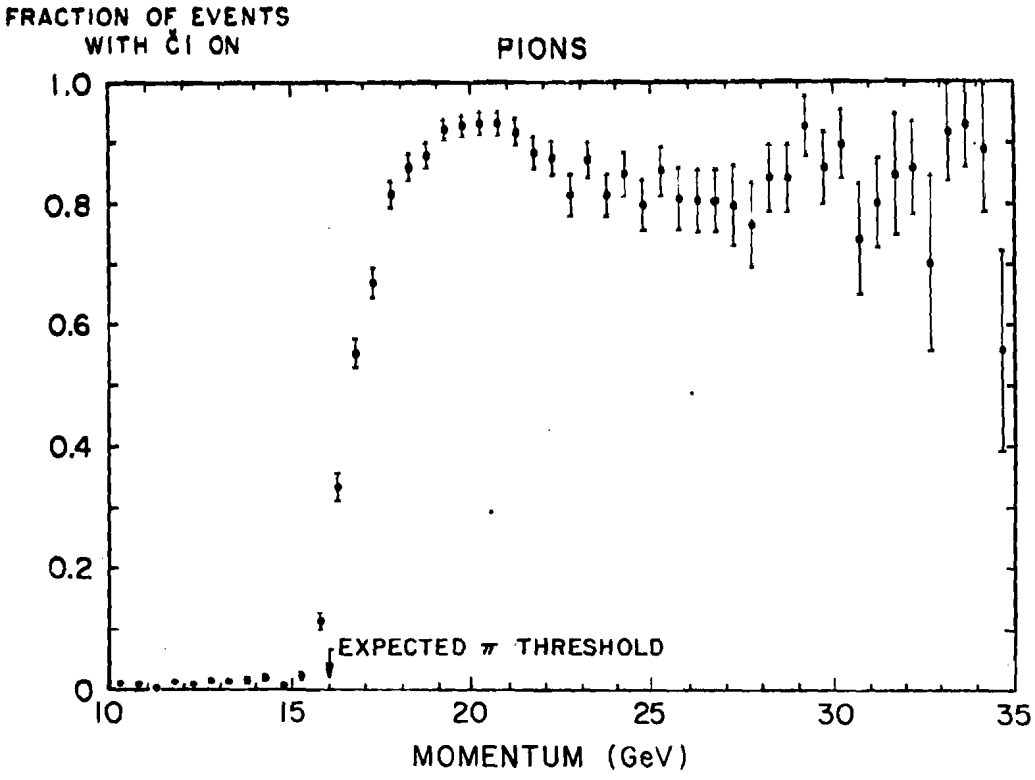

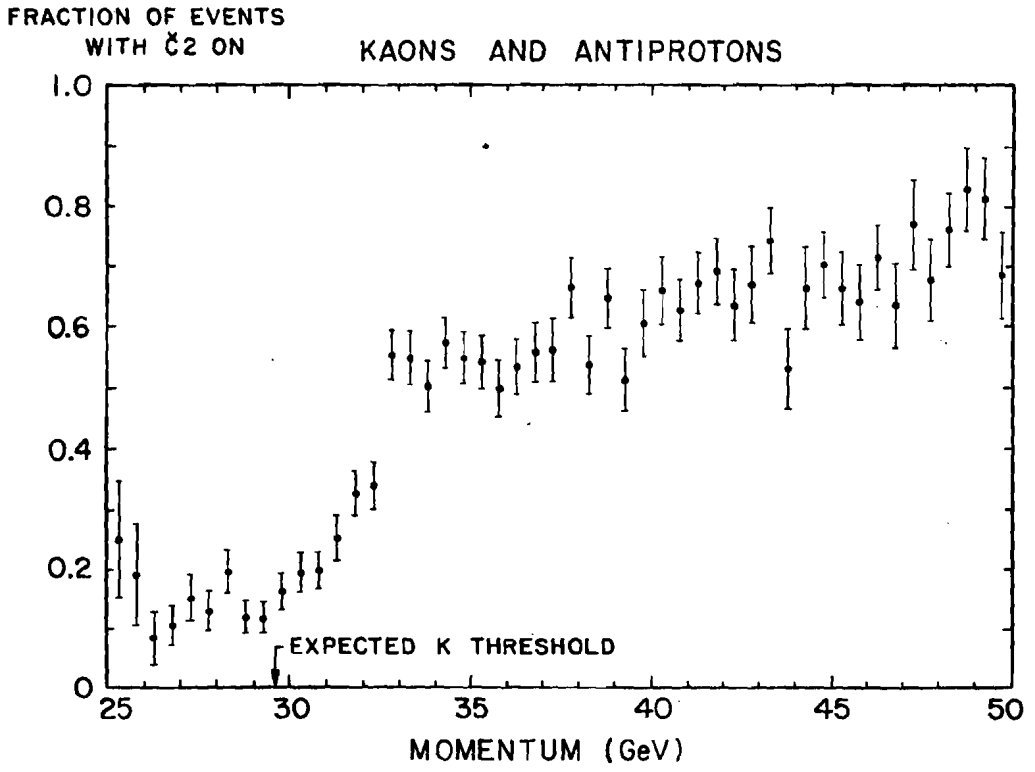

Fig. 20: Threshold curves for $\check{C}_1$ and $\check{C}_2$.

a) Pion threshold in $\check{C}_1$. The graph shows the fraction of particles in the spectrometer (and firing $\check{C}_2$) which also fired $\check{C}_1$. The drop at 23 GeV is due to kaons firing $\check{C}_2$(N_2 gas), contaminating the π sample.

b) Kaon threshold in $\check{C}_2$. Shown is the fraction of reconstructed tracks of negative charge not firing $\check{C}_1$, which fire $\check{C}_2$ (42% N_e, 58% N_2). Note the additional rise above 40GeV, where the p/K ratio begins to fall.

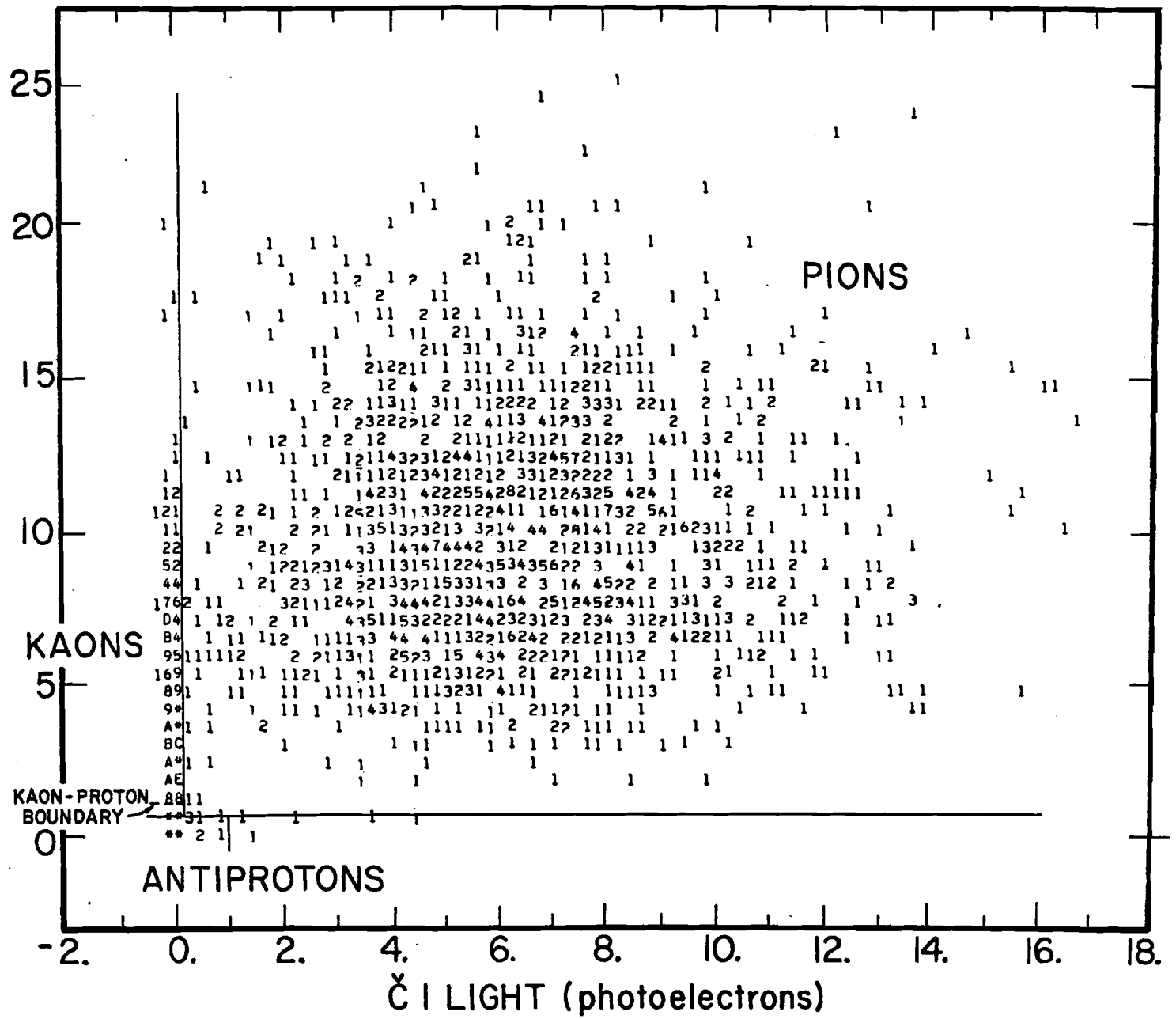

Fig. 21: The response of the two Cerenkov counter system to negative hadrons from 34 to 56 GeV (the triple identification band). Pions register in both counters, kaons only in $\check{C}_2$, and protons in neither counter (the overflow asterisks near the origin signify 35 or more events per bin). The thresholds (0.[illegible] photoelectrons in $\check{C}_1$, 0.2 in $\check{C}_2$) are shown as solid lines.

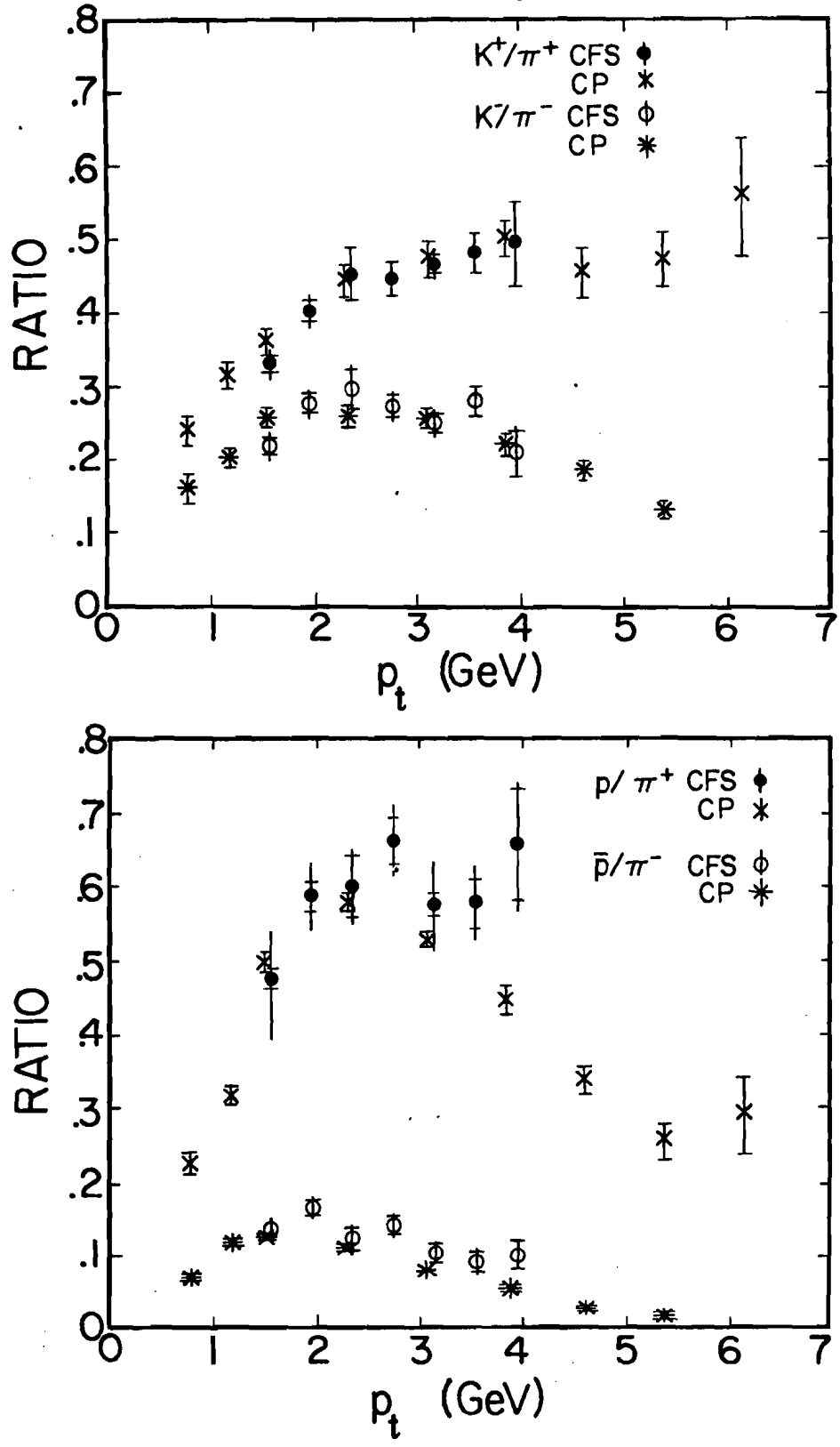

Fig. 22: Ratio of kaon and proton to pion production as a function of p_t. Data from this experiment (CFS) are compared to those from the CP experiment (Ref. 8). All data are from 400 GeV protons striking Beryllium targets.

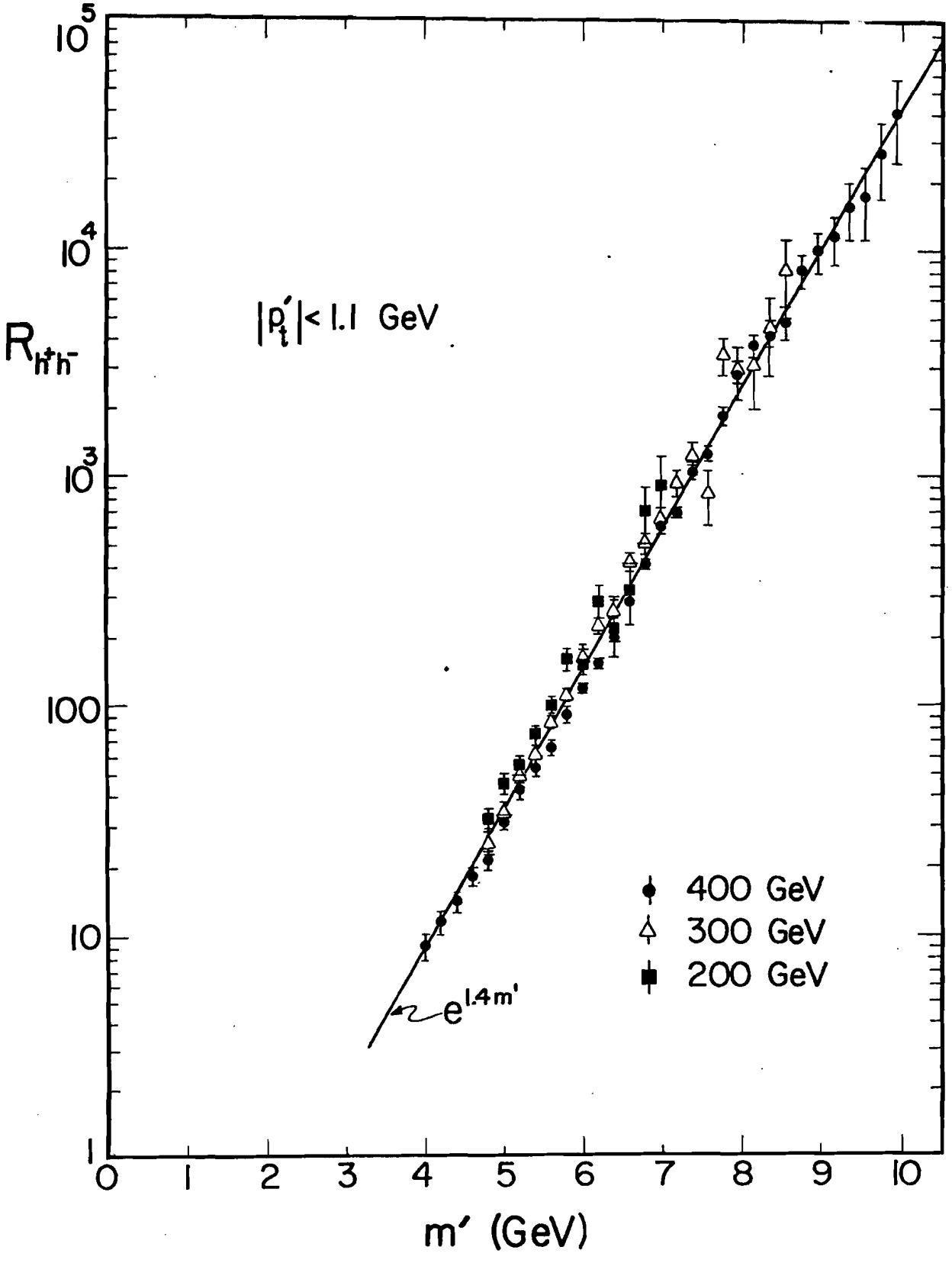

Fig. 23: The correlation function R (defined in the text) versus pseudomass m' for h^+h^- pairs in p-Be collisions (per Be nucleus). Nuclear enhancement is negligible for these symmetric pairs, but affects the single hadron cross sections in the denominator of R.

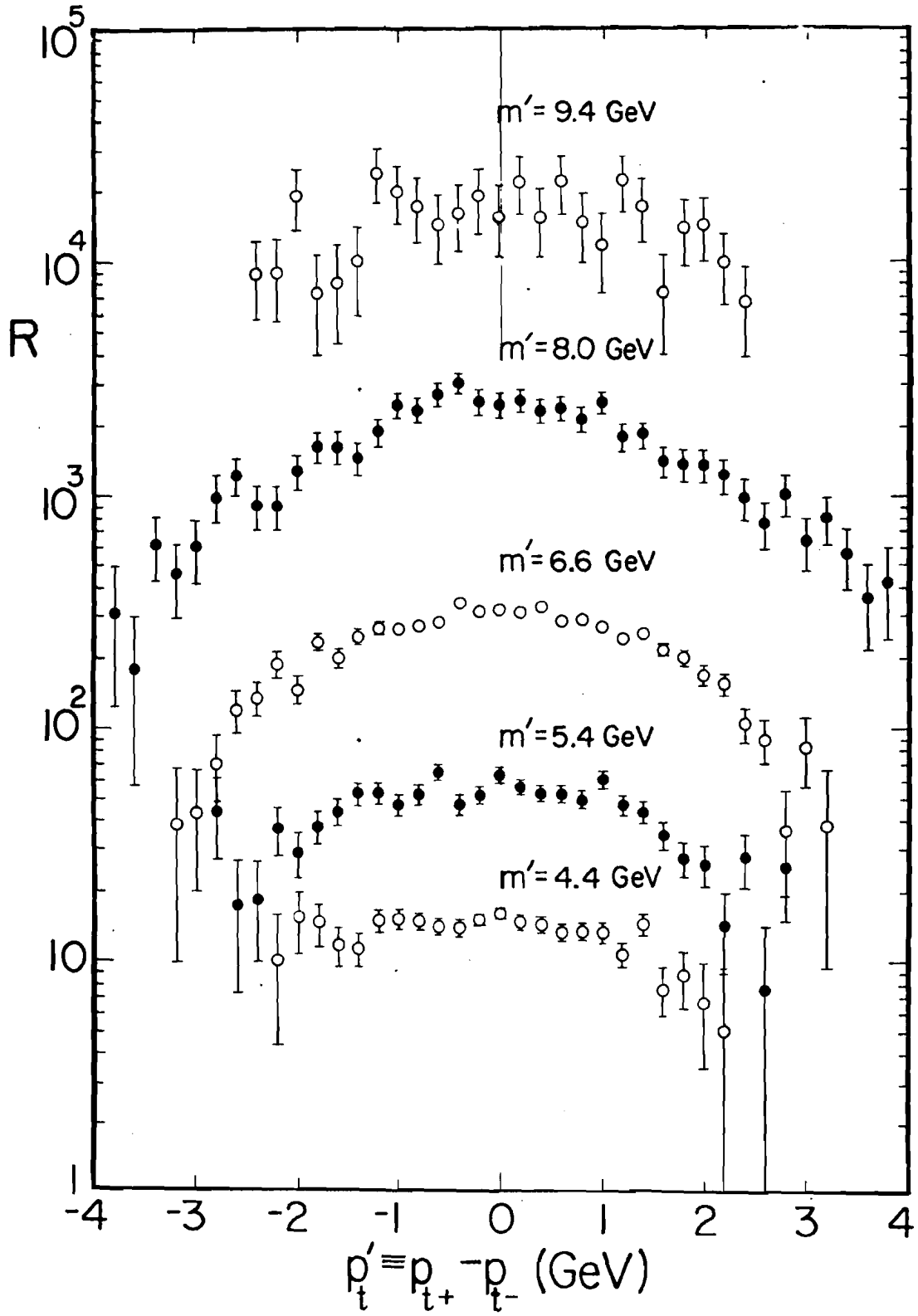

Fig. 24: The correlation function R for fixed m' versus p_t' in 400 GeV p-Be collisions (per Be nucleus).

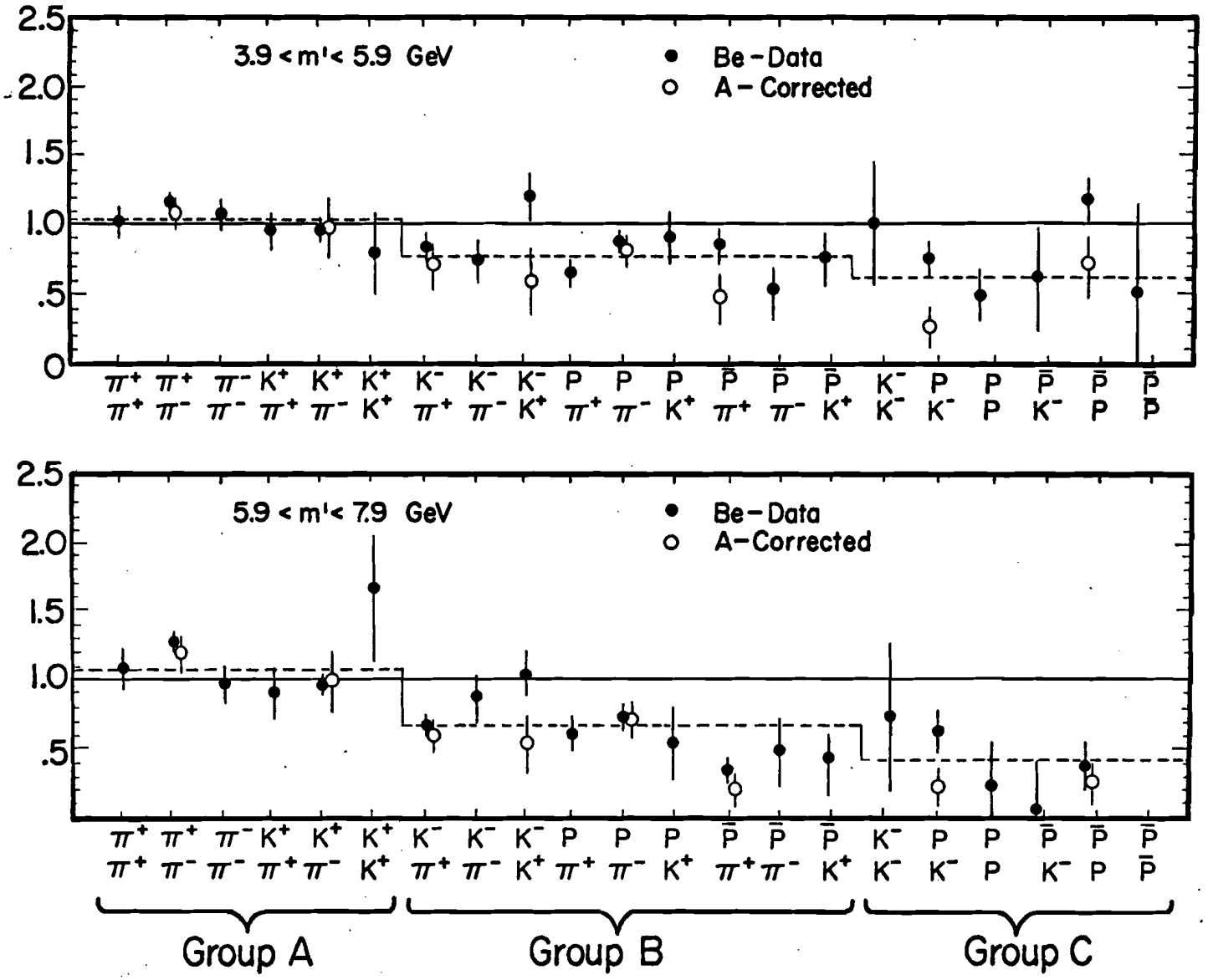

Fig. 25: Correlation function R averaged over the mass range 5.9 to 7.9 GeV (top) and 3.9 to 5.9 GeV (bottom) for identified pairs, normalized to the same function for h^+h^- pairs.

a) The full circles are Be data, while the open circles are data corrected (where measurements are available) for nuclear enhancement as a function of species.

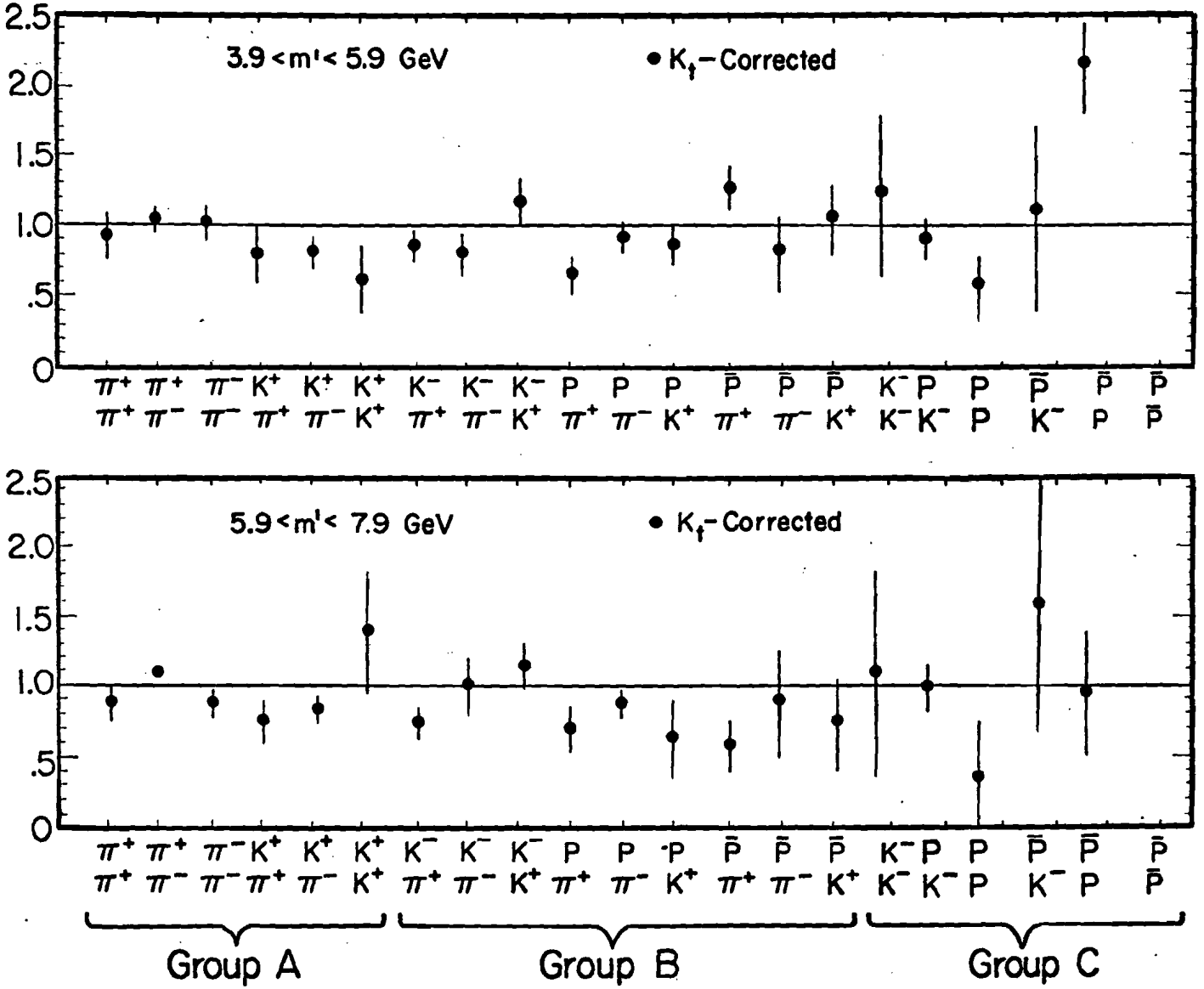

Fig. 25 b) The same normalized correlation function, corrected for constituent k_t (see text).

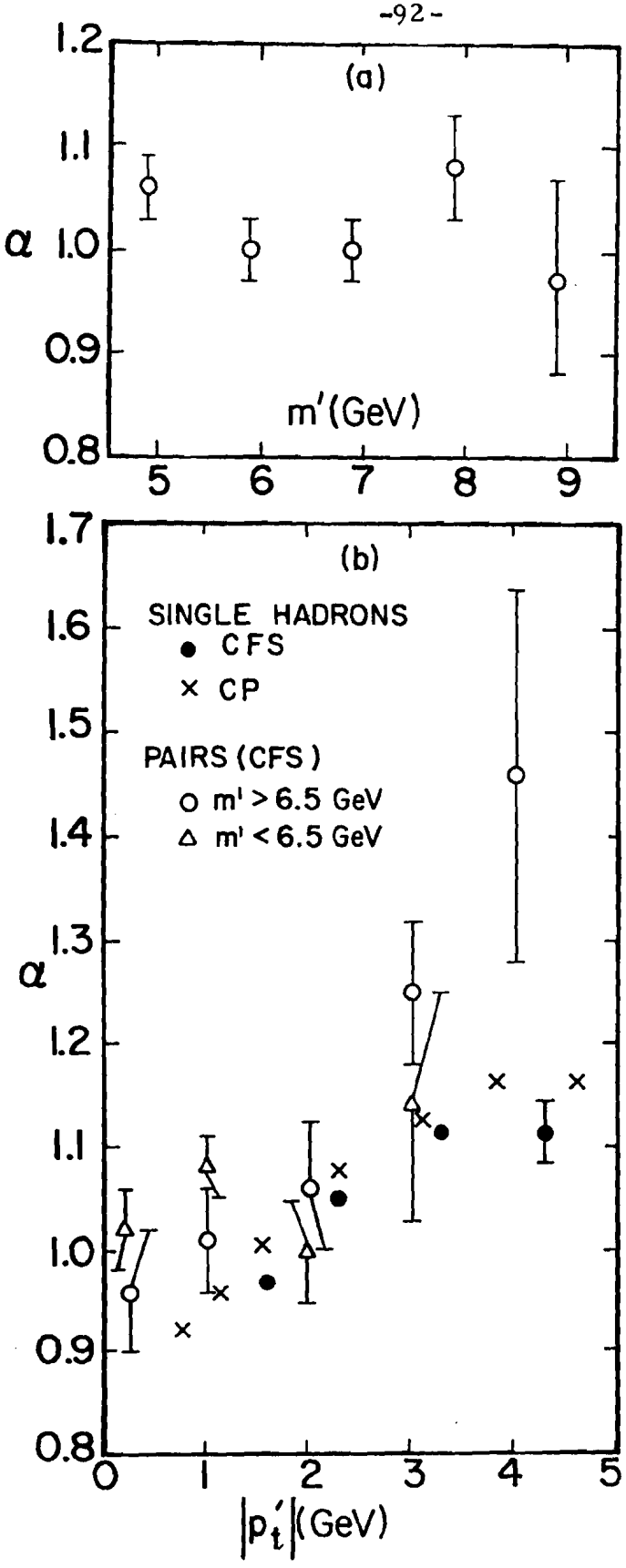

Fig. 26: The power α of the A-dependence of the invariant dihadron production cross section as a function for m' for all p_t' (top) and as a function of $|p_t'|$ for two mass ranges as indicated (bottom). Comparison is made to the nuclear enhancement in single hadron production [8]. Statistical errors are shown when they are larger than the symbols.

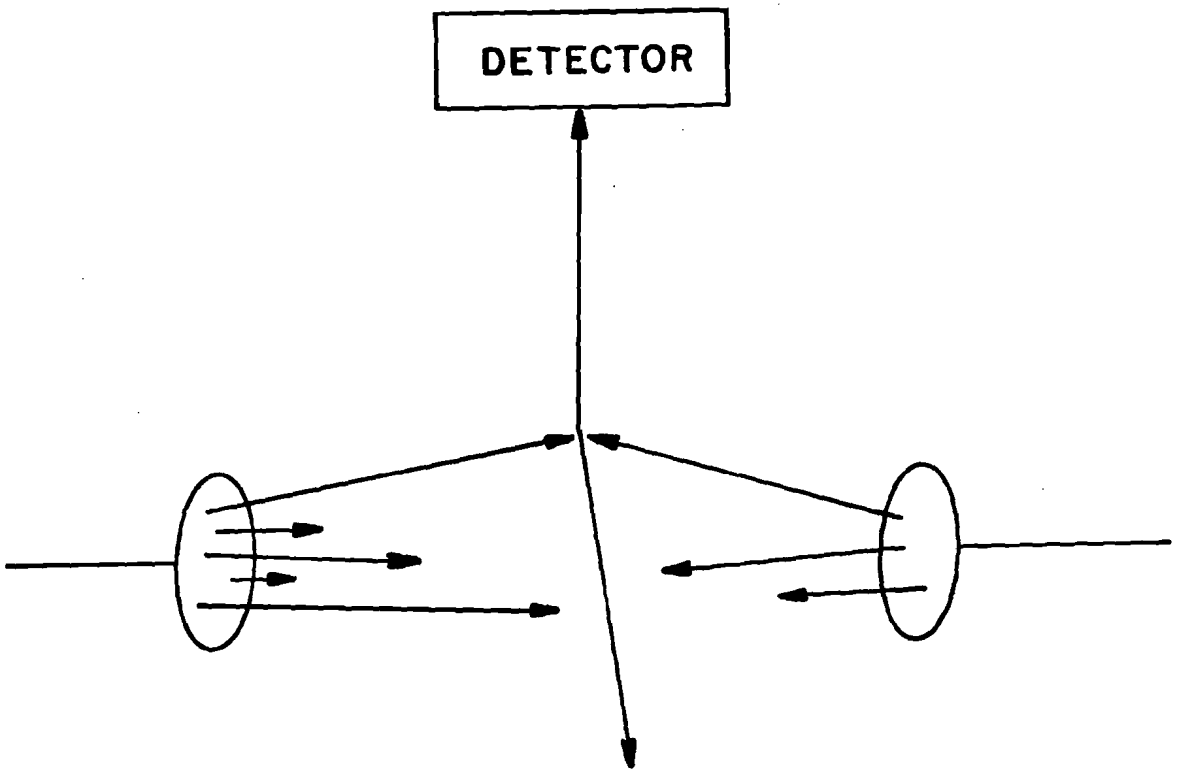

Fig. 27: "Trigger bias" in inclusive single hadron production at large p_t. At any p_t one sees mostly events originating from constituents starting out with their transverse momentum large and pointing toward the detector.

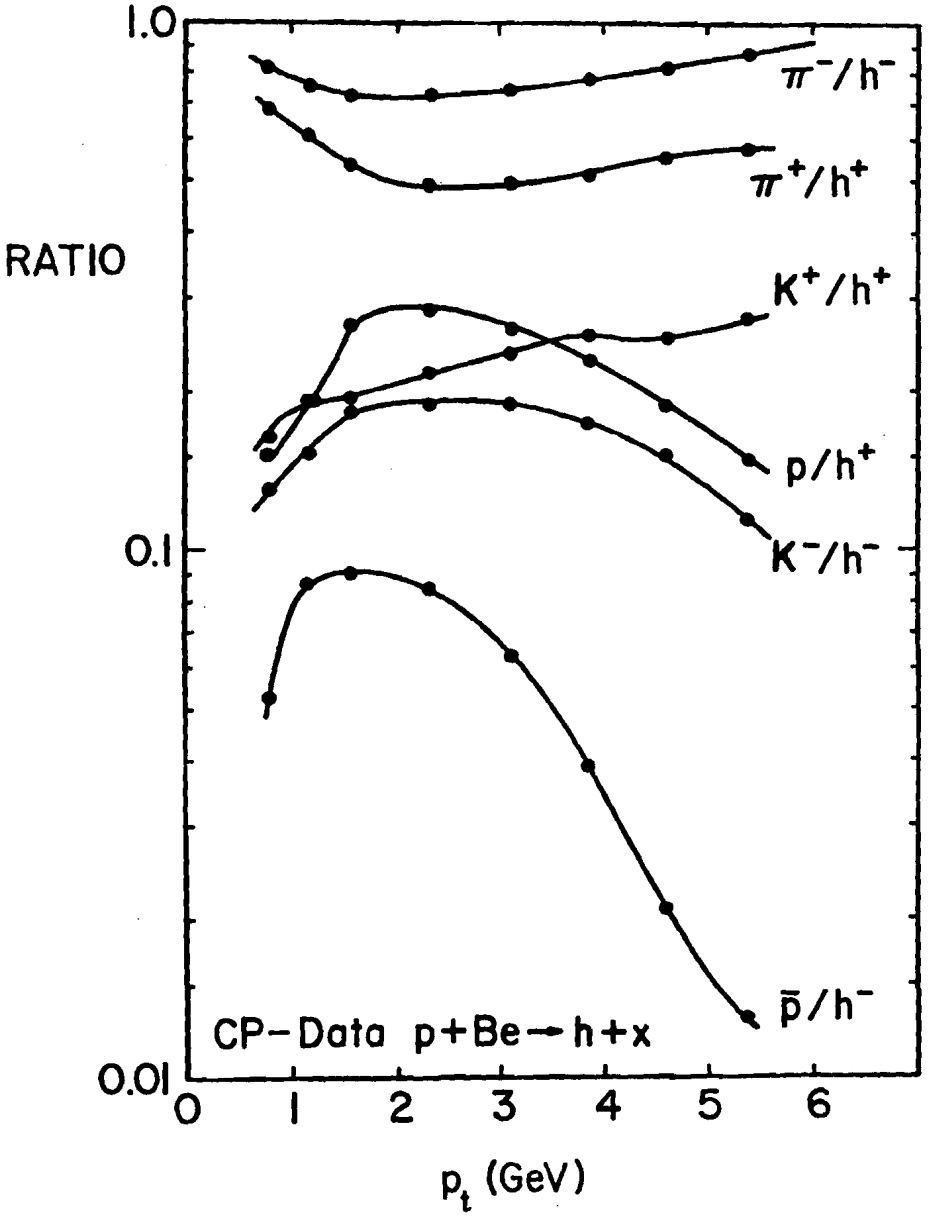

Fig. 28: The species composition of positive and negative hadrons as a function of p_t. The original data are from Ref. 8. Note that π^+, π^- and K^+ are flat or rising with p_t in the range of interest here (2-4 GeV), while K^-, p and $\bar{p}$ are falling.

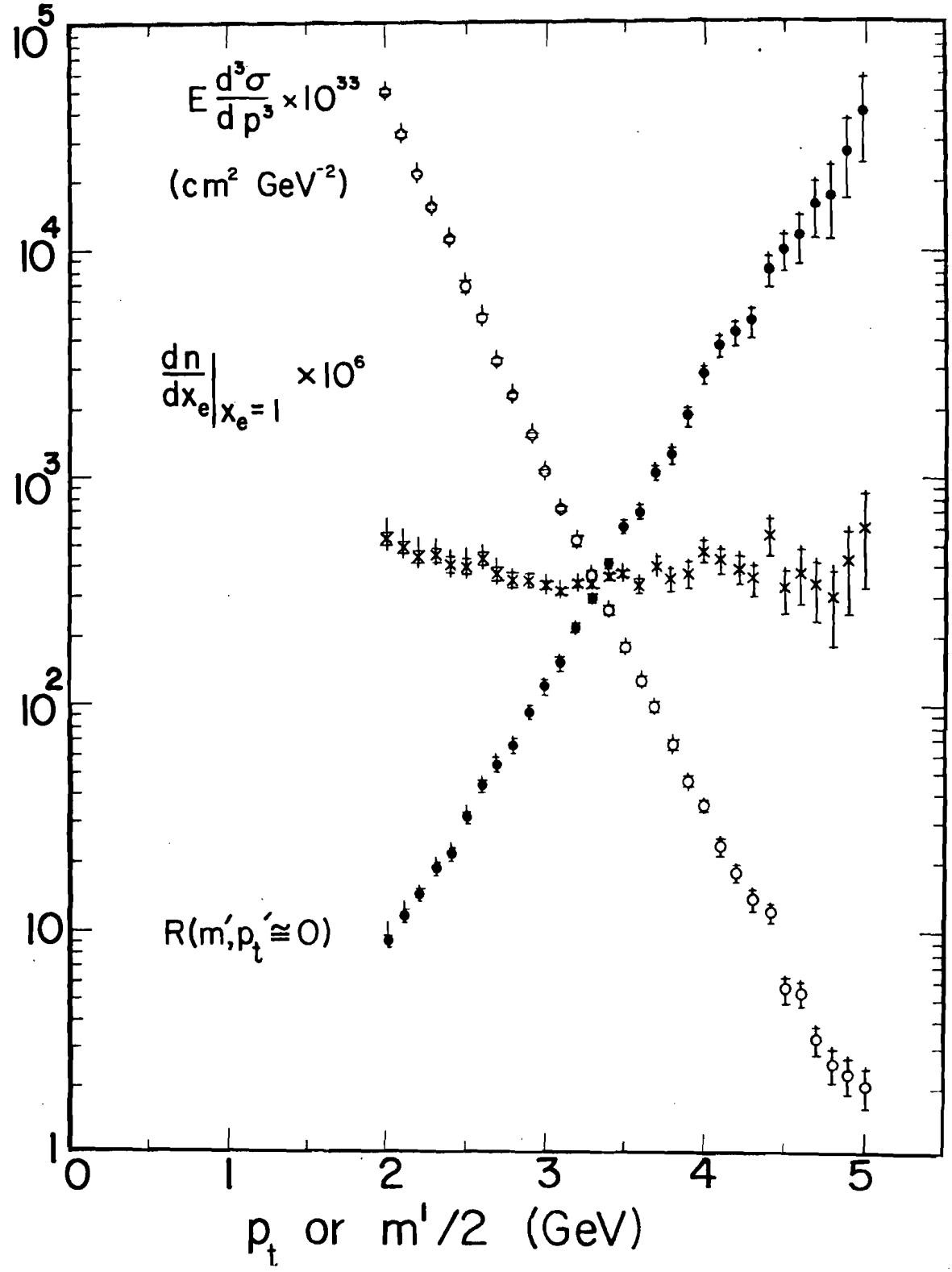

Fig. 29: The single hadron (h^-) invariant production cross section (ϕ), the correlation function R(ϕ) and the away side multiplicity dn/dx_e (defined in the text, ‡) versus p_t or $m'/2$. The correlation R is seen to rise just fast enough to cancel the drop in the single hadron production cross section, yielding a flat dn/dx_e distribution. The data are from p-Be collisions at 400 GeV.

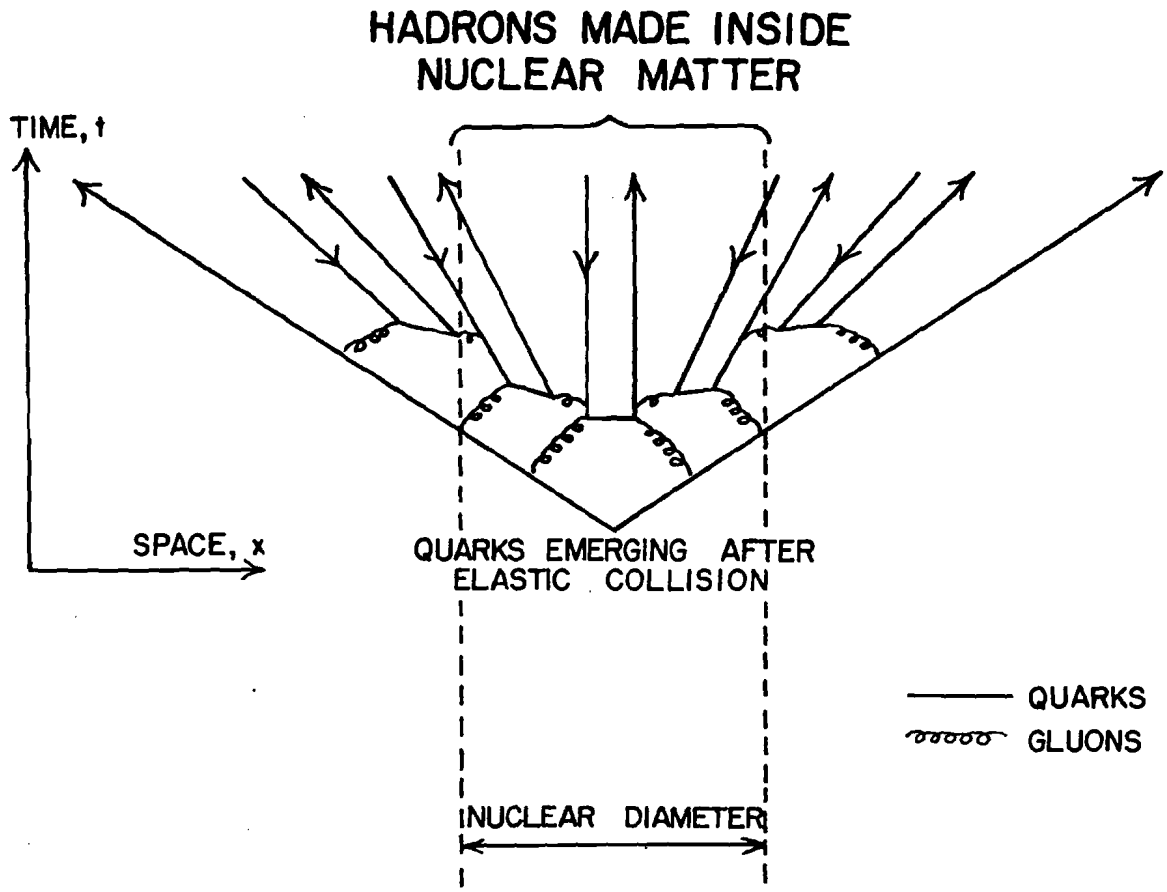

Fig. 30: A schematic picture of the time development of a pair of hadron jets from a pair of quarks. The slow (low z) hadrons in the center of the figure are made first, and therefore inside nuclear matter, which affects the process.

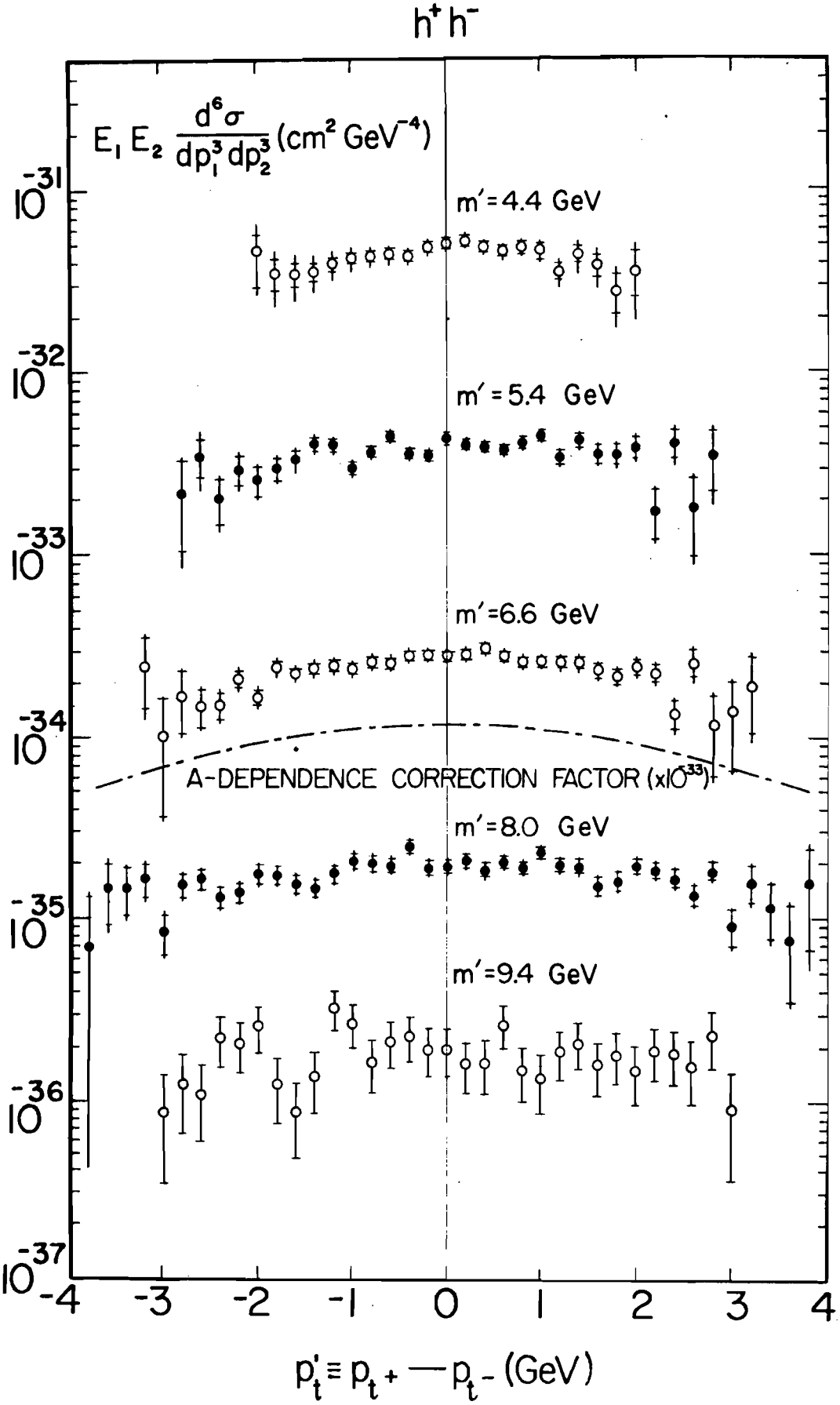

Fig. 31: The invariant two particle cross section S (defined in the text) versus p_t' in several mass ranges for the reaction $p + Be \rightarrow h^+ + h^-$. To correct for nuclear enhancement, each data point should be multiplied by the value of the dashed correction function at the same p_t'.

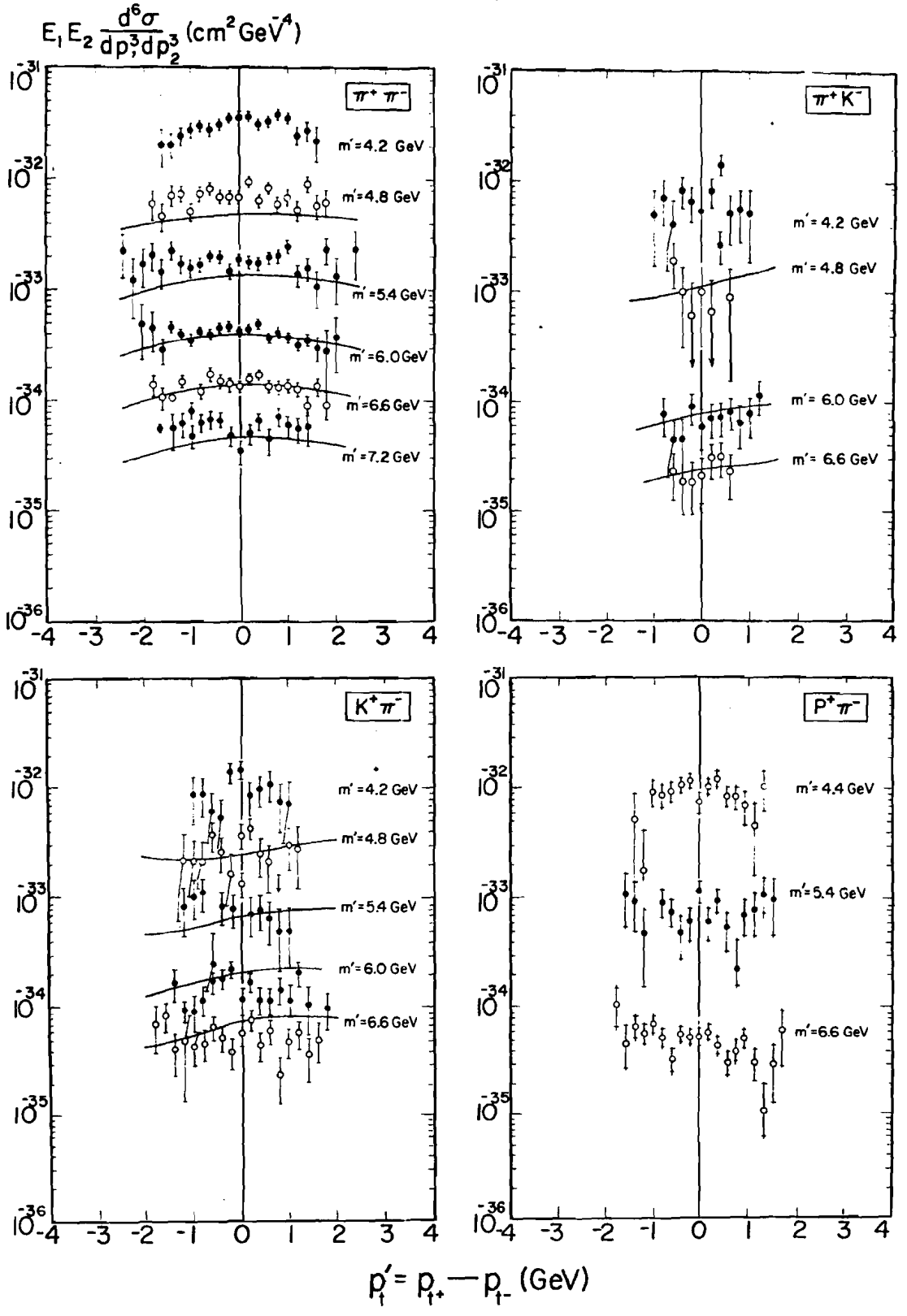

Fig. 32: The invariant two particle cross section S for 4 species combinations, plotted versus p_t'. The lines are from calculations by the Bielefeld group (Baier et al., Ref. 19) using a quark transverse momentum of $< k_t > = 0.95$ GeV inside the colliding hadrons, and a mean transverse momentum of 0.25 GeV of the produced hadrons relative to the quark from which they originated. The predictions were divided by 3.0.

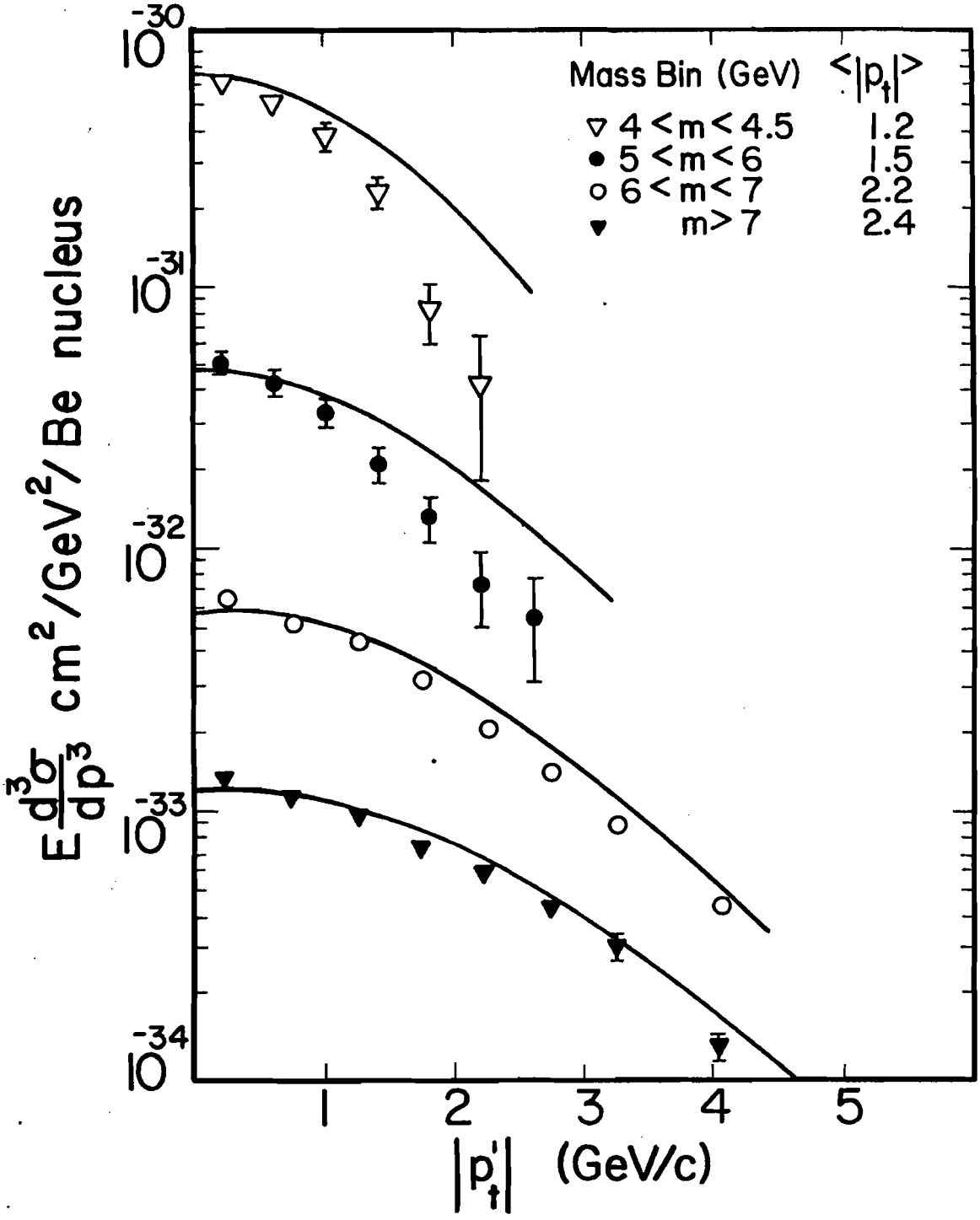

Fig. 33: Transverse momentum spectra at fixed m (Ref. 1), using the decay model acceptance. The data can be roughly described as being independent of p_t' at fixed pseudomass m': For each point (m,p_t') we first compute the pseudomass $m' \equiv p_{t,1} + p_{t,2} = \sqrt{m^2 + p_t'^2}$. The cross section at this value of m' for symmetric h^+h^- pairs is then calculated from fit h ($x_t \geq 0.24$) in Table X and normalized to the point at $p_t' = 0$.

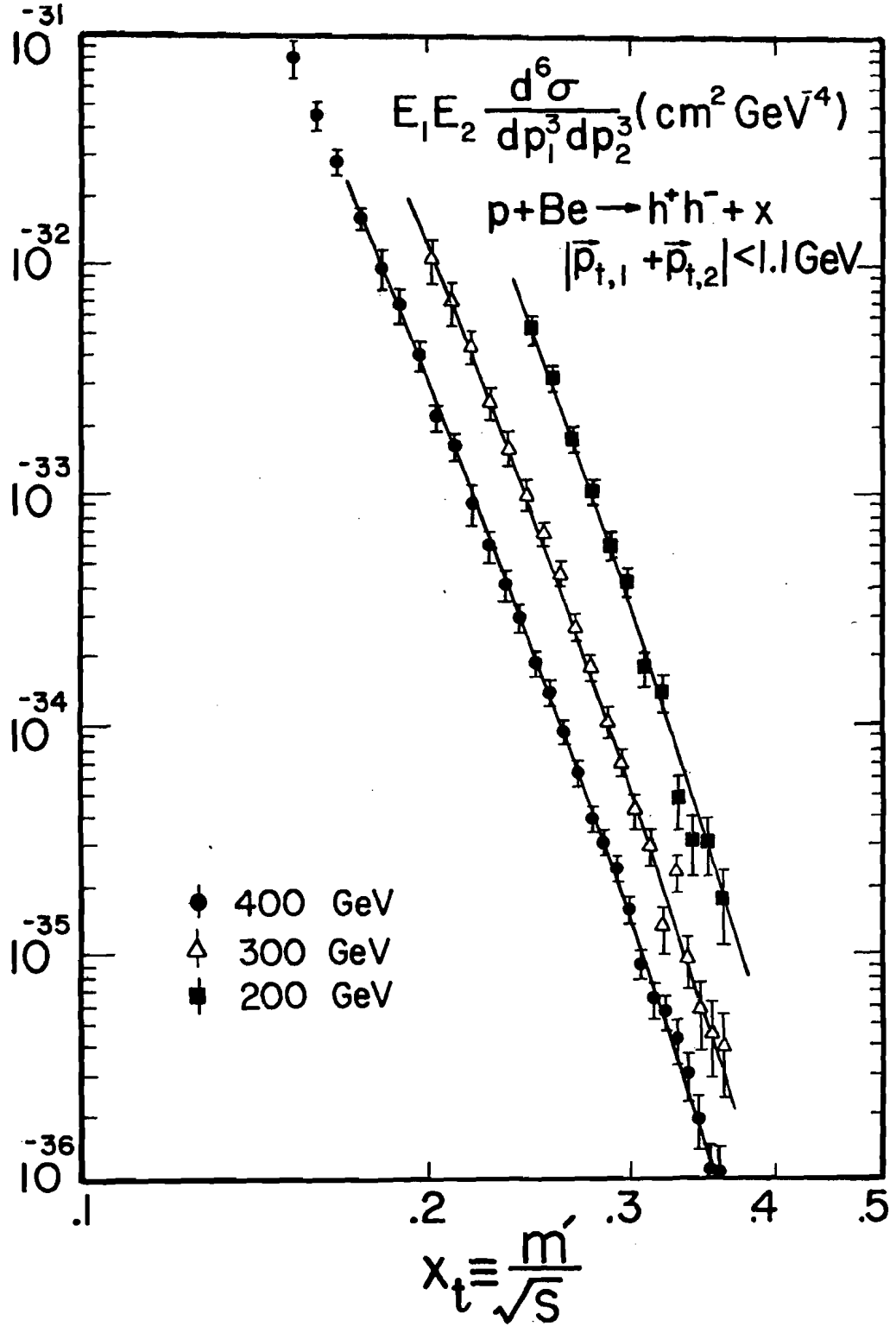

Fig. 34: The two particle invariant cross section S_+ plotted against the scaling variable x_t for symmetric h^+h^- pairs for three beam energies. The vertical separation between the data points at the same x_t yields the power k of p_t (defined as m'/2). The lines represent the fit function h for $x_t > 0.17$ from Table X.

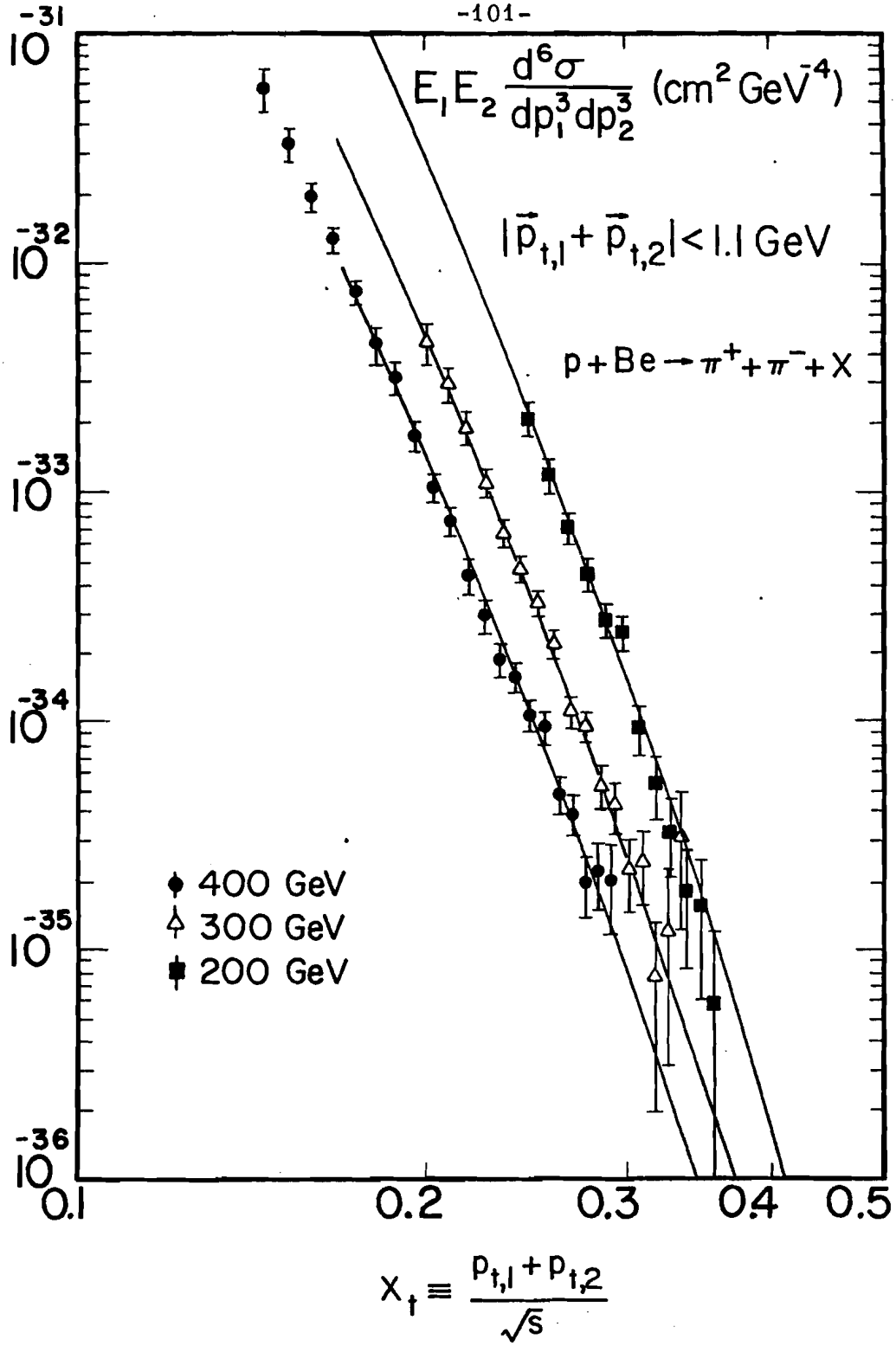

Fig. 35: Same as Fig. 34, but for $\pi^+\pi^-$ production.
The fits shown in this figure are to data above $x_t = 0.24$.